UPPSALA DISSERTATIONS IN MATHEMATICS

96

Modelling collective movement and transport network formation in living systems

Arianna Bottinelli

Department of Mathematics
Uppsala University
UPPSALA 2016

Dissertation presented at Uppsala University to be publicly examined in Häggsalen, Ångströmslaboratoriet, Lägerhyddsvägen 1, Uppsala, Friday, 25 November 2016 at 09:15 for the degree of Doctor of Philosophy. The examination will be conducted in English. Faculty examiner: Professor Renaud Lambiotte (University of Namur).

Abstract
Bottinelli, A. 2016. Modelling collective movement and transport network formation in living systems. *Uppsala Dissertations in Mathematics* 96. 56 pp. Uppsala: Department of Mathematics. ISBN 978-91-506-2599-8.

The emergence of collective patterns from repeated local interactions between individuals is a common feature to most living systems, spanning a variety of scales from cells to animals and humans. Subjects of this thesis are two aspects of emergent complexity in living systems: collective movement and transport network formation. For collective movement, this thesis studies the role of movement-mediated information transfer in fish decision-making. The second project on collective movement takes inspiration from granular media and soft mode analysis and develops a new approach to describe the emergence of collective phenomena from physical interactions in extremely dense crowds. As regards transport networks, this thesis proposes a model of network growth to extract simple, biologically plausible rules that reproduce topological properties of empirical ant trail networks. In the second project on transport networks, this thesis starts from the simple rule of "connecting each new node to the closest one", that describes ants building behavior, to study how balancing local building costs and global maintenance costs influences the growth and topological properties of transport networks. These projects are addressed through a modeling approach and with the aim of identifying minimal sets of basic mechanisms that are most likely responsible of large-scale complex patterns. Mathematical models are always based on empirical observations and are, when possible, compared to experimental data.

Keywords: animal collective behaviour, transport networks, crowd dynamics, complex systems, ants, fish

Arianna Bottinelli, Applied Mathematics and Statistics, Box 480, Uppsala University, SE-75106 Uppsala, Sweden.

ISSN 1401-2049
ISBN 978-91-506-2599-8
urn:nbn:se:uu:diva-303943 (http://urn.kb.se/resolve?urn=urn:nbn:se:uu:diva-303943)

Essentially, all models are wrong,
but some are useful.
George E. P. Box

List of papers

This thesis is based on the following papers, which are referred to in the text by their Roman numerals.

I **A. Bottinelli**, A. Perna, A Ward, D.J.T. Sumpter. How do fish use the movement of other fish to make decisions? *Proceedings of the European Conference on Complex Systems 2012*. Springer International Publishing (2013)

II **A. Bottinelli**, E. van Wilgenburg, D.J.T. Sumpter, T. Latty. Local cost minimization in ant transport networks: from small-scale data to large-scale tradeoffs. *J. R. Soc. Interface*, 12 20150780 (2015)

III **A. Bottinelli**, R. Louf, M. Gherardi. Optimal tradeoffs between building and maintenance costs in growing transport networks. *arXiv:1609.06470 [physics.soc-ph]*, *in review*, (2016).

IV **A. Bottinelli**, D.J.T. Sumpter, J.L. Silverberg. Emergent Structural Mechanisms for High-Density Collective Motion Inspired by Human Crowds. *arXiv:1606.08835 [physics.soc-ph]*, *in review*, (2016).

Reprints were made with permission from the publishers.

Contents

1. Introduction

The emergence of collective patterns from local interactions is a common feature to most living systems, spanning a variety of scales from cells to animals and humans [1, 2]. Bird flocks, fish schools, ant colonies, human crowds: across species we observe the emergence of similar collective phenomena in absence of centralised control [Fig. 1.1]. What is the *physics of emergence* in living systems? Is it possible to identify few simple principles to explain the emergence of complexity across scales and systems? At the level of a single entity, the physical, cognitive, and behavioural variables can often be measured through experiments, and individual interactions described in mathematical terms. At the level of the group, the empirical observations of collective patterns can be quantified statistically. However, what are the general mechanisms connecting these two separate levels is still an open, fundamental question.

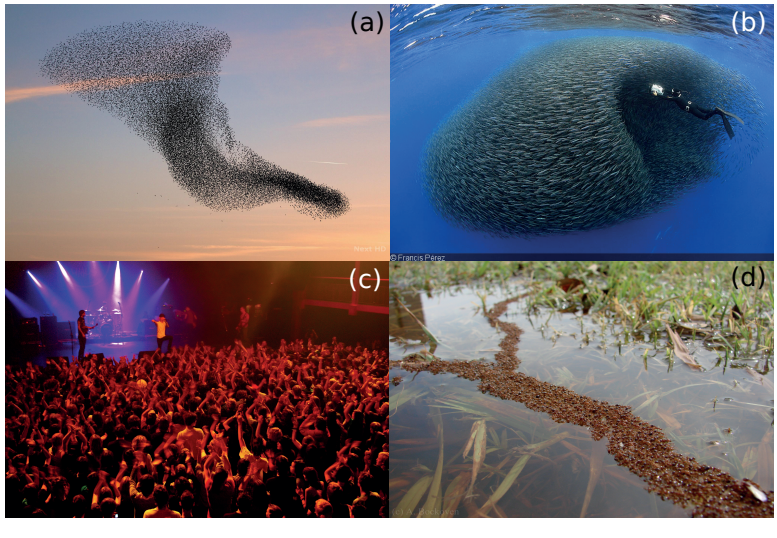

Figure 1.1. Examples of collective behaviour in living systems. (a) Starlings murmuration. (b) Fish "mill". (c) Crowd at Heavy metal concert. Credit: Ulrike Biets. (d) Floating trail made by Fire ants. (a),(b),(d) publicly available on the internet.

This thesis focuses on identifying the basic mechanisms that are most likely responsible for group-level patterns in living systems. The first unifying theme in this thesis is the idea of adapting tools from physics and mathematics to describe and understand biological and human complexity. For example, statistical mechanics provides a formal connection between the large-scale behaviour of a system and the small-scale behaviour of its constituents. Although the microscopic laws of mechanics governing the interactions between two particles are known, the lack of knowledge about each particle's state makes it impossible to extract the macroscopic dynamics of a gas by using classic mechanical laws. Similarly, knowing the details of one single bird's, or fish's, behaviour and shape, is not enough to understand how a thousand birds can flock cohesively, or how a thousand fish can produce a mill [Fig. 1.1(a) and (b)].

Group behaviour of both living and non-living systems is "more than the sum of its parts", and the result of repeated interactions between a large number of individuals. It is thus very natural to attempt to approach biological collective behaviour by adapting tools that have proven successful in describing and understanding collective behaviour in physical systems.

The second unifying theme in this thesis is the aim of making parallels between the mechanisms that underly decentralised organisation in different biological systems, and explore their potential application in human centric infrastructures. Sometimes, apparently unrelated systems turn out to be more alike than what we would have guessed at first sight. It may be about some specific feature, some hidden underlying dynamics, or just about looking at them in the right perspective, or at the right scale. As fish groups decide to turn together, ants collectively decide where to build their trails. The way they exchange information is different, as well as the way they move, and the environment they live in. In both cases, collective decisions are taken without any central control: there is no leader-fish, no engineer-ant. Although no one would mistake a man with an ant, both men and ants build transport networks, allowing one to compare the way ant trail networks and human-made infrastructures form.

Therefore, apparently very different systems—from fish, to ants trails, to transport networks and human crowds—are studied here through the same process: models founded on empirical observations give insights into specific systems, while also allowing us to abstract away from these systems, to understand general mechanisms, and to draw parallels. In this thesis, mathematical models are always based on real-world observations and are, when possible, compared to empirical data. Such approach is grounded on the belief that the model-experiment iteration is a virtuous cycle generating consistent theories about the mechanisms of emergence of collective patterns from individuals' interactions.

2. Background: a brief excursion in the field of complexity and collective behaviour

The idea that everything is made of parts, and that parts themselves are made of parts, has deeply influenced the development of philosophy and science since the 5th century BC. Since then, a lot of effort has been devoted to understand and describe these parts, splitting them further into sub-parts, down to the indivisible fundamental constituents of nature. By the 19th century, technological advances allowed different research areas to focus on different scales and systems, from atoms and stars in physics, to molecules in chemistry, to cells and human beings in biology and medicine. Nowadays, science has gained the awareness that everything is composed of the same fundamental building blocks — currently quarks, or maybe strings — and the knowledge of how these blocks work. In the meantime, it has become more and more clear that the world is not just made of parts, but of systems of parts, and that what characterises a specific system are the interactions between these parts [3].

Complex systems research is the cross-disciplinary branch of science that studies how interactions between parts on some scale result in a collective outcome on a larger scale, which properties could not be predicted by knowing the properties of one part alone [4]. For example, atoms interact to give molecules, molecules aggregate in genes, genes' interactions determine the whole set of biochemical processes that are necessary to an individual's life. In the meantime, the interaction between billions of neurones allow individuals to make everyday life decisions, such as when and how to interact with others. Insects aggregate in colonies, mammals aggregate in groups, humans build cities and form societies, and the interaction between such different systems impacts on global climate, having deep consequences on these same systems.

As many disciplines, from physics to psychology, have addressed how interactions lead to ubiquitous collective outcomes in living and non-living systems, it is difficult to find a broad, formal definition of what a complex system is [3]. A general and evocative definition of complex system is that of a whole which is "more than the sum of its parts" [Gell-Mann citing Arisototele], suggesting some contrast with mathematics, where a whole is always exactly the sum of its parts. However, in the last 40 years the study of complex phenomena has seen a close collaboration between physics, mathematics, chemistry and biology, which has quickly expanded to medicine, economics, psychology, and sociology. Indeed, most techniques and concepts that are applied to describe and investigate such phenomena are adapted and evolved from

mathematics, statistical physics, information theory and dynamical systems theory [1, 5].

In a mathematical framework, a complex system can be defined as a system composed by a large number of similar parts that interact in a disordered way to form an aggregate featuring robust organisation [3]. This definition encloses a number of concepts that recur when talking about complexity in diverse fields: emergence, self-organisation, interdependence, nonlinearity, and feedback loops.

Emergence refers to the formation of collective behaviours, and to the causal relationship between the properties of an aggregate and the properties of, and interactions among, the parts composing it. In particular, ordered collective patterns emerge spontaneously from disordered interactions, meaning that group-level order is not encoded in how single parts behave, nor is it the result of external control: the system self-organises [6, 2]. For example, crystallisation occurs when many disorderly-interacting molecules self-organise their position in a regular lattice: while the status of the system changes from liquid to solid, the nature of the interactions between molecules does not. A school of fish is able to turn at unison not because of the presence of a leading fish, but because of the way how fish respond to their neighbours' behaviour [1].

As a result of the strong interdependence between the parts composing the system, the large-scale effect of small-scale perturbations can be strongly amplified or dampened by feedback loops. In this sense, complex systems are said to display non-linear behaviour, making it hard to predict what will be the large-scale effect of perturbations at the small-scale level. Finally, complex patterns are said to be robust, meaning that introducing or subtracting a few individuals to the system does not change the collective outcome.

The separation between different levels of description, or scales, is another fundamental idea that cuts across all the above concepts, and that is strictly linked to measuring the degree of complexity of a system. One possible measure of complexity is defined as the amount of information needed to describe a system [7]. The smaller is the scale at which a system is observed, the larger is the precision of the description, but also the amount of details needed for such a description [4]. For example, describing a solid crystal at the large-scale requires a few macroscopical notions such as shape, weigh, temperature. Describing it at a small-scale requires knowing the position of billions of atoms or molecules. Similarly, a fish school can be described through the speed of its mass centre, its spatial extension and density, or through each single fish position and speed. In turn, each fish may be described as a synergistic ensemble of organs, each organ as the collective outcome of an ensemble of cells, down to atoms.

Often, complex systems display nested levels of complexity, and, as a general rule, the amount of information needed to describe the same object increases as the scale at which it is described shrinks [Fig. 2.1, red line]. This is very different compared with random (e.g. a gas of atoms at equilibrium) and

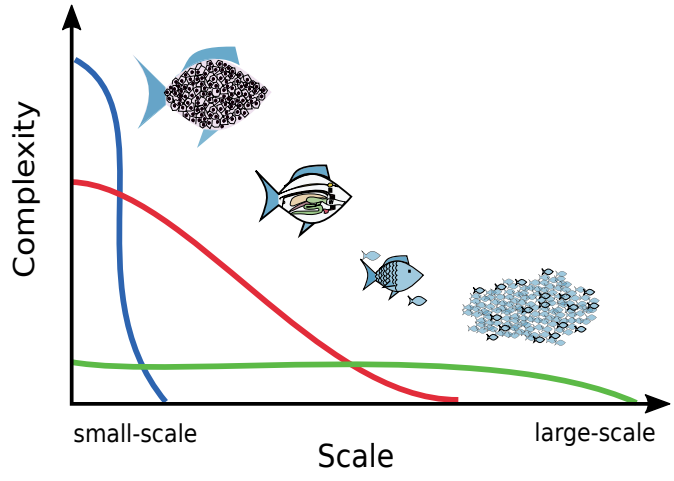

Figure 2.1. Complexity and scale of description of a system. The amount of information needed to describe complex systems increases as the scale at which it is described is diminished (red line). For random (blue line) and coherent (green line) systems the amount of information is almost independent of the scale of description. [4]

coherent systems (e.g. a gas of atoms forced to move all in the same direction), where the level of complexity is almost scale-independent [Fig. 2.1, blue and green lines respectively]. Choosing the right scale of analysis is thus fundamental to be able to observe and explain emergent group properties, and has to be taken into account when studying and modelling complex systems [1].

3. Modelling Living Systems

The expanding interest in complex systems and collective behaviour from diverse disciplines has been matched with the development of theoretical tools, often inspired by physics, aimed at formalising and unifying domain-specific empirical knowledge [1]. Describing two-body interactions through functions called potentials is a well established process in physics, whether it is about two planets or two charged particles. However, modelling the emergent properties of many-body systems requires a different set of tools, such as mean field theory, dynamical systems theory, Monte Carlo approaches, and more in general statistical physics [5, 8].

The idea that mathematical models constitute a rigorous way to compute consequences from assumptions [9] can as well be applied to complex systems to understand what are the most likely characteristics and interactions at the level of parts that give rise to collective behaviours at the level of the whole [1, 10]. However, a model is a simplified mathematical representation of a system, and a big deal of work is to connect the assumptions about its composing parts to the real world. First, a complex system might feature several nested levels of complexity, requiring to choose *a priori* what level of description is most convenient to model the emergence of a certain pattern. Second, the basic working hypothesis in complex systems research is that interacting parts should be identical, requiring to abstract the relevant features that characterise all parts' behaviour. Finally, extracting basic mechanisms requires to reduce the number of assumptions to the minimum set that is necessary to reproduce a certain pattern.

Such process of simplification is even more critical when searching for the general principles of collective behaviour in living systems [11]. Unlike physical systems, biological complexity is indeed the result of evolution through natural selection. Therefore, the diversity of behavioural interactions in living systems is by far larger than the diversity of the interactions in physical systems [2]. Here, identifying and retaining only the few features that are considered to be essential to understand a certain phenomena becomes less and less straightforward as biological complexity increases. As a consequence, models strongly depend on the analysed system and on the research questions.

Group decision making, collective dynamics, and infrastructures construction are examples of complex phenomena displayed by the same system: human society. Therefore, understanding human society passes through the description and modelling of these aspects, requiring to identify the different characteristics of human beings that are most relevant to each phenomena.

While psychological aspects may be of primary importance in decision making, collective dynamics has mainly a physical nature, and infrastructures are driven by socio-economical considerations. Modelling requires to simplify a person's psychological and physical complexity by choosing the right level of description and by identifying common behavioural rules, discarding the details that would characterise a single individual. Intuitively, if our final aim is to describe large crowds' collective motion it is not convenient to model how muscles work together to make a person walk, nor it is generally necessary to distinguish pedestrians' sex. Similarly, modelling cells motility would be convenient in order to understand the formation of internal organs, but not to understand how a fish or a school of fish move, as this would cross too many levels of organisation [Fig. 2.1]

Integrating theory and experiments is fundamental for abstracting the individual relevant features that are needed to investigate the principles underlying collective behaviour across levels of biological organisation [1]. One usually starts by choosing a model to represent some collective pattern observed in nature. Different systems, or different patterns within the same system, lend themselves to be better represented through different models. For example, decision making is often modelled using differential equations, collective dynamics through agent-based models, and infrastructure planning through network theory [1]. By observing how individuals within a group behave, one has then to make assumptions about the basic rules that describe how each individual responds to other individual's behaviour, formalising qualitative observations into a mathematical framework. Comparing the model's prediction against experimental data allows one to have an insight on the initial assumptions and to better understand a specific system. It might happen that one has to change some assumptions to better fit the model to empirical data, compute new predictions, and iterate the comparison with experimental evidence in order to match data better and better.

Sometimes, the same pattern can be explained by more than one model or more than one set of assumptions about the system producing it. When this is the case, Occam's razor can help identifying the simplest theory that explains the largest amount of data. Also, testing a theory's predictivity through new experiments allows us to increase our knowledge about a system while nailing down the basic set of behavioural rules that explains a certain pattern. Ideally, iterating the model-experiment process provides consistent theories about the most plausible mechanisms underlying the emergence of collective patterns from individuals' interactions.

Interestingly, this process often reveals that the same model can explain patterns observed in very different systems, suggesting that there are few underlying mechanisms behind a variety of phenomena observed in different fields and at different scales. Reducing systems to their fundamental, biologically plausible, ingredients makes it possible to draw parallels between them, and to make predictions about a system by applying the knowledge about another

system. For example, in Paper II I implement a model to find the basic rules of trail construction in ants, and find that their behaviour can be abstracted and described through a simple mechanism of local optimisation. In Paper III, I explore the large-scale properties of this mechanism and its relevance in the construction of human infrastructures.

On the one hand, mathematical models provide simple explanations of complex biological phenomena, allowing us to link together different levels of complexity and to qualitatively compare different systems. On the other hand, integrating models with specific data provides a quantitative, detailed description of systems, unifying the knowledge about different aspects of the same system and allowing us to make predictions. Typical models used in this context are ordinary, partial, and stochastic differential equations, Markov chain models, network models, agent-based models, and spatially explicit models [1]. The choice of a model depends on the studied system. Usually, basic algorithms describing how a system works are implemented in computer simulations, allowing us to visualise the predictions of different sets of assumptions and to compare them with empirical data.

In what follows, I present the models used in this thesis to investigate collective motion in fish and crowds (Papers I and IV), and the formation of ant and man-made transportation systems (Papers II and III).

3.1 Modelling Collective Motion

Collective motion is displayed by a wide variety of living and non-living systems, from vibrated granular materials, to cells, to mammals, where moving and interacting units give rise to spatially ordered patterns [12, 13].

A convenient way to model this kind of phenomena is to take a Newtonian approach and describe each unit as a Self-Propelled Particle (SPP), that is, a particle that moves in a 1, 2 or 3 dimensional space due to an internal propulsion, and that interacts locally with other particles [12, 1]. Such a model embodies most ideas within the definition of complex systems: every individual is simplified to be described as a particle, responds only to the presence and behaviour of close-by neighbours (also called "interacting neighbours"), and all individuals follow the same rules of motion and interaction. The shape of these interactions varies with the system that one intends to model. Typical ingredients are repulsion from, attraction towards, and alignment with, interacting neighbours. Further ingredients may be body collision forces, in which case body size is relevant to the modelled system, and interactions with the environment. These interactions are complemented with rules of motion such as the tendency to move at a certain preferred speed or towards some direction, and random noise that represents the effect of stochastic and unknown deterministic factors affecting the motion of the considered organisms. All these ingredients, described as forces acting on each particle i, are computed

at discrete times and summed up to update the equations of motion for speed ($\vec{v}_i$) and position ($\vec{r}_i$) of a usually large number of particles N.

Self-Propelled Particle models thus implement local interaction rules through a set of coupled differential equations, and are suited to investigate how the emergent properties of a system as a whole depend on the behaviour of single individuals [12, 1]. Usually, the evolution of a large system of such particles is analytically intractable, due to the complicated nature of interactions and to the large number of particles, and is typically studied through computer simulations. Numerical simulations also allow one to easily visualise the collective outcomes originating from different interaction rules, and lend themselves very well to test hypothesis about the relevant interactions underlying collective behaviour in living systems. As a result, some SPP models are extremely elaborated and specialised to represent the details of certain biological systems [14, 15]. However, this requires us to introduce many parameters at the expense of understanding basic mechanisms. An opposite trend is instead to search for minimal models, that is, to identify the set of interactions and rules of motion necessary and sufficient to reproduce natural patterns [16, 17, 18, 19, 20].

This minimal approach was initiated by physicists, who start from the assumption that collective motion is an ordered phase of a many-body system, and use tools developed in statistical mechanics, such as order parameters, scaling laws, and correlation functions, to identify universal classes of collective patterns [12]. When taking such an approach, one must be aware that SPP systems are fundamentally out-of-equilibrium due to the ability of active units to self-propel, and thus to transform free energy in persistent motion [21]. This feature has two main consequences distinguishing active systems from equilibrium ones: the total momentum of an active system is not conserved[1], and the Mermin-Wagner theorem[2] is violated, i.e. these systems show true long-range order even in two dimensions.

3.1.1 The Vicsek Model

The first step towards modelling collective motion by using active particles was made by Vicsek in 1995, who developed a model of flocking self-propelled units inspired by ferromagnetic continuous spins [16]. The parallel exploits the similarity between a flock's velocity field and oriented spins during the ordered phase of a ferromagnet, and the analogy between random noise and temperature. As such, the model implements three of the ingredients mentioned above: the tendency to move at a certain preferred speed, to align with

[1] One has to consider the system and the fluid where it moves, then the total momentum is conserved [22].

[2] The Mermin-Wagner theorem states that in a thermal equilibrium model at nonzero temperature with short-ranged interactions, it is impossible to spontaneously break a continuous symmetry [23].

neighbours, and random directional noise. In particular, the i-th individual (of N) is described as a point particle situated at a position $\vec{r}_i(t)$ and having speed $\vec{v}_i(t) = v_0\, e^{i\theta_i(t)}$, where v_0 is a constant. At each time step, each individual updates its direction of movement θ_i by averaging on the directions of all the neighbours within an interacting range R, to which is added a random angle $\eta_i(t)$ extracted from a uniform distribution of zero mean and standard deviation Δ:

$$\theta_i(t+1) = \langle \theta_j(t) \rangle_R + \eta_i(t), \tag{3.1}$$

$$\vec{r}_i(t+1) = \vec{r}_i(t) + v_0(\cos\theta_i(t+1), \sin\theta_i(t+1)). \tag{3.2}$$

Where $\langle\rangle_R$ represents the average over the neighbours j such that $|\vec{r}_i(t) - \vec{r}_j(t)| < R$. Since the flock moves, interacting neighbours may change during the evolution of the dynamics.

Similar to the classical Heisenberg model, this simple model shows a phase transition driven by noise, or equivalently by density, between disorder (for $\Delta > \Delta_c$) and order (for $\Delta < \Delta_c$), corresponding to the birds moving in random directions and to a polarised flock where all birds move in the same direction respectively. The order of the transition has been longly debated and appears to be a consequence of how noise is introduced into the model [24]. Independent of its order, the transition can be observed by using the average velocity of the flock $\langle \vec{v} \rangle = \sum_{i=1}^{N} \vec{v}_i/(v_0 N)$ as order parameter, and the variance of noise Δ as temperature. However, unlike ferromagnets, the transition between order and disorder occurs at a critical noise level which is larger than zero $\Delta_c > 0$, breaking continuous rotational invariance. While this would never be possible in an equilibrium system, where continuous invariances can be broken only at zero temperature, self-propulsion leads the system towards non-equilibrium, thus allowing it to get around the Mermin-Wagner theorem [22].

This feature has profound consequences on the expected properties of flocks, which have been examined analytically by Toner and Tu [25] by taking a hydrodynamic approach that coarse grains the bird's density and velocity field. Such an approach makes it possible to explain the emergence of true long-range order in $d = 2$ due to the suppression of orientational fluctuations at large scale. Furthermore, the Goldstone theorem[3] implies the existence of sound-like waves due to the breaking of rotational symmetry. This phenomena is known as the "Goldstone mode of the flock", which corresponds to long wavelength fluctuations perpendicular to the direction of motion that are easily excited and slow to decay, and implies giant fluctuations in the individual's density [21].

The Vicsek model is thus a minimal model that sheds light on the general principles underlying the physics of flocking, and on the emergence and

[3]The Goldstone theorem states that the spontaneous breaking of a continuous symmetry generates Goldstone bosons, i.e. massless long-wavelength fluctuations in the corresponding order parameter [26, 27]

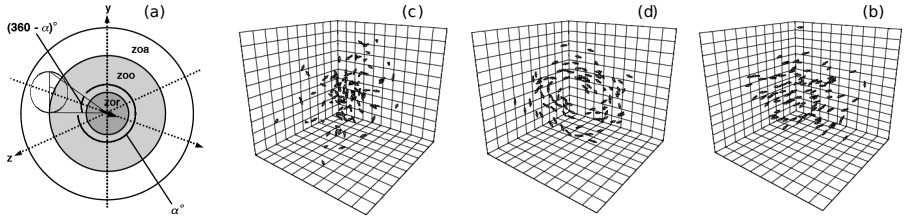

Figure 3.1. 3D model for fish collective motion by Couzin et al., figure adapted with permission from [34]. (a) Each fish is represented as a point particle that is repelled by the individuals within the repulsion zone (zor), tends to align with the individuals in the orientation zone (zoo), and is attracted by the individuals in the attraction zone (zoa). The fish does not interact with individuals in the "blind volume" at the rear (α). Collective motions exhibited by the model at increasing zoo and fixed zor and zoa: (b) swarm, (c) torus or "mill", (d) dynamic polarised group.

properties of an ordered state in active systems. It also provides an example of how collective phenomena can be interpreted using concepts from hydrodynamics, statistical mechanics, and condensed matter physics. Recently, a similar approach has been successfully applied to datasets of starling flocks in $d = 3$ taken in the field, allowing to better understand how birds choose their interacting neighbours [28], to detect Goldstone modes [29], and scale-free correlations [30].

In Paper IV, I adapt and use the vibrational theory of soft condensed materials to analyse the emergence of collective phenomena in a SPP model inspired to dense crowds.

3.1.2 Modelling Animal Collective Motion

The Vicsek model produces only two phases, random and polarised, and does not reproduce most complex patterns observed in nature, such as swarming, milling, and internal dynamics [31]. While the first known individual-based model was developed by Reynolds in 1986 to reproduce realistic flocks in computer vision [32], variations of the Vicsek model have been proposed to reproduce a wider variety of natural patterns [33]. These variations included for example purely attractive or repulsive interactions [18], or body exclusion [19], or restricted the individuals' field of vision [34], or tried to obtain polarised flocks by not explicitly encoding alignment in the rules of motion [17, 35].

For example, Couzin [34] proposed a model of fish in $d = 3$ where the individuals' circular interaction area is divided in three zones, repulsion zone at short range (zor), orientation zone (zoo), and attraction zone (zoa), plus a blind zone at the rear [Fig. 3.1(a)]. As a consequence, modelled fish try to avoid other fish which are too close, tend to orient in the same direction

as nearby fish (i.e. to align), and to join conspecifics which are far away, but do not respond to fish behind them as they cannot see them. By keeping the radii of repulsion and attraction constant, the model obtains a wide range of collective patterns by tuning the radius of orientation [Fig. 3.1(b)(c)(d)]. In particular, when the radius of orientation increases, the school undergoes a transition from a stationary disordered swarm, to a torus (or mill), to a polarised group moving in a common direction. This model is an example of how self-organised patterns that are found in real fish schools can be reproduced by using a relatively simple SPP model featuring a low number of parameters.

In Paper I, I use a SPP model in a 2D set-up to investigate which are the relevant movement-mediated interactions between fish that allow for a successful collective decision making process that involves escaping a predator.

3.1.3 Modelling Human Collective Motion

In human crowds, as in many biological systems, a variety of collective behaviours emerge from repeated local interactions of both psychological and physical nature. Examples of the resulting patterns of motion are alternating flows at bottlenecks [36], the formation of trails [37] and traffic lanes [38], as well as more dramatic collective phenomena as stop-and-go waves and crowd turbolence [39]. In all these cases, individuals behave according to their own motivations, but local interactions generate organization at the scale of the crowd without centralized planning or external control. The physics community has therefore devoted a lot of theoretical effort to the quantitative study and qualitative modelling of pedestrian crowds dynamics. Models of pedestrian crowds have important fields of application in evacuation simulations, and understanding the emergence of dramatic phenomena such as turbolence is fundamental to enhance crowd management strategies and public space design [40].

In parallel with the work by Vicsek, in 1995 Helbing initiated a class of individual-based models, known as "social force models", aimed at specifically reproducing the dynamics of human crowds [41, 20]. Helbing described pedestrians as Newtonian particles subject to "social forces" measuring the internal motivations of individuals to perform certain movements. In particular, he included a driving force, that reflects pedestrian's desire to move in a given direction at a certain speed, repulsive forces, describing the desire of keeping a certain personal distance from other pedestrians and from walls or obstacles, and attractive forces towards other individuals or objects. He assumed that the total motivation of each pedestrian i could be represented by the sum of these forces $\vec{F}_i$, so that its motion is modelled through two nonlinearly coupled Langevin equations:

$$\frac{d\vec{w}_i}{dt} = \vec{F}_i + \text{fluctuations}, \tag{3.3}$$

$$\frac{d\vec{r}_i}{dt} = \vec{w}_i\, g\left(\frac{\vec{v}_i^{\max}}{|\vec{w}_i|}\right). \tag{3.4}$$

Here, $\vec{r}_i$ is the position of individual i, $\vec{w}_i$ is its speed, and $\vec{v}_i^{\max}$ is its maximum possible speed. The function g is equal to 1 if its argument is larger than 1 and equal to its argument otherwise, so that $\vec{w}_i$ cannot exceed $\vec{v}_i^{\max}$. Finally, fluctuations represent random behavioural changes. By means of numerical simulations, Helbing was able to show that spatio-temporal patterns, such as lane formation and oscillatory flows at bottlenecks [Fig. 3.2(a) and (b)], emerge due to non-linear interactions between pedestrians, even without assuming strategical considerations, communication, or imitative behaviour. This result suggests that, even in human crowds, complex coordinated behaviour may arise from simple automatic responses rather than as the result of intelligent human actions.

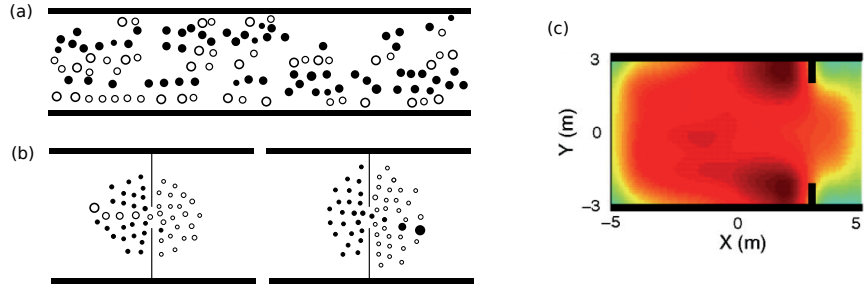

Figure 3.2. Simulation results of the social forces model for human collective motion from Helbing et al. [41], and of the variant taking into account body contact forces by Moussaid et al. [42] (adapted with permission). The original social force model by Helbing et al. reproduces (a) lane formation in pedestrian conterflows and (b) alternating flows at bottlenecks. Pedestrians are represented by circles which size is proportional to individual speed, white move towards the left and black towards the right. (c) Characterisation of turbulent flows in front of a bottleneck by mean of local body compression, which reveals two critical areas of strong compression in front of the bottleneck (dark red), from Moussaid et al. [42].

Empirical observations showed that, at increasing crowd density, people become more and more constrained and the crowd undergoes a transition from laminar flow, to stop and go waves, to turbolence [39]. In this particularly dangerous situation, crowd motion is characterised by random unintended displacements which push people around causing falling and trampling, and local body compression can reach deadly levels. In such high-density situations, conventional social norms completely break down and the dynamics is dominated by physical interaction between contacting bodies. To capture this kind of extreme behaviour, models typically introduce a body repulsion force and a sliding friction force in analogy with the physics of granular media [43].

Adding body contact forces results in a contribution to the equations of motion of pedestrian i of the form

$$f_{i,j}(t) = k\Theta(\rho_i + \rho_j - d_{i,j})\hat{n}_{i,j} + h\Theta(\rho_i + \rho_j - d_{i,j})\Delta v^t_{i,j}\hat{t}_{i,j}, \tag{3.5}$$

for each pedestrian j in contact with it. In particular, h and k are constants, ρ_i is the radius of i, $d_{i,j}$ is the distance between i and j, $\hat{n}_{i,j}$ and $\hat{t}_{i,j}$ indicate the normal and tangential directions to the vector pointing from i to j, and $\Delta v^t_{i,j}$ is the velocity difference between i and j in the tangential direction. Analysing the local body compression (or the crowd pressure, defined as local density times the local velocity variance) produced by simulating this model, made it possible to identify areas at high risk of crowd turbolence, as for example the areas in front of bottlenecks [Fig. 3.2(c)].

Along these lines, further models based on Newtonian dynamics [44, 45, 46, 47], have been successful in reproducing most self-organised phenomena observed in real crowds [40], also exploiting the similarity with granular media [36, 48, 49]. Since these models are relatively hard to calibrate, alternative approaches have also been developed, for example by implementing a cognitive heuristics based on visual cues that drives individual behaviour [42]. Other models in this field have attempted to describe crowds as a fluid [50], by means of cellular automata [51], or by taking a continuum approach where a global potential field specifies the movement of all pedestrians present within the field without agent-based dynamics [52, 53].

In Paper IV, I define a force model featuring only body contact forces, noise, and self propulsion to represent dense crowds, and use it to investigate the emergence of collective phenomena by applying tools inspired to the physics of granular materials.

3.1.4 Criticism

While the presented models demonstrate that few simple rules may produce diverse biologically plausible collective patterns, some criticism has been made against this kind of individual-based models. For example, different combinations of rules may provide very similar patterns [54], thus reducing their predictive power [55]. Arbitrary modelling choices, such as how to introduce noise (as exemplified in Section 3.1.1), the choice of a metric or topological interaction scheme, the assumption of a certain equilibrium distribution for a stochastic model, may also have profound impact on the large-scale outcome of simulations [10]. Beyond modelling, implementing computer simulations requires to make further arbitrary decisions about, for example, boundary conditions, the updating scheme, how to integrate the equations of motion, etc. that may affect the final outcome in unpredictable ways, creating artefacts which might be mistaken for original properties of the system [56].

As a consequence, different approaches to modelling collective motion have been developed. In contrast with the "microscopic" or individual-based ap-

proach described so far, researchers have also tried to model collective motion through a "macroscopic" approach that evolves field variables such as the group's density and speed [25, 57, 58, 52]. Such an approach sacrifices the knowledge of each individual's position and behaviour, but it is more analytically tractable and significantly reduces the computational effort, therefore it is often used to model human crowds in evacuation scenarios [53] or to study the statistical mechanics of active systems [25, 57].

3.2 Modelling Transportation Systems

Transportation systems are ubiquitous in nature. They are vital to the existence of most organisms and support functions that are fundamental to both human society and animal groups [59, 60, 61, 62, 63, 64, 65, 66, 67]. They allow for efficient travelling and for the exchange of resources, nutrients, or information between physically separated locations. Examples are railways and roads, power grids and sewing systems, the internet, ant trails and biological foraging networks, but also blood vessels, leaf veins, and neural networks [Fig. 3.3].

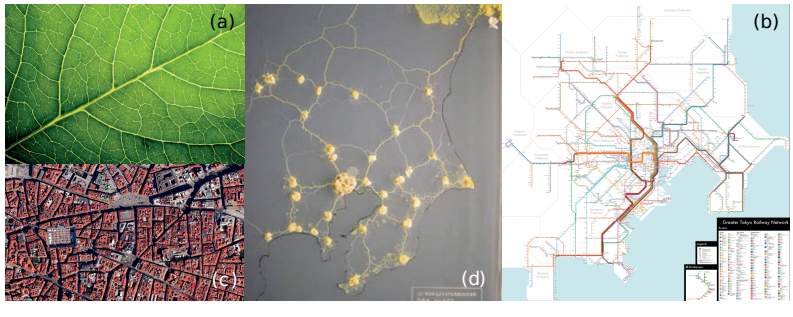

Figure 3.3. Examples of man-made and natural transport networks. (a) Leaf veins (publicly available on the internet). (b) Top view of the road network in Madrid. From Google Earth. (c) The *slime mould* builds a foraging network reproducing the main features of the great Tokyo railway network. Adapted from [60] with permissions. (d) Map of the great Tokyo railway system (publicly available on the internet).

Research in this area, from quantitative geography to medicine, aims at characterising the shape and the formation processes of transportation structures in order to understand the features of the organisms that build and rely on them [68]. For example, the growth of blood vessels is an important aspect in developing cancer treatments [69], the brain's cognitive functions are deeply connected with the structures arising from billions of physical connections between neurons [70], and the evolution of man-made infrastructures is tightly entangled with social, economical and political aspects [71, 72].

Despite transportation structures feature large-scale complex patterns, most often they are the result of an iterative local process involving repeated interac-

tions between agents and their environment, rather then the product of central planning [68]. While this is intuitive for natural networks such as blood vessels and neural networks, it might be considered surprising in the case of ant trails and human infrastructures.

The formation of well a defined trail running for several meters between the garden and a food source, for example in our kitchen, looks like a structure that would require a big deal of coordination, and possibly some kind of central control. However, it is explained by a local mechanism of positive reinforcement of chemical trails [1, 73]. In particular, each ant is able to recognise and lay a chemical substance, the pheromone. As long as one ant finds a food source, it starts going back and forth on the same route, carrying food to the nest and laying pheromone behind. Each ant that comes across the pheromone trace is able to follow the chemical gradient to the food, and starts going back and forth as well. This simple behaviour has the effect of making the trail stronger and stronger, while other traces of pheromone disappear due to evaporation, until all foraging ants follow the same trail (and find our kitchen).

This simple mechanism based on positive reinforcement is responsible for trail formation in several ant species [67], but also in other living systems such as mammals and even humans [37]. It does not require any external coordination, nor a global knowledge of the environment on the ant's side, and has been observed in laboratory conditions as well as in the field. The formation of one or few trails is often studied by taking an individual-based approach (SPP models, cellular automata, Monte Carlo simulations), which addressed the behavioural rules followed by individuals to build transport structures [37, 74, 75, 76, 66]. Similar to collective motion research, this approach aims at finding the simple mechanisms of behaviour that are essential to reproduce the geometrical properties observed in empirical trails. Remarkable examples are the ability of ant colonies to choose the shortest path between two points [77] or to build the shortest-length network between several food sources [78].

3.2.1 Spatial Network Approach

A convenient way to model large transportation systems is to take a coarse-grained approach and to represent them as networks, where nodes are stations of arrival and departure of resources, individuals, or information, and links are physical connections between these nodes [68, 79]. For this reason, transportation systems are often referred to as "transport networks". This approach discards the individual's behavioural details, and assumes that links are built according to macroscopical rules that are the result of an underlying microscopic process (foraging ants, car traffic, human activity and mobility). The advantage of such a representation is that it allows us to exploit most con-

cepts and tools developed in graph and complex networks theory to analyse and describe transportation systems [68, 80]. In particular, linking traditional topological measures to real-world quantities allows us to classify transport networks through their structure [81], and to connect such structure to the resulting properties of the network. Moreover, it provides a formal framework to understand the basic environmental and evolutionary constraints that shape transport systems during their growth, and how they relate to the specific functions the network is meant to perform [82].

An aspect common to both natural and man-made transportation systems is that space poses a fundamental constraint on the growth and structure of these networks [68]. For example, recent research has shown that closer brain regions are more likely to be connected to each other due to the biological cost of axons [70]. Building physical connections has a immediate cost in terms of material, and then what is built needs to be maintained until it is destroyed or abandoned, resulting in further costs that have to be sustained for the whole life of the network [83, 84, 72]. Since these costs are extensive, that is, the longer the connection the higher the cost for building and maintaining it, one would expect that long and expensive links should bear some advantage, for example by providing a connection to a node with high centrality or connectivity. The topology of transport networks is thus strictly related to spatial aspects, which can be taken into account by embedding these networks into a metric space, often the euclidean 2-dimensional space (but, for example, neural networks are embedded in 3 dimensions). This allows us to define measures that mix topology and space and that complement "classical" topological measures (such as degree distribution, clustering coefficient, assortativity etc), enabling a thorough description of spatial networks [68].

Measures on Transport Networks

By embedding a network into euclidean space, the *costs* associated to building and maintaining a connection are naturally represented by the length of the connection itself, and the total length of a network is usually used as a proxy for its total cost [68]. In particular, the total length of a network G built on N nodes can be written as:

$$l_T(G) = \sum_{e \in \mathscr{E}(G)} l_e, \tag{3.6}$$

where e is a link belonging to $\mathscr{E}(G)$, the set of links of G, and l_e is the euclidean length of the link. Real costs will be proportional to the total length through some constant (e.g. the cost per meter), and building and maintenance costs may have different proportionality constants. In the literature, however, the quantity defined in Eqn. 3.6 is often directly referred to as the "cost" of the network [85, 86, 87, 88, 89, 90]. Furthermore, such a definition does not take into account the fact (which is very likely for a transport system) that the current network's structure may be the result of an iterative process involving

building and destroying more links than the ones displayed in the network. Paper III starts from this observation to argue that Eqn. 3.6 is a good indicator of maintenance costs but not of building costs, and further discusses how these two costs affect the evolution and the structure of transport systems through a model of network growth.

Other typical measures that describe relevant properties of transportation networks by mixing space and topology are *efficiency* and *robustness* [91, 60, 64]. *Efficiency* represents how fast it is to travel between any two nodes of the network [92, 93], and can be computed by comparing the length of the path separating two nodes with their euclidean distance [92]:

$$E(G) = \frac{1}{N(N-1)} \sum_{i \neq j \in G} \frac{d^e_{i,j}}{d_{i,j}}. \tag{3.7}$$

i and j are nodes in G, $d^e_{i,j}$ is their euclidean distance and $d_{i,j}$ is the length of the shortest path connecting them on the network G, i.e. the sum of the length of links constituting the shortest path. With such a definition, E takes values between 0 (minimum) and 1 (maximum efficiency). The quantity $q(i,j) = d_{i,j}/d^e_{i,j}$ is also known as *route factor* or *detour index*, and sometimes used as an alternative measure of transport efficiency [59].

Another desirable property of transport systems is *robustness*, i.e. that no part of the network remains isolated in case of failure of one connection due to a targeted or random disruption [94, 95], which is usually quantified as the probability that the network remains connected under the removal of a random link [60]. Robustness is achieved through the presence of loops[4], which allow for multiple paths between different nodes. Further quantities involving space are defined to measure the density of links and to detect communities and recurring structures (motifs), and are relevant when studying traffic on networks [68].

Optimal Structures

The measures defined above can be applied to transport networks to describe their large-scale structure and to assess their performances. For example, the *Euclidean minimum spanning tree* (MST) is the network of shortest length that connects a set of N nodes [88] [Fig. 3.4(a)]. The MST is the most economical transport network, however, it is not very efficient as it features a large average shortest path, and it completely lacks robustness as the failure of one connection is enough to disconnect the network. Since it optimises cost, it is often used as a term of comparison to assess the trade-off between cost and efficiency, or cost and other design goals, in real transport networks [78, 91, 61, 65, 59]. Another notable network is the *maximal planar graph* [Fig. 3.4(b)], the graph with the maximum number of non-intersecting

[4] Loops, or cycles, are sequences of adjacent links starting and ending at the same node, such that there are at least two non-overlapping paths between any two nodes of the same cycle.

links[5]. This graph optimises robustness and efficiency by casting the maximum number of connections, but as a result it has a high cost [68]. Finally, the *star graph* is a complete bipartite graph[6] where several peripheral leaves are connected with one link to a unique internal node [Fig. 3.4(c)]. It provides the lowest route factor between the leaves and the internal node but it is suboptimal in terms of total length. It is a useful reference graph to compare transport networks constituted by a central source and many sinks, as in electric, water, or distribution networks (or the way around as in the case of ant colonies [65]), or by one main node and several secondary nodes, as in railway or metro networks [59].

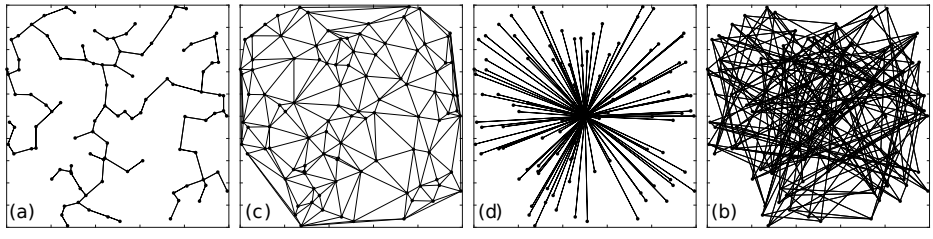

Figure 3.4. Examples of optimal networks generated on the same set of 100 randomly placed nodes. (a) Minimum spanning tree. (b) Maximal planar graph. (c) Star graph. (d) Small-world graph.

As a general observation, increasing efficiency and robustness of a network requires adding further links, which in turn increases building and maintenance costs. Therefore, another feature common of artificial and natural transport networks is that there is a trade-off between cost, efficiency, and robustness. These design goals cannot be optimised together, and natural and man-made transport systems often feature a balance between them rather than prioritising one over the others [94, 96, 59]. While such a balance may be carefully planned in artificial networks, in the case of natural network it is the consequence of a decentralised process [65, 64, 67].

A lot modelling effort has therefore focused on how competing optimisation principles affect the topology and the metric properties of transport networks. Given a set of nodes, a typical approach is to find the network configuration that minimises a convex combination of competing quantities of the form [97, 86, 87, 88]

$$\mathscr{C} = \lambda Q_1 + (1-\lambda) Q_2. \tag{3.8}$$

[5] A spatial graph is said to be planar if its links intersect only at a node. A maximal planar graph would loose its planarity if any link is added to the existing set.

[6] A bipartite graph is a graph where nodes can be divided into two disjoint sets and links connect only nodes belonging to different sets. Such a graph is complete if every node in one set is connected to every node in the other set.

At changing $\lambda \in [0,1]$, the obtained networks can be classified in terms of some topological measure, for example the degree distribution [97], allowing one to link emerging network properties and optimisation principles.

Overall, the optimisation approach sheds light on how different topological structures can arise as optimal solutions of the interplay between competing design goals. Conversely, given a real network, such an approach can help us understand what optimisation principles are likely to have shaped the observed structure. One has to be aware that optimisation studies typically consider a static set of nodes and are based on the underlying assumption that networks can be centrally planned in order to satisfy global optimisation constraints, which is a useful viewpoint for engineering and abstract problems, and may also reproduce the actual building process in the case of some artificial networks [98, 89, 99]. In the case of self-organised networks, for example natural networks, such an approach can be justified by the more subtle assumption that the observed system is the result of an evolutionary process that maximised some fitness [100], but is unlikely to provide a description of the actual process of network formation. However, optimal networks have been useful in the study of circulatory systems and river networks [101], and to assess the structures created by slime moulds or ants when compared with the MST [78, 91, 65, 60, 102].

Transport Network Growth

Most natural and artificial transport systems evolve in time, increasing or decreasing their service area as a result of a decentralised process [68]. For example, the internet grows by adding new routers and physical cables [103], railways by building new stations [59], and polydomous ants by building new nests when existing ones are overcrowded[7] [104]. Modelling transport systems as networks allows us to represent growth and regression through the insertion and deletion of nodes and links. The general aim of network growth studies is to identify the local rules that govern such insertions and deletions, and how they give rise to global patterns.

The seminal work by Price [105], and Barabasi and Albert [106] showed that a simple model where nodes are added iteratively and connected preferentially to the more highly connected nodes[8] leads to networks characterised by the presence of few highly connected nodes (hubs) and many nodes with a few connections, and asymptotically to power-law degree distributions. Such "scale-free" networks are very common in nature, from the WWW, to social networks, to the network of world airports [107], and feature remarkable properties in terms of fault tolerance, resilience and traffic efficiency. Further studies have shown that this mechanism of *preferential attachment* (and its varia-

[7] The colonies of polydomous ants consist of several nests (and possibly food sources, such as trees) connected by physical trails used by ants to travel and transfer food, eggs and larvae.

[8] The probability of a node i to connect to another node j is proportional to the degree of j, k_j, i.e. to the number of its connections.

tions) can produce a wide subclass of scale-free networks, while more general research has also focused on the properties emerging from different wiring mechanisms [108].

In the case of transport systems, the position of nodes and their distance have to be taken into account due to connection costs. Spatial aspects pose a constraint on wiring mechanisms, affecting the final properties and topology of transport networks [68]. A way to take this into account is to generalise the preferential attachment mechanism so that the probability of connecting a new node to another depends also on the distance to it [109, 110]. Usually, this probability decreases with distance in order to represent the idea that longer links are more expensive and can be created only if they provide a connection to a node with very high degree (hub). As a result, short distance connections are favoured, leading to the formation of local hubs that are tightly connected to spatially close nodes, and that are connected to each other through few long links.

Particularly relevant to understand the growth of transport networks are local optimisation models, which account for the costs of adding each single link to existing networks. Similar to the global optimisation model, this is implemented by defining a local cost function $\mathscr{C}_{i,j}$ that has to be minimised every time a node is added by choosing the most convenient link. Such cost function is typically a combination of euclidean distance and another topological or geometrical quantity [68]

$$\mathscr{C}_{i,j} = \lambda d_E(i,j) + Q_j. \tag{3.9}$$

When adding a node i, the model computes the cost function for all possible links between i and each other node j, and creates the connection that minimises it.

Such an approach has been used to explain the emergence of the power-law degree distribution of the Internet by setting Q_j to be a measure of the centrality of j [103]. The main focus of this article was to show that power-law degree distributions emerge for intermediate values of λ. However it is interesting to note that when only euclidean distance is minimised (i.e. at large λ), each new node gets connected to the closest one, iterating a paradigm of local cost minimisation that can be seen as a dynamical version of the minimum spanning tree (dMST).

Most local optimisation models have been developed to represent the growth of human transport networks and are not generally used to address the formation of biological transport networks. However, distance related costs are relevant also in biological networks, and a similar approach could be applied to understand the growth of animal transport networks by relating costs and benefits to quantities that may be relevant for animal groups, such as the presence of food, obstacle avoidance, or shelter availability [67]. In Paper II I investigate the rules of formation of meat ant trail networks by testing different biologically plausible wiring mechanisms against field data.

3.2.2 Human Transport Networks

Since the 70's, research in the field of quantitative geography aims at developing tools to characterise human transportation systems, at understanding the influence of space, and more in general of the geography of a territory, on the growth and shape of such infrastructures, and how this relates to local human activity and mobility [79, 68]. Along with the numerous contributions made by geographers, economists, urbanists, and sociologists, important advances in this field have been achieved by representing transportation systems as spatial networks, so that complex networks theory could be exploited to correlate topological and spatial aspects. Also, new extensive datasets have been gathered thanks to recent technological developments, for example from mobile phone data, satellite pictures, Geographic Information Systems, opening the way to quantitative studies of real-world transport networks and allowing researchers to validate and integrate theoretical models with empirical knowledge.

From a complex systems standpoint, it is interesting to notice that both central optimisation and self-organisation are likely to be relevant aspects in the formation of human transport networks [68]. Often, global rational planning has to compromise with local economical and political interests, resulting in solutions that may seem suboptimal from a large-scale point of view [79]. Moreover, even when centralised planning is possible, the evolutionary time scale of most infrastructures largely exceeds the time-horizon of planners. For example, railways and roads have been evolving for centuries, and in this time attempts of central planning alternated with several local uncontrolled rearrangements. Therefore, the structures we observe today can be thought of, at least on the large scale, as the result of a local optimisation process [111]. Furthermore, despite most man-made transport networks have been shaped by geographical, historical, and socio-economical mechanisms, empirical studies have shown that there are quantitative similarities between, for example, road networks patterns of very different cities [112, 61]. Such an observation suggests that the local processes at play may be based on similar detail-independent mechanisms. For these reasons, different models have taken a coarse-grained approach to study the optimisation of human transport networks, and to investigate their growth from local mechanisms.

Examples of coarse-grained models

Brede et al. [86] explore the interplay of cost and efficiency in communication infrastructures constituted by a fixed set of nodes on a one-dimensional lattice. They pose $Q_1 = l_T$ and $Q_2 = \langle l \rangle$ in Equation (3.8), representing the cost of the network through its total length and taking the average shortest path $\langle l \rangle$ as a measure of transport efficiency. At $\lambda = 1$ the model minimises the average shortest path, and the resulting network is a complete graph, where every couple of nodes is connected by a link. At $\lambda = 0$ the model minimises the

total length by building the minimum spanning tree. At intermediate values of λ, the model interpolates between these two extremes, and optimal networks range from wheels, to star graphs, to hierarchical trees. In particular, the phase diagram of several measures (for example the average degree, the clustering coefficient, the average length of a link) as a function of λ allows the authors to find transition points and to analyse how network properties depend on the optimisation constraints. Similarly, Mathias et al. [100] show that small-world networks[9] may arise from the same optimisation process in two dimensions [Fig. 3.4(d)].

An example that considers both network structure and local growth is the work by Gastner and Newman, who assessed the global optimisation of the Boston commuter rail network and of other distribution networks, and then proposed a growth mechanism to explain their large-scale structure [59]. First, the authors made a quantitative analysis of the empirical networks' structure by computing their total length and route factor, which is inversely proportional to transport efficiency [for measures definition see Section 3.2.1]. By comparing these measures with the MST and the star graph built on the same set of nodes, they showed that the analysed networks constitute a good compromise between these two extremes, i.e. they simultaneously have low route factor and low total length, possessing the benefits of both but not the drawbacks [Fig. 3.5].

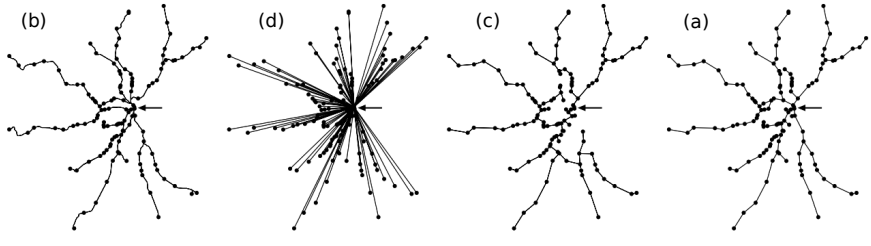

Figure 3.5. Example of how man-made transport networks can be analysed by comparison with optimised networks. Adapted with permission from [59]. (a) The Boston commuter rail network. Nodes are train stations and links are connecting railways, the arrow indicates the root of the network, i.e. the central station. (b) Star graph and (c) Minimum spanning tree built on the same set of nodes. (d) Result of the optimisation model proposed in [59] applied to the same set of nodes.

They then suggest a growth model based on local optimisation which explains the emergence of a balance between global design criteria. In the model, they randomly place a set of N nodes and one central root node (which has

[9] A network is said to be small-world if it has a large clustering coefficient but a small characteristic path length (increasing as $logN$), thus laying in between regular lattices and random graphs. Many real-world networks feature this characteristic, from neuronal networks, to social and computer networks [113, 107].

label 0) in the two-dimensional plane, and iteratively grow the network by adding the link that minimises the weight $w_{i,j} = d^e_{i,j} + \beta d_{j,0}$, where $d^e_{i,j}$ is the euclidean distance between two nodes i and j, and $d_{j,0}$ is the sum of the length of the links between j and the route. At changing β, the model interpolates between a MST ($\beta = 0$) and a star graph (at large β), and at intermediate values of β the networks self-organise to have simultaneously low route factor and low total length, similar with empirical networks. Figures 3.5 (b) to (d) illustrate this same procedure on the set of nodes of the Boston rail network. It is worth noticing that the weight function is similar to the one adopted by Fabrikant et al. in [103] for modelling the internet growth [see Section 3.2.1], however the resulting network at $\beta = 0$ is not a dMST but the actual MST, as they assume that the position of all nodes is initially known.

Louf et al. [85] take an analogous approach to explore the growth of a transportation network between several centres of human activity (cities for example). They randomly place a set of nodes in the two-dimensional plane and add one link at a time so that the cost-benefit function $R_{i,j} = B_{i,j} - C_{i,j}$ is always maximised. Benefits $B_{i,j}$ are related to human activity as they are proportional to the expected traffic between two cities i and j, while costs $C_{i,j}$ are assumed proportional to the length of links. Interestingly, this model also interpolates between the MST and a star graph, but in an intermediate regime it reproduces a structure where various local hubs control geographically separated areas, explaining how large-scale spatial hierarchy (which is observed in many real-world networks) may emerge from local cost-benefit considerations.

Criticism

Similar to the examples above, most models of network growth do not adequately take into account the separation between the time scales of self-organisation and of global planning characterising most man-made transport networks. Indeed, when considering self-organisation mechanisms, they assume that the position of all the nodes composing the network is known ahead of time, which is a rare condition for networks which have evolved for a long time, such as railway or road networks, but also electric grids and sewing systems of old cities. More generally, most existing models that aim at explaining the structure of real-world transportation systems either take a global optimisation approach, or assume that such networks are the result of a decentralised process. They therefore address only one of these two aspects, while they are both likely to be relevant for understanding the current structure and properties of transport networks.

In Paper III I explore the interplay of global planning and local optimisation in minimising the costs of building and maintaining a transport network that grows by adding nodes which position is not known ahead.

3.2.3 Ant Transport Networks

In nature, ant colonies provide a remarkable example of decentralised efficient behaviour. They are able to dig large underground nests composed of tunnels and chambers [114, 115], to solve complicated optimisation problems such as shortest-path detection [77, 116, 117] or shelter quality assessment [118], and to organise their colony as a system of spatially separated nests connected by a network of physical trails [119, 120, 121]. In particular, most ant species are able to form transportation networks to help foraging, exploration, and migration tasks [1, 67]. Depending on the species of ant considered and on the tasks these networks are used for, they can last for a few days, as for exploration networks, up to months or years. In both cases, it appears that trail formation is mainly due to a basic mechanism of pheromone laying and detection, as described at the beginning of Section 3.2 [73], although long lasting trails are usually cleared of vegetation and gravels, remaining visible also when no ant travels on them [1].

In natural conditions for example, meat ant colonies (*Iridomyrmex purpureus*) build physical trails that connect several spatially separated nests and one or more trees where these ants feed. The meat ant's trails are quite large and kept clear of vegetation and debris, so that ants do not encounter obstacles when travelling on them, can be up to 80 meters long, and typically last for several years [119, 104]. Clearly, building and maintaining this kind of network requires an active effort that increases with the length and width of trails, and that is compensated by a reduction in the effort ants have to put in transportation. Similarly, pheromone trails have the advantage of providing a direct trace between food sources and the nest, preventing ants from taking inefficient detours, but have to be maintained by ensuring a minimum passage rate, otherwise pheromone evaporates and trails disappear [73]. Therefore, ant colonies face similar trade-offs as in human transport systems, needing to achieve a balance between the competing design criteria of cost, robustness and efficiency.

Research in this area is mainly focused on finding correlations between the shape of ant transport systems, their functions, their formation process, and the behaviour of individual ants [67]. While the connection between ant's behaviour and trail formation is usually addressed through individual-based models [66, 74, 75, 76], a network approach provides a useful framework to analyse the topology of transport networks and to understand how this relates with the network's properties and functionality [122, 93, 91]. Typically, mapped trail systems are represented as networks by identifying nests, food sources, intersections, and dead ends with nodes, and the physical trails connecting these points with links. When looking at the topology of these networks, many studies have found that ant colonies remarkably find near-optimal solutions to transport network design problems [67].

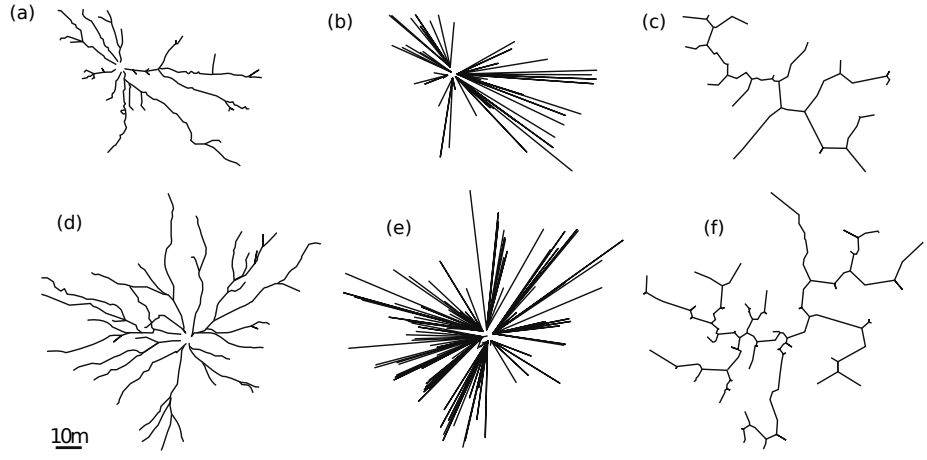

Figure 3.6. Two examples of wood ant's trail networks compared to optimised networks built on the same set of nodes. Adapted with permission from [65]. (a) and (d) are the original networks, the central node is the nest, resources are represented by peripheral nodes, and trails by links. (b) and (e) are the corresponding star graphs that connect each resource by a direct link to the central nest. (c) and (f) are the approximate Steiner trees connecting all resources (small plain circles) to the central nest (larger black circle) by minimising the total length of trails.

For example, Buhl et al. [65] address the problem of optimal network design for the colonies of the wood ant (*Formica aquilonia*). These colonies are constituted of one central nest from which several branched trails depart towards the trees where the ants feed. The authors represented each colony as a network where the central nest is a sink node, trees are source nodes, and branching points are marked and considered a separate set of nodes. Following the same approach taken by Gastner and Newman [59], Buhl et al. quantify cost and efficiency of these networks by computing the total length and the average route factor of the trails connecting source nodes to the central nest. They compare empirical values with the ones obtained for the star graph (which minimises the route factor) and for the Steiner tree[10] (which minimises the total length accounting for branching in the trails) built on the same set of nodes, showing that wood ants find a remarkably good balance between cost and efficiency [Fig. 3.6]. In particular, their networks appear to be an intermediate solution which obtains a low route factor and a low total length, similar with what observed by Gastner and Newman for man-made networks, but in the complete absence of centralised control. Interestingly, ants obtain such a result by introducing branching points, which is not the case for the artificial networks studied in [59].

[10]The Steiner tree is the network of shortest length that connects a set of nodes by introducing a set branching points.

Although Buhl et al. do not analyse the mechanisms underlying network formation, a possible explanation of the remarkable topology of wood ant networks is given by the individual-based "active walker" model [123]. In this model, each ant can orient itself towards the food source, and can lay and detect pheromone. When a large number of ants compromise between following an existing pheromone trace and going straight to the food source, branched Y-shaped trails emerge, with similar properties as wood ants foraging networks.

Other species of ants build transport networks that balance between the cost of building and maintaining the infrastructure and travel efficiency. A recent study has shown, for example, that meat ants build networks that balance between cost, efficiency, but also robustness, by introducing loops to achieve a higher resilience against disruptions [91]. Similarly, the analysis of several ant transport networks by Cook et al suggested that, in the field, most polydomous ant species tend to balance between these three design criteria [93].

Interestingly, this does not seem to be the case in laboratory experiments, where colonies of Argentine ant (*Linepithema humile*) have been observed to form minimum spanning trees or stainer trees between the nest and available food sources, minimising the cost of trails rather then balancing it against efficiency [78]. This might be due to a different mechanism of trail formation: in this specie of ants, foragers explore the territory creating a large number of trails, then once one or more food sources are detected, most of these trails get pruned so that only the shortest connections are kept between the nest and food sources [66]. However, Heller et al. show that Argentine ants in natural conditions build more robust transport networks that feature redundant links [124].

Such a difference within the same ant specie seems to support the hypothesis that the environment, and how resources are distributed in space, plays an important role in determining the large-scale patterns of ant transport networks [125]. On the other hand, the fact that several species of ant, and in very different conditions, tend to balance between design criteria, suggests that the formation of trail networks may be described by few, simple and detail-independent wiring rules [1]. Both these observations should be taken into account when modelling the morphogenesis of ant transport networks. So far, research in this field has addressed the individual-based mechanisms of trail formation mainly through individual-based models, using network theory only to describe the static structure of ant transport systems and their properties in terms of cost and efficiency.

In Paper II, I define a model of network growth to investigate the process of growth and expansion observed in the colonies of meat ant, and find two simple wiring rules that allow to reproduce the topology of empirical networks through a dynamical process.

4. Paper Summary

Papers are presented in chronological order.

4.1 Paper I

A. Bottinelli, A. Perna, A. Ward, D.J.T. Sumpter. How do fish use the movement of other fish to make decisions? *Proceedings of the European Conference on Complex Systems 2012*. Springer International Publishing (2013).

Animals living in groups are required to make collective decisions about where to collect food, the timing and direction of group travel, the choice of a new shelter, the detection and avoidance of predators etc. Typically, larger groups are predicted to be more accurate in making decisions than smaller groups or single group members, as they benefit of pooling information from several individuals. However, this may come at a cost in terms of the speed of decision, as sharing information and reaching a consensus is expected to become slower as the size of the group increases. The trade-off between accuracy and speed in decision-making characterises many biological systems [126, 127], and is supported by our every-day experience as members of human society.

However, an experiment by Ward et al. [128], showed that moving fish groups detect hidden predators and collectively decide about a new direction of motion both faster and in a more accurate fashion than isolated individuals. The research team hypothesised that this remarkable ability was a consequence of the fact that fish communicate through movement. Therefore, the information about the predator's position could be transferred quickly because of how fish responded to the movement of their neighbours.

In this paper I tested Ward et al.'s hypothesis through mathematical modelling, investigating the link between movement and information transfer underlying the emergence of a collective decisions in fish. This work constitutes a first attempt to relate two areas that are typically studied separately: physical rules of motion and group decision-making. The goals of this work were to describe how fish react to the movement of other fish through simple rules of motion, and to identify the minimal set of such rules that allowed fast and accurate decision-making in groups of increasing size. I used a self-propelled particle approach combined with numerical simulations. Fish were modelled as moving particles subject to social forces in order to capture the connection

between fish's social interactions and spatial movement. By mean of numerical simulations I reproduced the experiment by Ward at al. and fit it to the empirical data.

The analysis suggested that two biologically plausible social forces were necessary and sufficient to reproduce collective predator avoidance: the tendency to aggregate (attraction) and to swim in the same direction (alignment). Alignment in particular, was the leading interaction allowing the information about the predator's position to travel rapidly through fish schools. A possible interpretation of this result is that keeping cohesion through attraction is fundamental for visual-based communication, however relevant information are enclosed in the individual's direction of movement and in the deviations from such a direction.

Once the model was fitted to experimental data, I tested its robustness by simulating it in a different environment than the one used by Ward et al. Here, I found that the interactions found in the previous environment allowed larger groups of fish to better escape a predator chasing them. This result suggests that keeping a strong alignment with other group members is fundamental for information to spread quickly and for the group to avoid predation. An interesting outlook of this work would be to fit the same model to different species of fish performing the same decision-making task, and to test wether the relevant interactions change or remain the same.

4.2 Paper II

A. Bottinelli, E. van Wilgenburg, D.J.T. Sumpter, T. Latty. Local cost minimisation in ant transport networks: from small-scale data to large-scale tradeoffs. *J. R. Soc. Interface*, 12 20150780 (2015).

Transport networks, such as railway lines and ant trails, are a fundamental mean for distributing resources and exchange information in many human and biological systems. Most networks trade-off between *efficiency* (travel time between two points), *cost* (total network length) and *robustness* (against the loss of connections). Since the simultaneous optimisation of these design criteria is not possible, human transportation systems are often planned to balance between them. In nature, some ant species build transport networks of trails that connect multiple nests and food sources within the same colony, allowing for the exchange of eggs, larvae and food between physically separated nests. These networks are constrained by the same trade-offs found in human systems, however, they are built without any centralised planning.

Recently, a large dataset reporting the spatial structure of 140 transport networks built by the Australian meat ant (*Iridomyrmex purpureus*) became available [129], and statistical analysis on the structure of these networks showed that these ants balance efficiency and cost without giving up robustness [91].

In collaboration with Dr. Latty, a biologist from The University of Sydney and co-author in the above study, I led a project that aimed at identifying simple, decentralised and biologically plausible building rules to explain the balance observed in meat ant's networks. The challenge in this project was that the dataset provided only static information about the structure of networks of different size, which can be thought of as representative for different stages of growth of the same colony, but did not provide information about growth processes. Furthermore, meat ant networks can take up to 80 years to fully develop, making it unlikely to observe the process of construction of nests and trails in the field.

To overcome this issue I took a coarse grained approach and formulated a model of network growth based on empirical observations about the meat ant's building habits. Using this model, I found that the simple rule of "linking to the closest neighbour" together with a greedy heuristics based on distance for linking to food sources were the key to reproduce the balance observed in meat ant networks. Therefore, taking a coarse grained approach may suggest biologically plausible building mechanisms for the process of network formation when observing it directly is difficult or expensive.

Finally, I explored whether the rules suggested by ants could be relevant for other spatial self-organised networks, for example to inspire decentralised design principles for human transport networks. Similar with ants, many man-made distribution networks are constituted by sources (e.g. water stations, power plants) and sinks (e.g. our homes), grow in time, and need to be dynamically connected so to obtain efficient distribution but low infrastructure cost. Scaling the model up to a size relevant for man-made transport networks (i.e. from 15-20 nodes up to 2000 nodes) showed that local length minimisation builds transport networks that balance between efficiency and cost also on the large scale. However, in order to recover a balance with robustness, it was necessary to introduce a new parameter that represents the catchment area of sources.

4.3 Paper III

A. Bottinelli, R. Louf, M. Gherardi. Optimal tradeoffs between building and maintenance costs in growing transport networks. *arXiv:1609.06470 [physics.soc-ph]*, *in review*, (2016).

This project originates from the observation that the simple rule of "linking to the closest node", described in Paper II, is a local mechanism minimising the length, and therefore the cost, needed to connect a new node to the existing network. This growth mechanism was also considered by Fabrikant et al. [103] in the framework of a model for the growth of the Internet, and named "dynamical minimum spanning tree" (dMST). However, the focus of the authors

was on the intermediate regimes where local cost minimisation was balanced with centrality, and little attention was given to the dMST alone.

When considering the dMST in the context of growing spatial networks, linking each new node to the closest one minimises local building costs, but it results sub-optimal for the long term maintenance costs. In fact, maintenance costs are minimised by minimising the total length of a transport network, i.e. if the transport network is a minimum spanning tree. However, minimising the total length every time a node is added may require to destroy existing links and rebuild new ones, which would in turn increase building costs. The trade-off between building and maintenance costs is a feature common to all transport networks that evolve in time, however no model so far has taken this into account, assuming that building and maintenance costs pose the same constraint on network growth.

Interestingly, this aspect is strictly related to other issues that are relevant for understanding the structure and the formation of transportation systems, and that are not adequately taken into account by many models in this field. First, transport networks grow and evolve in time, and their structure is likely tied to their history. Second, most models that consider the growth of transport networks do so on a set of nodes which position is known ahead, despite in most real-world scenarios future developments are beyond the horizon of network planners. Third, most man-made transport networks have evolved for decades, and attempts of central planning necessarily alternated with locally optimised expansions. However, existing models that aim at explaining the structure of real-world transportation systems address only one of these two aspects, either taking a global optimisation approach, or assuming that such networks are the result of a completely decentralised process.

Therefore, I defined a model that grows spatial networks without the knowledge of future developments, and that implements the trade-off between building and maintenance costs by optimising a convex combination of competing quantities. Since minimising building cost can be achieved by mean of local decentralised optimisation, while minimising maintenance cost requires a central organisation that minimises total network's length, in this work I also addressed the interplay of central planning and local growth characterising the evolution of many man-made transport networks.

Combining mean field analysis and numerical simulations, I showed that balancing infrastructure costs is a minimal sufficient ingredient giving rise to emergent properties, such as the balance between the network's total length and efficiency, usually explained by more system-specific organising principles. By changing the balance between building and maintenance cost, the parameter space divides into three "phases", with a phase boundary characterized by power-law temporal correlations. Remarkably, the growth strategies that alternate local length minimisation with global reorganisations of the network are optimal in that they minimise the long-term total costs of construction, constituted by the sum of building and maintenance costs. Finally,

I discuss the relevance of this model in the context of understanding the optimisation principles underlying the growth of biological transport networks by comparing it to the transport networks built by different species of ants.

4.4 Paper IV

A. Bottinelli, D.J.T. Sumpter, J.L. Silverberg. Emergent Structural Mechanisms for High-Density Collective Motion Inspired by Human Crowds. *arXiv:1606.08835 [physics.soc-ph]*, *in review*, (2016).

In human crowds, as in many living systems, a rich variety of collective patterns emerge from repeated local interactions of both psychological and physical nature. Examples range from the formation of pedestrian lanes to the more dramatic phenomena of "crowd turbolence". During these hazardous situations, people loose control of their movement, they can be involuntary displaced meters away or fall, density waves can propagate through the crowd and body compression can reach deadly levels. In high-density situations, conventional social norms no longer apply and dynamics is dominated by physical interaction between contacting bodies. Understanding the emergence of these dramatic phenomena is fundamental to enhance crowd management strategies and public space design.

In recent years, the physics community has devoted a lot of effort to the quantitative study and qualitative modelling of pedestrian crowds. Modelling pedestrians as self-propelled particles subject to social forces allows to qualitatively reproduce most crowd self-organising phenomena and is used to advise space design and evacuation strategies. However, these models are hard to calibrate and require quantitative experimental validation.

This paper proposes a new approach to crowd dynamics based on the resemblance between high-density crowds and disordered granular packings. In the context of jammed granular materials, vibrational analysis allows to connect local structural properties of the system to its dynamics by computing the correlation matrix of the displacements of each grain around its equilibrium position. The eigenvectors (also called modes) corresponding to the largest eigenvalues of the correlation matrix convey information about the system's structural stability, the response to perturbations, and coherent and localised motion. In this work, I adapted and applied these tools to analyse the structural mechanisms underlying collective motions in simulations of large high-density crowds and to identify the causes of dangerous scenarios.

As a case study, I simulated a large number of people pushing towards a common point of interest located at one edge of a simulation box. Each person is modelled as a disk that self-propelles towards the point of interest, and subject to soft-body collision forces, random fluctuations, and a wall collision force. The model is intentionally as simple as possible, as the study aims

at identifying minimal mechanisms of emergence of collective phenomena. However, it is inspired to real-world examples, such as attendees at heavy metal concerts trying to get as close as possible to the stage, customers congregating at the entrance of a store during Black Friday sales, participants to a pilgrimage.

Traditionally, vibrational analysis studies inert materials under external stresses. Here I adapted it to study an active system vibrating under self-produced stress. In parallel with granular media, the modes corresponding to the lowest eigenvalues are vector fields predicting how the crowd would collectively move in response to perturbations. Analysing the structure and the coherence of these modes, I identified three candidate mechanisms to underly crowd collective movement:

1. The first mode is the Nambu-Goldstone mode arising from broken translational symmetry. This mode carries a system-spanning displacement modulation that couples with the propagation of density waves. When excited in a real crowd, a large number of people would be suddenly displaced resulting in dangerously high pressures, a phenomenon known as "crowd crush".
2. The individuals undergoing the largest displacements in each mode cluster in the same region near the core of the crowd, revealing the existence of a "soft spot". In jammed granular media, soft spots correlate with structural rearrangements and dynamical instability. In crowds, these areas indicate the individuals who would displace the most during collective movements, thus undergoing the greatest risk of falling and trampling.
3. When introducing a fraction of individuals agitating more to account for behavioural heterogeneity, vibrational analysis predicted the emergence of multiple distinct long-range highly correlated modes reminding of the stochastic resonance phenomena. The activation of such modes would enhance the propagation of shock waves, explaining why injurious outcomes are more likely in extreme social situations such as riots, protests, and escape panic.

If found in real crowds, these three self-organised mechanisms would provide a simple explanation of how tragic crowd incidents could arise from purely physical and structural considerations.

5. Sammanfattning på Svenska

Modellering av kollektiv rörelse och transportnätverksformation i levande system

Uppkomsten av kollektiva mönster från upprepade lokala interaktioner är ett vanligt kännetecken för de flesta levande system på alla nivåer; från celler till djur och människor. Levande system, såsom fågelflockar, fiskstim, myrkolonier och människor i grupp: oavsett vilken art som observeras uppstår liknande komplexa fenomen i frånvaro av central styrning. Hur ser fysiken bakom uppkomsten av dessa levande system ut? Är det möjligt att identifiera ett fåtal enkla principer som kan beskriva denna komplexitet tvärs över skalor och system? För enskilda enheter kan man ofta observera och kvantifiera fysiska och kognitiva variabler och beteendevariabler genom experiment och individuell interaktion går att beskriva med matematik. På gruppnivå går det att kvantifiera kollektiva mönster med hjälp av statistik. Det som återstår är att undersöka och formulera kopplingen mellan nivåer. Målet med denna avhandling är att besvara denna öppna fråga.

Denna avhandling belyser två aspekter av uppkomsten av komplexa levande system: kollektiv rörelse och formation av transportnätverk.

Inom ämnet kollektiv rörelse så studerades rollen av rörelseinitierad informationsutbyte för fiskars beslutsfattande. Analysen visade att den primära egenskapen som avgjorde fiskars möjlighet att undvika predatorer var tendensen hos dem att simma åt samma håll (alignment). Ett annat resultat belyser uppkomsten av kollektiva fenomen relaterade till den fysiska dynamiken i extremt täta grupperingar.

Inom ämnet transportnätverk så utvecklades en modell för att kunna reproducera utbyggnaden av nätverksspår som kopplar samman ett flertal bon hos *Iridomyrmex purpureus*, en myrart vanligt förekommande i Australien. Den enklaste förklaringsmodellen för att koppla ihop varje ny nod till dess närmaste grannar visade sig är huvudingrediensen bakom att kunna reproducera den karaktäristiska balansen mellan de relevanta designkriterierna som observerats empiriskt.

I ett annat projekt studerades hur byggnations- och underhållskostnader påverkar utbyggnaden av transportnätverk. Det visade sig att den tillväxtstrategi som alternerar lokal optimering, vilket minimerar byggnadskostnader, och har centralt planerad omorganisation för att minimera underhållskostnader är det som mest troligt minimerar den sammanlagda kostnaden för nätverket.

Målet med dessa projekt är att identifiera den grundläggande mekanismen som är den mest sannolika för att beskriva mönster i levande system och de strukturer de konstruerar.

Det första förenande temat i denna avhandling är tanken att adaptera verktyg från fysiken och matematiken för att beskriva och förstå biologisk och mänsklig komplexitet. Gruppbeteende för både levande och icke-levande system är mer än summan av dess delar, och resultatet av upprepad interaktion av ett stort antal av individer. Det är därmed mycket naturligt att försöka att närma sig biologiskt kollektivt beteende genom att ta till sig verktyg som har visat sig framgångsrika i att beskriva och förstå kollektivt beteende i fysikaliska system.

Det andra förenande temat beskrivet i denna avhandling är målet att hitta paralleller mellan mekanismerna som ligger bakom decentraliserad organisation i olika system och utforska dess potentiella tillämpning i infrastrukturer rörande människor. Det händer att till synes oberoende system är mer lika varandra än vad som man hade kunnat tro vid en första anblick. Det kan handla om någon specifik egenskap, någon gömd underliggande dynamik, eller så gäller det att bara studera systemet utifrån rätt perspektiv, eller på rätt skala.

Därmed kan till synes väldigt olika system, från fiskar och myrstigar till transportnätverk och mänskliga folkmassor studeras genom samma process: matematiska modeller som bygger på empiriska observationer som ger insikt in i speciella system, men också möjliggör för oss att på ett abstrakt sätt att förstå generella mekanismer, och att kunna dra paralleller. I denna avhandling bygger matematiska modeller på observationer från verkligheten och är, när det är möjligt, jämförda med empirisk data. Ett sådant närmande är grundat i tron att modell-experiment-upprepningen är en bra cykel för att generera konsekventa teorier om mekanismerna bakom kollektiva mönster från individuell växelverkan.

6. Riassunto in Italiano

Modelli di movimento collettivo e di formazione delle reti di trasporto nei sistemi viventi

L'emergenza di fenomeni collettivi da semplici interazioni locali è una caratteristica che accomuna la stragrande maggioranza dei sistemi viventi, e che si presenta su una moltitudine di scale, dalle cellule, agli animali, agli esseri umani. Stormi di uccelli, banchi di pesci, colonie di formiche, folle umane: spesso, comportamenti collettivi similari emergono in sistemi molto differenti tra loro e senza il bisogno di coordinazione esterna. Qual'è la fisica che descrive l'emergenza di fenomeni collettivi nei sistemi viventi? È possibile identificare pochi semplici meccanismi che spieghino l' emergere della complessità su diverse scale e in diversi sistemi? A livello delle singole entità, gli esperimenti permettono di misurare quantità fisiche, cognitive, e comportamentali, di osservare le interazioni tra gli individui, e queste osservazioni possono essere formalizzate in termini matematici. A livello del gruppo è possibile osservare i comportamenti collettivi e quantificarli tramite strumenti statistici. Tuttavia, quali siano i meccanismi generali che connettono questi due livelli rimane ancora una questione aperta.

L'oggetto di studio di questa tesi è l' emergenza di fenomeni complessi nei sistemi viventi in due manifestazioni principali: il movimento collettivo e la formazione delle reti di trasporto.

Nell'ambito del movimento collettivo, questa tesi si occupa di come il movimento dei singoli individui permetta di trasferire informazioni all'interno di un gruppo di pesci così da ottenere decisioni collettive accurate. L'analisi qui descritta suggerisce che la tendenza dei pesci a nuotare allineati con i propri vicini sia il meccanismo che permette a gruppi numerosi di sfuggire a un predatore con più probabilità rispetto a gruppi più piccoli o a singoli individui. Il secondo progetto sul comportamento collettivo si ispira all'analisi spettrale nell'ambito della fisica della materia granulare per sviluppare un nuovo contesto in cui studiare la dinamica delle folle umane. Questo lavoro propone un nuovo approccio per descrivere l'emergenza di fenomeni collettivi in situazioni di alta densità, in cui le persone interagiscono principalmente tramite contatto fisico.

Per quel che riguarda le reti di trasporto, in questa tesi ho sviluppato un modello per rappresentare il processo tramite cui le formiche australiane della

carne (*Iridomyrmex purpureus*) costruiscono delle reti di trasporto fatte di sentieri che collegano diversi nidi appartenenti alla stessa colonia. Confrontando il modello con i dati sperimentali, ho dimostrato che la semplice regola di connettere ogni nuovo nido al nido più vicino riesce a riprodurre le reti osservate in natura, ed in particolare l'equilibrio tra la robustezza della rete, l'efficienza nel trasporto, e il costo di costruzione dei sentieri. Il secondo progetto sulle reti di trasporto contenuto in questa tesi, studia come lo sviluppo di queste reti sia influenzato dai costi di mantenimento e costruzione delle connessioni tra nodi tramite un modello di crescita dinamica. In particolare, ho dimostrato che i costi totali di una rete di trasporto possono essere minimizzati alternando l'ottimizzazione del costo di costruzione a livello locale e la minimizzazione dei costi di mantenimento tramite azioni di controllo centralizzato.

L'obbiettivo comune di questi progetti è stato di identificare i meccanismi che più probabilmente sono alla base dei comportamenti collettivi nei sistemi viventi, o delle proprietà su larga scala delle strutture costruite da questi ultimi.

Un altro tema che unifica i progetti in questa tesi è l'idea di adattare strumenti tipicamente usati in fisica e matematica per descrivere e comprendere la complessità dei sistemi biologici. Sia nei sistemi fisici sia in quelli viventi, i comportamenti collettivi sono "più della somma delle singole parti", nel senso che derivano dalla ripetuta interazione di un grande numero di individui. Sembra quindi molto naturale l'idea di studiare il comportamento collettivo di sistemi biologici tramite strumenti che si sono rivelati appropriati nel descrivere il comportamento collettivo di sistemi fisici.

L'ultimo tema che unifica questa tesi è l'intenzione di tracciare paralleli tra i meccanismi che guidano l'emergenza di comportamenti collettivi in sistemi differenti, ed esplorare come questi meccanismi potrebbero potenzialmente essere applicati in un contesto umano. Talvolta infatti, sistemi apparentemente molto diversi possono risultare più affini di quanto si possa immaginare da una prima analisi. Questa similitudine potrebbe essere legata a qualche particolare caratteristica dei sistemi osservati, alle proprietà che ne governano il funzionamento, o semplicemente alla scala e alla prospettiva in cui li si studia.

Per questo motivo, questa tesi analizza sistemi apparentemente molto diversi tra loro—pesci, formiche, reti di trasporto, folle umane—tramite lo stesso procedimento. Partendo dalle osservazioni empiriche, i modelli matematici vengono applicati per studiare le caratteristiche dei singoli sistemi e, nel contempo, per individuare gli aspetti più universali, astraendo i meccanismi generali che rendono possibile trovare le similitudini tra sistemi diversi. I modelli matematici in questa tesi sono sempre basati su osservazioni empiriche e, quando possibile, le predizioni ottenute tramite i modelli sono comparate ai dati sperimentali. Questo approccio è fondato sulla convinzione che integrare modellizzazione e sperimentazione, teoria e osservazione, sia fondamentale per generare teorie coerenti sulla realtà che ci circonda.

7. Acknowledgements

Getting to the end of this long PhD-journey has been possible thanks mainly to my supervisor David Sumpter. David has been there to support, encourage, explain, teach, listen, prod, reproach (etc) exactly when I needed it, becoming a firm point of reference in my academic development as well as a person I trust. The biggest thank you is for letting me follow my scientific interests, making me a more independent researcher and a happier person.

The diverse projects that are part of this thesis follow from as many collaborations. In these years I've had the privilege to work with amazing scientists who co-supervised me, showing me different aspects of working in an interdisciplinary environment and contributing to getting me closer to a real researcher.

First, thanks to Andrea Perna, my first officemate, who welcomed me in Uppsala, accompanied my first steps in the field of collective behaviour, taught me how to use Matlab, and shared my suffering when drinking Swedish coffee.

Thank you to Tanya Latty who, over a cappuccino in Sydney, told me about her ongoing projects, offered me a collaboration, and gave me the inspiration to come back from my gap year and to keep doing research.

Thank you to Marco Gherardi, who has provided priceless input and support for our network project, hosting me in his already overcrowded office in Milan and patiently listening to and skimming through all my more or less eccentric ideas.

Finally, thank you to Jesse Silverberg, whose enthusiasm for science (and heavy metal and cats) has been a great source of inspiration and a strong motivation during the last year.

Next to the purely academic considerations, thanks to all of you for not only being collaborators, but also friends.

Not only have I been supervised, but I also had the chance of co-supervising Andreas Gådin and John Svensson, whom I thank for their patience and feedback. I hope that this experience has been useful for them as much as it was for me.

I enjoied being part of the Collective Behaviour group, which I have seen evolving for quite a while now, and has always been a lively and fun environment. I am grateful to Daniel, Qi, Richard, and Boris, who welcomed me when I arrived in 2011, for all the nights spent at the pub or in a Nation. To Shyam, Natasha, Stam, and Viktoria for shared lunch-breaks and chats. Max, Teddy, Hongli, Alex, Ernest, Emil, Björn, Linnéa, Line: thank you for never giving up on calling me for coffee breaks, games and pub nights. As you can

see, it eventually worked out. A special mention goes to Björn and Linnéa for helping me translating the summary in Swedish, and to Alex for proofreading part of this thesis.

During these years of PhD studies I had the chance to meet excellent scientists whose research contributed to expand my interests and to whom I owe inspiring conversations: Irene Giardina, Andrea Cavagna, Mehdi Moussaid, Andrea Baronchelli, Vito Latora, Manlio De Domenico, Guy Theraulaz, Jean-Louis Deneubourg, Simon Garnier, Roberto di Leonardo, Hugues Chaté, and Audrey Dussutour.

I also met friends who are definitely on their way to become excellent scientists, but were not of less inspiration: Sarah, Remi, whom I also collaborated with, Domenico, and Elisa.

I would like to thank Renaud Lambiotte for hosting me in Namur, for spending some time discussing my research work (some ideas that came up during that conversation actually made it into my future research projects), and finally for accepting to be my opponent.

I am grateful to the Centre for Interdisciplinary Mathematics for funding my PhD and for supporting my participation in workshops and conferences, allowing me to meet most of the people mentioned above and below.

I'd like to thank the researchers and the staff at the Mathematics department, in particular Warwick Tucker, Elisabeth Bill, Inga-Lena Assarsson, Susanne Gauffin, and Fredrik Lannergård who have always been very patient and helpful with all my administrative issues. And of course the other PhDs, Felipe, Dan, Kostas, Jakob, Marta, Katia, with whom I shared some wasting hardcore-math course at some point, and Hannah, for being such a kind officemate.

A thank you goes to Valeria, Johan, Marianna, Saman, José, Juan, Anke, and Nattakarn at the department of Wave Energy for hosting me during many lunches in their kitchen, and for the nice and entertaining chats.

During these years I have spent quite some time wandering between Milan and Uppsala. The time I have spent in Uppsala has been brightened by the presence of many friends, and I am sure I wouldn't have made it through many of these winters without them and without the serious amount of Italian food, wine, and chats we had together! Valeria, Johan, Pasticcino, Diego, Francesca, Niccoló, Tony, Alberto, Paola, Chiara, Beppe, Luca, Matteo, Valentina, Riccardo, Andrea, Sara, Alessandro, Carlotta (and possibly other people who will hopefully forgive my forgetfulness): thank you.

I want to thank the friends at my old department of Theoretical Physics in Milan; Marco, Bruno Bassetti, Pietro, and Sandro, for hosting me every now and then and for their availability in discussing what I was working on at the moment, providing advices and new viewpoints.

Another thank you goes to the department of Nuclear Engineering at Politecnico di Milano, for hosting me in their offices or in their small kitchen, for the tv series and fun conversations over lunch, and for always making me feel part of their group.

One of the most rewarding feelings every time I'm back in Milan is to meet with few but incredibly long-lasting friends, who make me feel like I've never left: Mary, Filo, Luca, Roby (who's not exactly in Milan but will forgive me for the approximation), Simona, Marchino. Not to mention Sara, Eleonora, Simona, Giovanni, Davide, with whom we manage to keep in touch despite they are scattered across Europe.

I'd like to thank my family, cats included, for supporting me in all my decisions and for the warmth, love, and understanding they give me both from distance and every time we manage to get together.

Last but not least, Ale, thank you for being my fixed point in the chaotic life of these last years.

So Long, and Thanks for All the Fish.
— The Dolphins

References

[1] David JT Sumpter. *Collective animal behavior*. Princeton University Press, 2010.

[2] Scott Camazine. *Self-organization in biological systems*. Princeton University Press, 2003.

[3] James Ladyman, James Lambert, and Karoline Wiesner. What is a complex system? *European Journal for Philosophy of Science*, 3(1):33–67, 2013.

[4] Yaneer Bar-Yam. General features of complex systems. *Encyclopedia of Life Support Systems (EOLSS), UNESCO, EOLSS Publishers, Oxford, UK*, 2002.

[5] Stuart A Kauffman. *The origins of order: Self organization and selection in evolution*. Oxford University Press, USA, 1993.

[6] Murray Gell-Mann. Simplicity and complexity in the description of nature. *Engineering and Science*, 51(3):2–9, 1988.

[7] Murray Gell-Mann. What is complexity? In *Complexity and industrial clusters*, pages 13–24. Springer, 2002.

[8] Gregoire Nicolis, Ilya Prigogine, et al. *Self-organization in nonequilibrium systems*, volume 191977. Wiley, New York, 1977.

[9] Richard Phillips Feynman. *The character of physical law*, volume 66. MIT press, 1967.

[10] Robert M May. Uses and abuses of mathematics in biology. *Science*, 303(5659):790–793, 2004.

[11] Nino Boccara. *Modeling complex systems*. Springer Science & Business Media, 2010.

[12] Tamás Vicsek and Anna Zafeiris. Collective motion. *Physics Reports*, 517(3):71–140, 2012.

[13] Jean-Louis Deneubourg and Simon Goss. Collective patterns and decision-making. *Ethology Ecology & Evolution*, 1(4):295–311, 1989.

[14] Andreas Huth and Christian Wissel. The simulation of the movement of fish schools. *Journal of theoretical biology*, 156(3):365–385, 1992.

[15] Hanspeter Kunz and Charlotte K Hemelrijk. Artificial fish schools: collective effects of school size, body size, and body form. *Artificial life*, 9(3):237–253, 2003.

[16] Tamás Vicsek, András Czirók, Eshel Ben-Jacob, Inon Cohen, and Ofer Shochet. Novel type of phase transition in a system of self-driven particles. *Physical review letters*, 75(6):1226, 1995.

[17] D Grossman, IS Aranson, and E Ben Jacob. Emergence of agent swarm migration and vortex formation through inelastic collisions. *New Journal of Physics*, 10(2):023036, 2008.

[18] Hugues Chaté, Francesco Ginelli, Guillaume Grégoire, Fernando Peruani, and Franck Raynaud. Modeling collective motion: variations on the vicsek model. *The European Physical Journal B*, 64(3-4):451–456, 2008.

[19] Fernando Peruani, Andreas Deutsch, and Markus Bär. Nonequilibrium clustering of self-propelled rods. *Physical Review E*, 74(3):030904, 2006.
[20] Dirk Helbing. A mathematical model for the behavior of pedestrians. *Behavioral science*, 36(4):298–310, 1991.
[21] Sriram Ramaswamy. The mechanics and statistics of active matter. *arXiv preprint arXiv:1004.1933*, 2010.
[22] John Toner, Yuhai Tu, and Sriram Ramaswamy. Hydrodynamics and phases of flocks. *Annals of Physics*, 318(1):170–244, 2005.
[23] N David Mermin and Herbert Wagner. Absence of ferromagnetism or antiferromagnetism in one-or two-dimensional isotropic heisenberg models. *Physical Review Letters*, 17(22):1133, 1966.
[24] M Aldana, H Larralde, and B Vázquez. On the emergence of collective order in swarming systems: a recent debate. *International Journal of Modern Physics B*, 23(18):3661–3685, 2009.
[25] John Toner and Yuhai Tu. Long-range order in a two-dimensional dynamical xy model: how birds fly together. *Physical Review Letters*, 75(23):4326, 1995.
[26] Yoichiro Nambu. Quasi-particles and gauge invariance in the theory of superconductivity. *Physical Review*, 117(3):648, 1960.
[27] Jeffrey Goldstone. Field theories with «superconductor» solutions. *Il Nuovo Cimento (1955-1965)*, 19(1):154–164, 1961.
[28] Michele Ballerini, Nicola Cabibbo, Raphael Candelier, Andrea Cavagna, Evaristo Cisbani, Irene Giardina, Vivien Lecomte, Alberto Orlandi, Giorgio Parisi, Andrea Procaccini, et al. Interaction ruling animal collective behavior depends on topological rather than metric distance: Evidence from a field study. *Proceedings of the national academy of sciences*, 105(4):1232–1237, 2008.
[29] William Bialek, Andrea Cavagna, Irene Giardina, Thierry Mora, Oliver Pohl, Edmondo Silvestri, Massimiliano Viale, and Aleksandra M Walczak. Social interactions dominate speed control in poising natural flocks near criticality. *Proceedings of the National Academy of Sciences*, 111(20):7212–7217, 2014.
[30] Andrea Cavagna, Alessio Cimarelli, Irene Giardina, Giorgio Parisi, Raffaele Santagati, Fabio Stefanini, and Massimiliano Viale. Scale-free correlations in starling flocks. *Proceedings of the National Academy of Sciences*, 107(26):11865–11870, 2010.
[31] Julia K Parrish and William M Hamner. *Animal groups in three dimensions: how species aggregate*. Cambridge University Press, 1997.
[32] Craig W Reynolds. Flocks, herds and schools: A distributed behavioral model. *ACM SIGGRAPH computer graphics*, 21(4):25–34, 1987.
[33] Charlotte K Hemelrijk and Hanno Hildenbrandt. Self-organized shape and frontal density of fish schools. *Ethology*, 114(3):245–254, 2008.
[34] Iain D Couzin, Jens Krause, Richard James, Graeme D Ruxton, and Nigel R Franks. Collective memory and spatial sorting in animal groups. *Journal of theoretical biology*, 218(1):1–11, 2002.
[35] Daniel Strömbom. Collective motion from local attraction. *Journal of theoretical biology*, 283(1):145–151, 2011.
[36] Dirk Helbing, Anders Johansson, Joachim Mathiesen, Mogens H Jensen, and Alex Hansen. Analytical approach to continuous and intermittent bottleneck

flows. *Phys. Rev. Lett.*, 97(16):168001, 2006.
[37] Dirk Helbing, Joachim Keltsch, and Peter Molnar. Modelling the evolution of human trail systems. *Nature*, 388(6637):47–50, 1997.
[38] Serge P Hoogendoorn and Piet HL Bovy. Pedestrian route-choice and activity scheduling theory and models. *Transport. Res. B - Meth.*, 38(2):169–190, 2004.
[39] Dirk Helbing, Anders Johansson, and Habib Zein Al-Abideen. Dynamics of crowd disasters: An empirical study. *Phys. Rev. E*, 75(4):046109, 2007.
[40] Dorine C Duives, Winnie Daamen, and Serge P Hoogendoorn. State-of-the-art crowd motion simulation models. *Transport. Res. C - Emer.*, 37:193–209, 2013.
[41] Dirk Helbing and Peter Molnar. Social force model for pedestrian dynamics. *Phys. Rev. E*, 51(5):4282, 1995.
[42] Mehdi Moussaïd, Dirk Helbing, and Guy Theraulaz. How simple rules determine pedestrian behavior and crowd disasters. *Proc. Natl. Acad. Sci. U.S.A.*, 108(17):6884–6888, 2011.
[43] Dirk Helbing and Anders Johansson. *Pedestrian, crowd and evacuation dynamics*. Springer, 2011.
[44] Rainald Löhner. On the modeling of pedestrian motion. *Appl. Math. Model.*, 34(2):366–382, 2010.
[45] Hui Xi, Seungho Lee, and Young-Jun Son. An integrated pedestrian behavior model based on extended decision field theory and social force model. In *Human-in-the-Loop Simulations*, pages 69–95. Springer, 2011.
[46] Dirk Helbing, Illés Farkas, and Tamas Vicsek. Simulating dynamical features of escape panic. *Nature*, 407(6803):487–490, 2000.
[47] Wenjian Yu and Anders Johansson. Modeling crowd turbulence by many-particle simulations. *Physical review E*, 76(4):046105, 2007.
[48] Emiliano Cristiani, Benedetto Piccoli, and Andrea Tosin. Multiscale modeling of granular flows with application to crowd dynamics. *Multiscale Model. Sim.*, 9(1):155–182, 2011.
[49] Sylvain Faure and Bertrand Maury. Crowd motion from the granular standpoint. *Math. Mod. Meth. Appl. S.*, 25(03):463–493, 2015.
[50] LF Henderson. The statistics of crowd fluids. *Nature*, 229:381–383, 1971.
[51] Victor J Blue and Jeffrey L Adler. Cellular automata microsimulation for modeling bi-directional pedestrian walkways. *Transportation Research Part B: Methodological*, 35(3):293–312, 2001.
[52] RL Hughes. The flow of large crowds of pedestrians.
[53] Nicola Bellomo, Benedetto Piccoli, and Andrea Tosin. Modeling crowd dynamics from a complex system viewpoint. *Mathematical models and methods in applied sciences*, 22(supp02):1230004, 2012.
[54] Anders Eriksson, Martin Nilsson Jacobi, Johan Nyström, and Kolbjørn Tunstrøm. Determining interaction rules in animal swarms. *Behavioral Ecology*, 21(5):1106–1111, 2010.
[55] Christian A Yates, Radek Erban, Carlos Escudero, Iain D Couzin, Jerome Buhl, Ioannis G Kevrekidis, Philip K Maini, and David JT Sumpter. Inherent noise can facilitate coherence in collective swarm motion. *Proceedings of the National Academy of Sciences*, 106(14):5464–5469, 2009.

[56] José Manuel Galán, Luis R Izquierdo, Segismundo S Izquierdo, José Ignacio Santos, Ricardo Del Olmo, Adolfo López-Paredes, and Bruce Edmonds. Errors and artefacts in agent-based modelling. *Journal of Artificial Societies and Social Simulation*, 12(1):1, 2009.

[57] András Czirók, Albert-László Barabási, and Tamás Vicsek. Collective motion of self-propelled particles: Kinetic phase transition in one dimension. *Physical Review Letters*, 82(1):209, 1999.

[58] Alexander Mogilner and Leah Edelstein-Keshet. A non-local model for a swarm. *Journal of Mathematical Biology*, 38(6):534–570, 1999.

[59] Michael T Gastner and Mark EJ Newman. Shape and efficiency in spatial distribution networks. *Journal of Statistical Mechanics: Theory and Experiment*, 2006(01):P01015, 2006.

[60] Atsushi Tero, Seiji Takagi, Tetsu Saigusa, Kentaro Ito, Dan P Bebber, Mark D Fricker, Kenji Yumiki, Ryo Kobayashi, and Toshiyuki Nakagaki. Rules for biologically inspired adaptive network design. *Science*, 327(5964):439–442, 2010.

[61] J Buhl, J Gautrais, N Reeves, RV Solé, S Valverde, P Kuntz, and G Theraulaz. Topological patterns in street networks of self-organized urban settlements. *The European Physical Journal B-Condensed Matter and Complex Systems*, 49(4):513–522, 2006.

[62] S P Gorman and R Kulkarni. Spatial small worlds: new geographic patterns for an information economy. *Environment and Planning B: Planning and Design*, 31(2):273–296, 2004.

[63] Guido Serini, Davide Ambrosi, Enrico Giraudo, Andrea Gamba, Luigi Preziosi, and Federico Bussolino. Modeling the early stages of vascular network assembly. *The EMBO Journal*, 22(8):1771–1779, 04 2003.

[64] Daniel P Bebber, Juliet Hynes, Peter R Darrah, Lynne Boddy, and Mark D Fricker. Biological solutions to transport network design. *Proceedings of the Royal Society B: Biological Sciences*, 274(1623):2307–2315, 2007.

[65] Jerome Buhl, Kerri Hicks, Esther R Miller, Sophie Persey, Ola Alinvi, and David JT Sumpter. Shape and efficiency of wood ant foraging networks. *Behavioral Ecology and Sociobiology*, 63(3):451–460, 2009.

[66] A. Perna, B. Granovskiy, S. Garnier, S. C. Nicolis, M. Labédan, G. Theraulaz, V. Fourcassié, and D. J. T. Sumpter. Individual Rules for Trail Pattern Formation in Argentine Ants (Linepithema humile). *PLoS Computational Biology*, 8:2592, July 2012.

[67] Andrea Perna and Tanya Latty. Animal transportation networks. *Journal of The Royal Society Interface*, 11(100), 2014.

[68] M. Barthélemy. Spatial networks. *Physics Reports*, 499(1–3):1 – 101, 2011.

[69] Alexander RA Anderson and MAJ Chaplain. Continuous and discrete mathematical models of tumor-induced angiogenesis. *Bulletin of mathematical biology*, 60(5):857–899, 1998.

[70] Ed Bullmore and Olaf Sporns. Complex brain networks: graph theoretical analysis of structural and functional systems. *Nature Reviews Neuroscience*, 10(3):186–198, 2009.

[71] William L Garrison and David M Levinson. *The transportation experience: policy, planning, and deployment*. Oxford university press, 2014.

[72] David Levinson. Paying for the fixed costs of roads. *Journal of Transport Economics and Policy (JTEP)*, 39(3):279–294, 2005.

[73] Bert Hölldobler and Edward O Wilson. *The ants*. Harvard University Press, 1990.

[74] James Watmough and Leah Edelstein-Keshet. Modelling the formation of trail networks by foraging ants. *Journal of Theoretical Biology*, 176(3):357–371, 1995.

[75] Jean-Louis Deneubourg, Simon Goss, Nigel Franks, and JM Pasteels. The blind leading the blind: modeling chemically mediated army ant raid patterns. *Journal of insect behavior*, 2(5):719–725, 1989.

[76] Leah Edelstein-Keshet, James Watmough, and G Bard Ermentrout. Trail following in ants: individual properties determine population behaviour. *Behavioral Ecology and Sociobiology*, 36(2):119–133, 1995.

[77] Ralph Beckers, Jean-Louis Deneubourg, and Simon Goss. Trail laying behaviour during food recruitment in the ant lasius niger. *Insectes Sociaux*, 39(1):59–72, 1992.

[78] Tanya Latty, Kai Ramsch, Kentaro Ito, Toshiyuki Nakagaki, David JT Sumpter, Martin Middendorf, and Madeleine Beekman. Structure and formation of ant transportation networks. *Journal of The Royal Society Interface*, 8(62):1298–1306, 2011.

[79] Feng Xie and David Levinson. Modeling the growth of transportation networks: a comprehensive review. *Networks and Spatial Economics*, 9(3):291–307, 2009.

[80] Peter Haggett and Richard J Chorley. Network analysis in geography. 2015.

[81] Feng Xie and David Levinson. Measuring the structure of road networks. *Geographical Analysis*, 39(3):336–356, 2007.

[82] Bhanu M Yerra and David M Levinson. The emergence of hierarchy in transportation networks. *The Annals of Regional Science*, 39(3):541–553, 2005.

[83] Patrick Edmund O'Sullivan. *Transport policy: geographic, economic, and planning aspects*. Rowman and Littlefield, 1980.

[84] John HE Taplin, Min Qui, Vivian K Salim, and Renlong Han. *Cost-benefit analysis and evolutionary computing: optimal scheduling of interactive road projects*. Edward Elgar Publishing, 2005.

[85] Rémi Louf, Pablo Jensen, and Marc Barthelemy. Emergence of hierarchy in cost-driven growth of spatial networks. *Proceedings of the National Academy of Sciences*, 110(22):8824–8829, 2013.

[86] M. Brede. Coordinated and uncoordinated optimization of networks. *Phys. Rev. E*, 81:066104, 2010.

[87] M. Brede. Optimal synchronization in space. *Phys. Rev. E*, 81:025202(R), 2010.

[88] M. Barthélemy and A. Flammini. Optimal traffic networks. *J. Stat. Mech.*, (07):L07002, 2006.

[89] M.T. Gastner and M.E.J. Newman. Optimal design of spatial distribution networks. *Phys. Rev. E*, 74:016117, 2006.

[90] Michael T Gastner and Mark EJ Newman. The spatial structure of networks. *The European Physical Journal B-Condensed Matter and Complex Systems*,

49(2):247–252, 2006.
[91] Guénaël Cabanes, Ellen van Wilgenburg, Madeleine Beekman, and Tanya Latty. Ants build transportation networks that optimize cost and efficiency at the expense of robustness. *Behavioral Ecology*, page aru175, 2014.
[92] Vito Latora. Efficient behavior of small-world networks. *Physical Review Letters*, 87(19), 2001.
[93] Zoe Cook, Daniel W Franks, and Elva JH Robinson. Efficiency and robustness of ant colony transportation networks. *Behavioral Ecology and Sociobiology*, 68(3):509–517, 2014.
[94] Vitor HP Louzada, Fabio Daolio, Hans J Herrmann, and Marco Tomassini. Generating robust and efficient networks under targeted attacks. *arXiv preprint arXiv:1207.1291*, 2012.
[95] Ellen Van Wilgenburg and Mark A Elgar. Colony characteristics influence the risk of nest predation of a polydomous ant by a monotreme. *Biological Journal of the Linnean Society*, 92(1):1–8, 2007.
[96] Reka Albert, Hawoong Jeong, and Albert-Laszlo Barabasi. Error and attack tolerance of complex networks. *Nature*, 406(6794):378–382, 07 2000.
[97] R. Ferrer i Cancho and R.V. Solé. Optimization in complex networks. In *Statistical Mechanics of Complex Networks*, volume 625 of *Lecture Notes in Physics*, pages 114–125. Springer, 2003.
[98] J.R. Banavar, A. Maritan, and A. Rinaldo. Size and form in efficient transportation networks. *Nature*, 399:130, 1999.
[99] John Glen Wardrop. Road paper. some theoretical aspects of road traffic research. *Proceedings of the institution of civil engineers*, 1(3):325–362, 1952.
[100] Nisha Mathias and Venkatesh Gopal. Small worlds: How and why. *Phys. Rev. E*, 63:021117, Jan 2001.
[101] A. Maritan, F. Colaiori, A. Flammini, M. Cieplak, and J.R. Banavar. Universality classes of optimal networks. *Science*, 272:984–986, 1996.
[102] Andrew Adamatzky. *Bioevaluation of World Transport Networks*. WORLD SCIENTIFIC, 2013.
[103] Alex Fabrikant, Elias Koutsoupias, and Christos H Papadimitriou. Heuristically optimized trade-offs: A new paradigm for power laws in the internet. In *Automata, languages and programming*, volume 2380 of *Lecture Notes in Computer Science*, pages 110–122. Springer, 2002.
[104] T. Greaves and R. D. Hughes. The population biology of the meat ant. *Australian Journal of Entomology*, 13(4):329–351, 1974.
[105] Derek J de Solla Price. Networks of scientific papers. *Science*, 149(3683):510–515, 1965.
[106] Albert-László Barabási and Réka Albert. Emergence of scaling in random networks. *science*, 286(5439):509–512, 1999.
[107] Luıs A Nunes Amaral, Antonio Scala, Marc Barthelemy, and H Eugene Stanley. Classes of small-world networks. *Proceedings of the national academy of sciences*, 97(21):11149–11152, 2000.
[108] Sergei N Dorogovtsev and José FF Mendes. *Evolution of networks: From biological nets to the Internet and WWW*. OUP Oxford, 2013.
[109] Alain Barrat, Marc Barthélemy, and Alessandro Vespignani. Weighted evolving networks: coupling topology and weight dynamics. *Physical review*

letters, 92(22):228701, 2004.
[110] Subhrangshu S Manna and Parongama Sen. Modulated scale-free network in euclidean space. *Physical Review E*, 66(6):066114, 2002.
[111] David Levinson and Bhanu Yerra. Self-organization of surface transportation networks. *Transportation Science*, 40(2):179–188, 2006.
[112] Alessio Cardillo, Salvatore Scellato, Vito Latora, and Sergio Porta. Structural properties of planar graphs of urban street patterns. *Physical Review E*, 73(6):066107, 2006.
[113] Duncan J Watts and Steven H Strogatz. Collective dynamics of small-world networks. *nature*, 393(6684):440–442, 1998.
[114] Andrea Perna, Sergi Valverde, Jacques Gautrais, Christian Jost, Ricard Solé, Pascale Kuntz, and Guy Theraulaz. Topological efficiency in three-dimensional gallery networks of termite nests. *Physica A: Statistical Mechanics and its Applications*, 387(24):6235–6244, 2008.
[115] Walter R Tschinkel. The nest architecture of the florida harvester ant, pogonomyrmex badius. *Journal of Insect Science*, 4(1):21, 2004.
[116] J-L Deneubourg, Serge Aron, Simon Goss, and Jacques M Pasteels. The self-organizing exploratory pattern of the argentine ant. *Journal of insect behavior*, 3(2):159–168, 1990.
[117] Ralph Beckers, Jean-Louis Deneubourg, and Simon Goss. Modulation of trail laying in the antlasius niger (hymenoptera: Formicidae) and its role in the collective selection of a food source. *Journal of Insect Behavior*, 6(6):751–759, 1993.
[118] Nigel R Franks, Katherine A Hardcastle, Sophie Collins, Faith D Smith, Kathryn ME Sullivan, Elva JH Robinson, and Ana B Sendova-Franks. Can ant colonies choose a far-and-away better nest over an in-the-way poor one? *Animal Behaviour*, 76(2):323–334, 2008.
[119] JD McIver. Dispersed central place foraging in australian meat ants. *Insectes Sociaux*, 38(2):129–137, 1991.
[120] NE Heller, KK Ingram, and DM Gordon. Nest connectivity and colony structure in unicolonial argentine ants. *Insectes Sociaux*, 55(4):397–403, 2008.
[121] David A. Holway and Ted J. Case. Mechanisms of dispersed central-place foraging in polydomous colonies of the argentine ant. *Animal Behaviour*, 59(2):433 – 441, 2000.
[122] S. Ellis, D. W. Franks, and E. J.H. Robinson. Resource redistribution in polydomous ant nest networks: local or global? *Behavioral Ecology*, 25(5), 2014.
[123] Dirk Helbing, Frank Schweitzer, Joachim Keltsch, and Péter Molnár. Active walker model for the formation of human and animal trail systems. *Physical review E*, 56(3):2527, 1997.
[124] N.E. Heller, K.K. Ingram, and D.M. Gordon. Nest connectivity and colony structure in unicolonial argentine ants. *Insectes Sociaux*, 55(4):397–403, 2008.
[125] Nigel R Franks, N Gomez, Simon Goss, and Jean-Louis Deneubourg. The blind leading the blind in army ant raid patterns: testing a model of self-organization (hymenoptera: Formicidae). *Journal of Insect Behavior*, 4(5):583–607, 1991.
[126] Nigel R Franks, Anna Dornhaus, Jon P Fitzsimmons, and Martin Stevens.

Speed versus accuracy in collective decision making. *Proceedings of the Royal Society of London B: Biological Sciences*, 270(1532):2457–2463, 2003.

[127] Jerome R Busemeyer and James T Townsend. Decision field theory: a dynamic-cognitive approach to decision making in an uncertain environment. *Psychological review*, 100(3):432, 1993.

[128] Ashley JW Ward, James E Herbert-Read, David JT Sumpter, and Jens Krause. Fast and accurate decisions through collective vigilance in fish shoals. *Proceedings of the National Academy of Sciences*, 108(6):2312–2315, 2011.

[129] E Van Wilgenburg and MA Elgar. Colony structure and spatial distribution of food resources in the polydomous meat ant iridomyrmex purpureus. *Insectes sociaux*, 54(1):5–10, 2007.

Paper I

Chapter 73
How Do Fish Use the Movement of Other Fish to Make Decisions?

From Individual Movement to Collective Decision Making

Arianna Bottinelli, Andrea Perna, Ashley Ward, and David Sumpter

Abstract Recent experiments by Ward et al. have shown that fish a moving fish group detects hidden predators faster and more accurately than isolated individuals. The increase in speed, in particular, seems to be a consequence of the movement-mediated nature of the interactions used by fish to share information. The present work aims at investigating the link between movement and information transfer underlying collective decisions in fish. We define an individual-based self-propelled particle (SPP) model of the decision-making process analyzed by Ward et al. We fit it to data in order to deduce the smallest set of interaction rules consistent with the experimentally observed behaviour. We infer the relative weight of different social forces on fish movement during the decision-making process. We find that, in order to reproduce the observed experimental trends, both the social forces of alignment and attraction have to be introduced in the model, alignment playing a more important role than attraction. We finally apply this model to make theoretical predictions about fish ability to detect and avoid a moving predator in a natural environment such as open water.

Keywords Collective animal behaviour · Decision making · SPP models · Fish

73.1 Introduction

Animals living in groups are required to make collective decisions about where to collect food, the timing and direction of group travel, the choice of a new shelter or the detection and avoidance of predators [1]. The decision-making accuracy of groups is typically predicted to be greater than that of the single group members, initially increasing with group size before leveling off [2]. This phenomenon can be explained by the fact that larger groups of animals are more effective than smaller

A. Bottinelli (✉) · A. Perna · D. Sumpter
Uppsala University, Uppsala, Sweden

A. Ward
University of Sidney, Sidney, Australia

T. Gilbert et al. (eds.), *Proceedings of the European Conference on Complex Systems 2012*, Springer Proceedings in Complexity, DOI 10.1007/978-3-319-00395-5_73,

groups or solitary individuals at gathering information, whereas single group members can exploit the informations collected by other members of the group and integrate them to take better decisions [3]. The "many eyes" hypothesis, that ability to detect predators increases with group size, could be one of the main evolutionary drives for the formation of animal groups [4, 5].

While pooling information from different group members increases accuracy, this improvement may come at a cost in terms of decision speed. Under this scenario, the speed-accuracy trade-off would be due to the additional time spent by different individuals for pooling their individual preferences and converge to a unitary decision. Interestingly, however, in experiments the integration of informations possessed by different group members in a fish school was found not have a great cost in terms of speed, allowing not only for more accurate, but also for faster decisions [6]. While the increase in accuracy with group size is successfully predicted by a model of optimal information transfer among group members, the increase of speed seems to be a consequence of the specific nature of the interactions used by fish to share information. Interactions are encoded into fish response to their neighbours' behaviour and mediated by movement, allowing information to spread quickly through the group [7]. Subsequently, information is filtered and integrated according to some simple local heuristic rule [8, 9]. Understanding these heuristics, as well as the relevant cues related to fish movement that support information transfer, is an important step towards a comprehensive understanding of decision-making's experimental outcomes and, in general, towards a mechanistic-based explanation of group behaviour.

In the present work we aim at investigating the specific nature of movement interactions underlying fast and accurate collective decision in fish as observed in [6]. In order to describe fish motion and the decision making process together we took a modeling-numerical approach where fish are represented as interacting self-propelled particles (SPPs). These particles move in a two dimensional space by updating their position according to their own driving force (represented as vectors), but also according to social forces related to the motion of other fish. The whole ensemble of forces driving the particle's movement are called their "rules of motion", and the relative influence of different forces on the motion process is represented by the length of the corresponding vectors, these lengths being parameters of the model. We numerically reproduce the decision-making experiment analyzed by Ward et al. in [6] by setting the simulation in an environment that reproduces the experimental set-up. Our main goal here is to infer the relative importance of the different contributions to fish movement and, in particular, the relevance of social interactions during the collective choice of a group direction in order to escape an hidden predator.

Once obtained the relevant interactions and their relative importance, a further step in our work is to make theoretical predictions about their effectiveness in a different environment such as open water. We generalized the model in order to simulate groups of fish swimming according to the inferred rules of motion but free of the constraints of a tank and under the threat of a moving predator. Through a numerical approach we tested whether the same rules of motion could lead to

increases in the success of predator avoidance with group size also in this more general set-up.

73.2 Experimental Background: The Y-Maze Experiment

Our analysis is based on the empirical data collected by Ward et al. in [6]. In these experiments, the authors put groups of different size of mosquitofish, *Gambusia holbrooki*, in a Y shaped tank. A plastic model of a predator was allocated to one of the arms of the Y-maze at random and suspended in midwater to simulate a real predator. In pilot trials, the fish showed a strong aversive response to the predator once they detected it. During the experiment, five different group sizes of fish (1, 2, 4, 8, and 16) were added to a container set in the stem of the Y, then the box was raised, releasing the fish. In all cases, the fish made their way down the Y and into one of the arms. All trials were filmed and the fish were subsequently tracked.

Ward et al. were able to define two zones for their analysis: the area immediately before the bifurcation point of the tank, where the decision-making process takes place, called "decision zone" and the area crossed before reaching the decision zone, called "approach zone". The boundary between the two zones corresponded to the changing point in the behavior of the experimental animals before and during the decision-making process, and is situated around 16 cm from the bifurcation point of the Y-maze. For a picture of the experimental setup see Fig. 73.2.

In both the approach and the decision zones, each fish was characterized in terms of speed, path tortuosity (defined as the ratio of the path taken by the fish to the straight line distance between the beginning and the end of that path), time spent in the considered zone and the accuracy of its decision. The fish is considered to have made an accurate decision if enters into the arm of the Y-maze that does not contain the replica of the predator.

Ward et al. observed that, while a single fish is able to avoid the predator only in the 55.6 % of trials, which is not significantly different from random choice, the proportion of fish making an accurate decision increased with group size: individuals in groups of 8 or 16 fish were significantly more likely to make accurate decisions (i.e., to avoid the replica predator) than fish tested in isolation. The rate of increase in accuracy with group size was compatible with a perfect many eyes theory, stating that, for small groups of animals, the probability of all individuals avoiding the predator is equal to that of at least one individual detecting it. In particular, given the probability that a single fish spots the predator is p^1_{spot}, the probability that a group of size n avoids the predator is given by

$$P_n = 1 - \frac{1}{2}\left(1 - p^1_{spot}\right)^n \tag{73.1}$$

In [6], p^1_{spot} was computed from the one-fish experiment and resulted equal to 0.11 (under the assumption that when the fish fail to spot the predator they take a random branch of the Y-maze). The factor $1/2$ in Eq. (73.1) accounts for the fact

that even if the group does not spot the predator it has a 50 % chance of choosing the correct branch.

Ward et al. also measured that in the decision-making zone swimming speed is an increasing function of group size, while path tortuosity decreased with increasing group size. In particular, solitary fish and those in pairs decreased their swimming speed in the decision zone compared with the approach zone, whereas those in larger groups did not. This result is inconsistent with and expectation that integrating information among a larger number of individuals would require a longer time to converge to a collective decision.

73.3 Model and Methods

73.3.1 Fish as Interacting Self-Propelled Particles (SPPs)

One of the simplest ways of modeling animal movement and interaction is the Self-Propelled Particles approach introduced in 1995 by Vicsek and collaborators [10–13]. Animals are described as point particles moving with a constant speed and updating their direction at discrete time increments by adopting the average direction of motion of the particles in their local neighbourhood, plus a random perturbation [10]. This approach allows the study of the different global behaviours emerging from the introduction of different rules of interaction between particles (see [14] for a recent review), and therefore is particularly suited for our purpose of finding the minimal set of social interactions allowing for fast and accurate decisions.

Here, we consider the self-propelled particle model used in [15], and adapted from [16]. Each fish is a particle characterized by a direction of movement, a constant speed, an interaction radius R and a blind angle (see Fig. 73.1). At each time step, every fish will interact with all the neighbours within distance R, except for the ones in the region behind them, corresponding to the blind angle. The interaction radius together with the blind angle define an interaction zone whose size is equal for all the simulated fish and deduced from empirical data. We set the interaction radius to around 16 cm, which is also compatible with the size of the decision zone and the blind angle is fixed at 60 degrees from experimental considerations on the visual system of fish [17].

The direction of motion of each simulated fish is determined by the combined effect of different forces that act on the single particle. These contributions are described through vectors whose magnitude is proportional to their relative importance on the particle's motion, while the direction of the vectors can change at each time step, depending, for example, on the neighborhood of each fish. Forces contributing to the fish movement can be divided in two main subgroups: "individual forces" and "social forces". Individual forces represent basic characteristics of the fish movement, they are independent of the local neighborhood surrounding a particular fish, and describe its behaviour when it is alone. Conversely, social forces represent the tendency to align with or to join conspecifics within the local interaction zone of

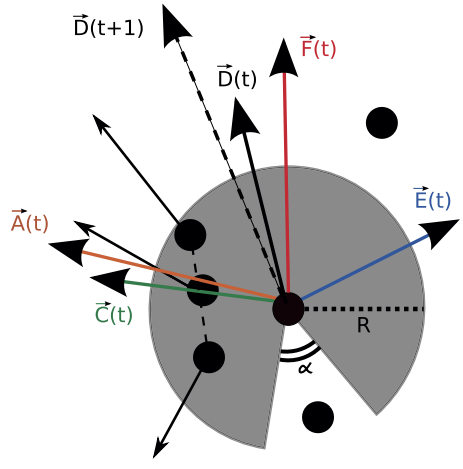

Fig. 73.1 Illustration of the SPP model. In the model fish are described as particles, each characterized by an interaction zone (*grey area* around the fish) defined by the interaction radius R and a blind angle α. While updating its position, the focal fish will take into account only the neighbours within this zone. The contributions to the movement of the fish are represented through forces acting on the particle (*arrows*), and we chose them to be the inertia in the current direction of movement $\vec{D}$, a force towards the favoured direction $\vec{F}$, an angular noise $\vec{E}$, the attraction towards the mass center of the interacting neighbours $\vec{C}$, and the alignment with their direction $\vec{A}$. The length of each vector represents the relative importance of the corresponding force, and is a parameter of the model. During simulations, at each time step all these contributions are computed and summed to give the new direction of movement of each fish $\vec{D}(t+1)$ (*dashed*)

each fish. As each fish experiences different interacting neighbourhood, these social forces are different for different individuals of the group.

The individual forces are inertia, aiming and a random force. The inertia $\vec{D}$ is the tendency to maintain the previous direction of motion. The "aiming force" $\vec{F}$ points towards the particles favoured direction. In the case of the y-shaped maze this point is the top shelter area of the maze. Then angular perturbation $\vec{E}$ represents uncertainty in the path. Lastly, at each time step the constant value of speed is perturbed by a Gaussian random error that is different for each fish and independent of neighbours. Note that this last addition does not introduce a further parameter since the value of speed is fixed according to the average speed measured from empirical data with the experimental standard deviation. These three forces together with the updating rule for speed are enough to describe the basic behaviour of a fish swimming alone [14].

Many options are available when it comes to introduce social forces, allowing to choose the level of detail in the description of individual behaviour [10–15]. Since our aim is to find the minimal set of interaction rules explaining experimental results, in the present model we introduce just two of them: the attraction towards the mass center of the interacting neighbours $\vec{C}$, and a force of alignment with their direction $\vec{A}$.

Given the above forces, the updating rule determining the actual motion of each fish is that at each time step all the described contributions are computed and summed to give the new direction of movement:

$$\vec{D}(t+1) = d\hat{D}(t) + f\hat{F}(t) + e\hat{E}(t) + c\hat{C}(t) + a\hat{A}(t) \tag{73.2}$$

Where all the forces have been decomposed in their modulus (small letter), which is the relevance of the force, as well as the unknown parameter of the model, and their unitary direction (capital, hatted letter). The resulting direction $\vec{D}(t+1)$ is then normalized, and each particle moves in the direction given by $\hat{D}(t+1)$ with speed taken from a Gaussian distributed around the mean experimental value.

73.3.2 Numerical Simulation of the Y-Maze Experiment

We simulated the decision-making process by running repeated simulations of groups of 1, 2, 4, 8 and 16 fish swimming in a Y-shaped environment of the same size of the experimental tank. Figure 73.2 shows the comparison between a typical run of the numerical simulations and a frame in an experimental trial with eight fish. In our simulated environment we distinguish three main zones, the approach zone, the decision zone and the zone after the bifurcation. The border between approach and decision zones is placed 16 cm from the bifurcation point, as in the experiments. At each run of the simulations the predator is randomly set in one of the two branches.

In a typical run of the simulation, the fish start from the beginning of the main branch of the Y maze, in the approach zone, with initial speeds, positions and entrance delays chosen according to experimental data. These delays are introduced to account for the fact that real fish do not all start moving through the maze at the same time. Since this is likely to have a consequence on the number of interacting neighbours per fish, we decided to reproduce such delays, as well as the other initial conditions, by randomly choosing a set of experimental initial conditions observed for a group of fish of the same size as the simulated one, and applying them to our simulations.

Once in the approach zone, fish move according to the rules of motions described in the previous section with, the force $\vec{F}$ pointing towards the top of the tank where the bifurcation is (see Fig. 73.2). This choice causes simulated fish to swim towards the decision zone and the branching point and reproduces the preference of real fish for deeper water and darker areas, as the two arms of the Y-shaped tank in experiments were [6].

The predator-avoidance task is numerically reproduced by assigning to each fish an individual probability $p^1_{spot} = 0.11$ of spotting the predator in the moment it enters in the decision zone. This probability is set according to experimental data so that on average a single fish has a final probability of 0.55 to avoid the predator, according to Eq. (73.1) [6]. In the case a fish spots the predator, it stops behaving according to the rules of motion and moves straight towards the safe branch

of the tank with the speed it had when entering the decision zone. Depending on the strength of the social forces compared to the individual ones, the influence of a spotting fish on its neighbours leads to different global outcomes, from the likely avoidance of the predator by the whole group in the case of strong social interactions, to the noninteracting case, in which the probability of avoiding the predator is 0.55 independent of the size of the group.

To fit the model, we ran repeated simulations of the decision-making process for a wide range of parameters' value, with the scale of interaction fixed to $d = 1$. The fitting procedure is divided in two steps: we first obtain the strength of the aiming direction f and of the noise e by matching data and simulations for one fish. We then used these values in simulations of larger groups (2, 4, 8, 16 fish) and compared them with the corresponding data sets to infer the values of the social forces of alignment a and attraction c.

In the first part of the fitting process we ran 108 numerical realizations of the decision-making process for one fish and for each couple (f, e) of the values representing the strength of the force towards the bifurcation point and of the angular noise. The number of realizations is the same number of experimental trials by Ward et al., and one realization is constituted of the average of 100 runs from the same randomly extracted initial condition. For each set of parameters and group size we computed two global observables in the decision zone, the path tortuosity described by Ward et al., and the circular standard deviation of fish turning. Circular standard deviation can be thought of as a measure of the entity of directional changes. It is given by

$$CStD(t) = \sqrt{-2\log\big(r(t)\big)}, \tag{73.3}$$

where, if $\theta_i(t)$ is the angular turning of the i-th fish at time t and N the group size, then

$$r(t) = \sqrt{\left(\frac{\sum \sin\theta_i(t)}{N}\right)^2 + \left(\frac{\sum \cos\theta_i(t)}{N}\right)^2}. \tag{73.4}$$

Once we obtained the average tortuosity (T) and circular standard deviation (CStD) for each couple of parameters (f, e), we selected only the values compatible with the empirical ones, i.e. the values that were within one standard deviation, and the corresponding sets of "good" parameters $(f, e)_T$ and $(f, e)_{CStD}$. We then chose the best values $(f, e)_{best}$ in the intersection of the above sets $(f, e)_\cap = (f, e)_T \cap (f, e)_{CStD}$ as the values for which the Euclidean distance between numerical and experimental observables was minimized:

$$(f, e)_{best} = \min_{(f,e)_\cap} \sqrt{(T_{sim} - T_{exp})^2 + (CStD_{sim} - CStD_{exp})^2}. \tag{73.5}$$

Note that the accuracy for a single fish was not calculated at this stage, since it was fixed by $p^1_{spot} = 0.11$.

In the second part of the fitting process, for each couple (a, c) of the values of the social forces we ran 16 numerical realizations for groups of 2, 4, 8 and 16 fish with the individual parameters $(f, e)_{best}$ inferred in the analysis described above.

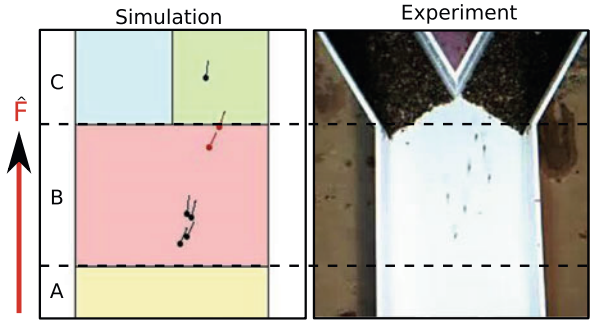

Fig. 73.2 Comparison between the visualization of our numerical set up and the experimental one. Following empirical results from [6], we distinguished three zones in our simulations: the approach zone (A), the decision zone (B) and the zone after bifurcation (C). Simulated fish started from the bottom of the tank, in the approach zone, with initial speeds, positions and entrance delays chosen according to experimental data. Fish swim across the tank due to the aiming force $\vec{F}$ that is set to point upwards, and have an individual probability $p^1_{spot} = 0.11$ of spotting the predator in the moment they enter the decision zone. This reproduces the experimental observed change in fish behaviour when crossing the threshold between zones A and B. The predator is randomly set in one of the two branches at the beginning of each run and a fish spotting it will stop behaving according to the rules of motion, swimming straight and with constant speed towards the safe branch

Again the number of numerical realizations is equal to the number of experimental trials in [6] and one realization is given by the average of 100 runs from the same randomly extracted initial condition. The process that allowed us to find the best values for alignment and attraction to neigbours follows a similar procedure as the one adopted to find the values of the individual forces. For each group size N, we computed the average accuracy (A) and tortuosity (T) and selected the couple of parameters $(a, c)^N$ corresponding to the values compatible with empirical results. We then intersected the couples of values obtained for tortuosity and accuracy $(a, c)^N_\cap = (a, c)^N_A \cap (a, c)^N_T$ at each group size, and subsequently took the union of these sets: $(a, c)_\cup = \cup_N (a, c)^N_\cap$. The best values $(a, c)_{best}$ are finally chosen from the union set $(a, c)_\cup$ as the values minimizing the Euclidean distance between experimental and numerical average for both accuracy and tortuosity:

$$(a, c)_{best} = \min_{(a,c)_\cup} \sqrt{\sum_N \left((A_{sim} - A_{exp})^2 + (T_{sim} - T_{exp})^2\right)_N}. \tag{73.6}$$

73.3.3 Simulations in Open Water

After fitting the parameters for the specific predator-avoidance task in the Y-maze, we adapted the model to numerically test the ability of the same fish to spot and escape a predator in different environmental conditions. Since the relevance of social interactions has been obtained for a very specific situation, we are interested

in whether the same rules of motion could lead to an increasing in the success of predator avoidance with group size also in a more general set-up. In particular, we simulate the model in open water for groups of shoaling fish of different size under the threat of a moving predator chasing them.

The first modification to the original model regards the set-up. Simulations take place in a squared tank centered in the axis origin and with a side that is one meter long. The predator is now free to move in the tank, and we now define some simple rules of motion. For the sake of simplicity, the only contributions to the predator's movement are inertia, which is set to be unitary, and a force of attraction towards the closest fish, which can be thought as the favourite direction of the predator. We chose this force to have the same strength as the aiming direction of fish $\vec{F}$ that we fitted from the Y-maze experiment. The speed of the predator is chosen to be constant and equal to 6 mm/frame, which is smaller than the lower average speed registered in experiments (that is, $v = 7.8$ mm/fr for one fish [6]). This choice, although arbitrary, is done in order to detect the advantage of the observed increasing in decision-making speed as a function of the group size. In the simulation, the predator starts from the upper-right corner of the tank, with an initial direction towards the origin of the axes.

The simulated fish are initially distributed with random positions and directions in a square of 10×10 centimeters, placed 30 centimeters away from the center of the tank. The initial speed of fish, as well as their speed throughout the whole simulations, is now extracted from the empirical distribution characterizing the corresponding group size in the Y-shaped tank experiment [6]. As regards the rules of motion of shoaling fish, the generalization of the model requires only a change in the favoured direction of the fish, i.e. in the direction of the aiming force $\vec{F}$, that in this set of simulations points towards the center of the tank. The effect of this choice is that the group will maintain a circular motion around the center of the tank without hitting the borders, preventing the definition of an interaction with walls.

In order to simulate the predator-avoidance task in open water, we assigned a spotting probability to each fish that is again $p^1_{spot} = 0.11$, but in this new environment a fish can spot the predator when their mutual distance is equal to the length of the decision zone. If this happens, the fish stops behaving according to the rules of motion, swimming straight and at a constant speed in the opposite direction with respect to the position of the predator, until it hits the walls of the tank. Once a fish reaches the border of the tank and exits it, it cannot go back and is considered to be "safe". As in the simulations of the Y-maze presented in the previous section, fish that do not detect the predator are influenced by the behaviour of the neighbours who did, and through social interactions has the chance to reach the border of the tank and avoid the predator. Conversely, a fish might not manage to escape the predator, whether it spots it or not, indeed if it gets closer than 6 cm from the point representing the predator[1] it is considered to be "eaten" and is canceled from simulations.

[1]This is chosen according to the fact that the predator replica used in [6] was 12 cm long.

In this setting, we ran 50 realizations for groups of fish of the same size as the ones analyzed in the Y-maze (1, 2, 4, 8 and 16), each realization being the average over 100 runs starting from the same initial condition and ending when all the fish are either "safe" or "eaten". For each group size we measured the proportion of fish avoiding the predator and the proportion of eaten fish. Among the "safe" fish, we then distinguished between these who avoided the predator because of detection and the ones escaping due to social interactions. Indeed, the latter quantity is the more relevant observable in order to assess the relevance of the social forces inferred in the Y-maze experiment in a predator-avoidance task.

73.4 Results

Initially we tried to describe fish as self-propelled particles interacting only by mean of attraction towards the mass center of neighbours, as in [16]. This was not sufficient to fit data. In fact, for each given group size the averaged observables assumed a value that was almost independent of the strength of attraction. Increasing with the value of the parameter c made little difference to the outcome, and even the best values did not compare favorably with experimental results. A similar situation was found when we tried to fit parameters by introducing only alignment with neighbours, as in [10]. Only the combination of these two social forces together provided significant variation in outcome as a function of parameters to allow us to successfully fit the data.

From the first step of the inference process, that is by matching the average simulated tortuosity and circular standard deviation with the corresponding experimental averages for one fish, we found the best values for the individual forces to be $(f, e)_{best} = (1.7, 2.7)$. Figure 73.3 shows the inference process leading to the obtained result. Here we plot the difference between the simulated observables (circular standard deviation and tortuosity respectively) and their empirical value for each couple (f, e) of the parameters. Both circular standard deviation and tortuosity increase with increasing angular noise and with decreasing aiming force, giving a regular surface whose difference with experimental values intersects zero in both cases. The black central band corresponds to the simulated quantities that are near to those found in experiments. The parameters (f, e) matching these values are reported in Fig. 73.3(C). This allows us to visualize the set $(f, e)_{\cap}$. This result is an intermediate step towards the fitting of social forces, but still it shows that randomness (e) is larger than the aiming force (f) and than inertia (d)

The second step was to look at simulations of groups of 2, 4, 8 and 16 fish. Varying the strength of social forces we finally fitted tortuosity and accuracy against data. Comparing simulated and experimental values at different values of the parameters (a, c) revealed that accuracy is an increasing function of both attraction and alignment. Tortuosity increases with attraction only, being a (slightly) decreasing function of alignment. Despite this trade-off between attraction and alignment in determining the trend of tortuosity, for all the group sizes it was possible to find

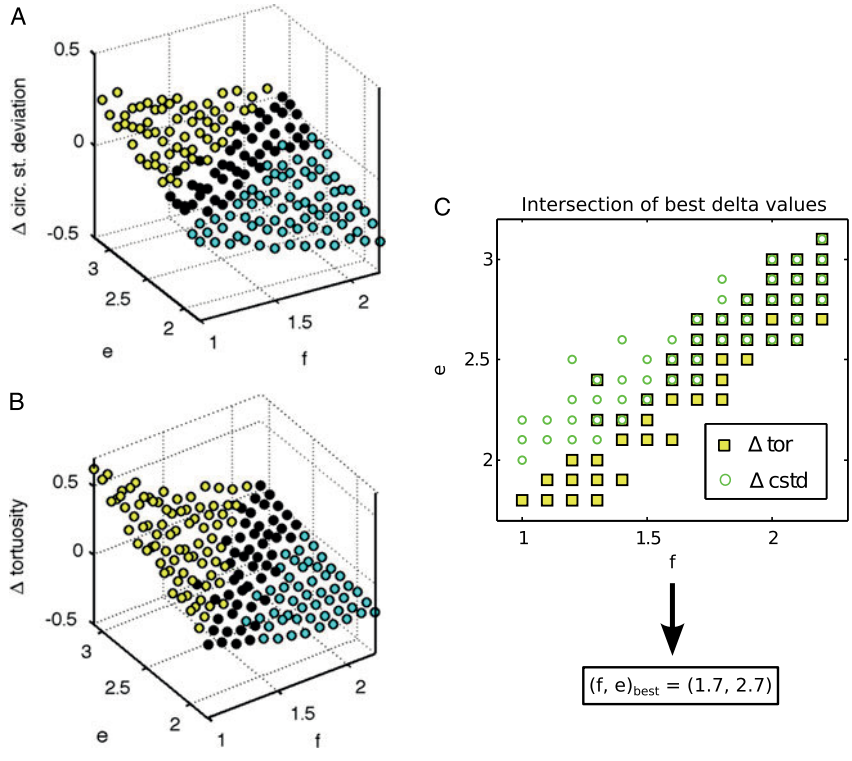

Fig. 73.3 Visualization of the inference process for the strength of individual forces. (**A**) and (**B**) The difference between the average of simulated observables (circular standard deviation and tortuosity respectively) for a single fish and their empirical value is plotted for each couple (f, e) of parameters. *The black central band* corresponds to the simulated quantities differing at most one standard deviation from the experimental values. (**C**) The couples of parameters (f, e) matching the black strip are reported in the same plane, square corresponding to the compatible values for tortuosity and circles for circular standard deviation. The couples of parameters corresponding to both a square and a circle constitute the set $(f, e)_{\cap}$, and a minimization on this intersection gave us $(f, e)_{best} = (1.7, 2.7)$

a set of parameters values for which simulations are compatible with empirical results. The final values of alignment and attraction resulting from the minimization process on the union of the compatible sets of parameters are $a = 4.2$ and $c = 3.1$. We do not show here the plots showing the variation of accuracy and tortuosity with the parameters (a, c), since they would not be particularly informative, and the visualization of the union set $(a, c)_{\cup}$ would be quite difficult due to the large number of subsets involved. Instead in Fig. 73.4 we show the match between our simulations and the data set from Ward's experiment. The simulations are in a good qualitative agreement with empirical data, reproducing quite closely the trends originally observed by Ward et al. These results suggest that alignment has a relevant role in the increasing of decision-making efficiency with group size. Notice that, despite circular standard deviation has been fitted to data only to retrieve the values of indi-

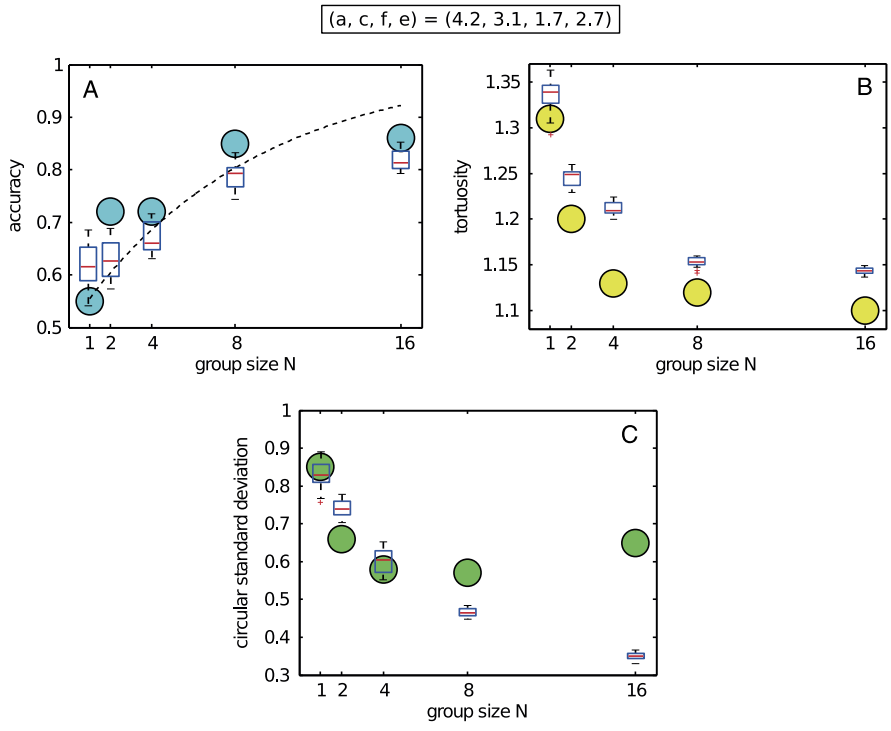

Fig. 73.4 Qualitative comparison between empirical data (*circles*) and numerical simulations (*boxes*). The model has been simulated with the parameters fixed to $(a, c, f, e) = (4.2, 3.1, 1.7, 2.7)$. Accuracy, tortuosity and circular standard deviation have been computed for each group size and plotted together with the corresponding experimental data. All the simulations are in a good qualitative agreement with empirical data, reproducing quite closely the trends originally observed by Ward et al. (**A**) Simulated accuracy is compatible with both empirical data and theoretical predictions at all group sizes. (**B**) Simulated tortuosity well resembles data for small group sizes, while at $N = 8$ and 16 decreasing is more difficult to achieve due to the trade-off between alignment and attraction in controlling this quantity. (**C**) Also the trend of circular standard deviation is reproduced, despite this observables has not been considered during the fitting of social interactions

vidual forces, the values of alignment and attraction obtained by fitting accuracy and tortuosity allow to also reproduce the trend of this third observable (Fig. 73.4(C)). Finally the robustness of the presented results have been tested by changing of the size of blind angle α from 0 to 180 degrees, showing no significant variation in the considered range.

We then tested the predator avoidance as a function of group size also in a more general set-up of open water. The test was performed by fixing the parameters according to the values obtained by fitting the Y-maze experiment, i.e. $(a, c, f, e) = (4.2, 3.1, 1.7, 2.7)$. The quantities that are relevant to assess the success in predator avoidance are the proportion of "safe" fish and the proportion of fish avoiding the predator due to social interaction only and not because they spot-

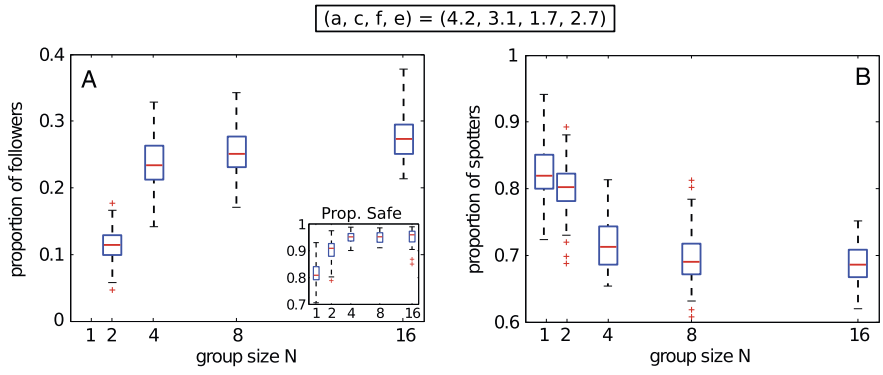

Fig. 73.5 Results of the simulations of the model in open water with $(a, c, f, e) = (4.2, 3.1, 1.7, 2.7)$. (**A**) The proportion of fish escaping due to social interactions only is an increasing function of group size, as well as the total proportion of safe fish (*inset*), meaning that the rules of motion fitted in the Y-maze make larger group more successful in predator avoidance also in different environment. (**B**) The proportion of spotting fish decreases with increasing group size, suggesting an important role of social interactions

ted it. The second quantity is particularly interesting, since it reveals how the actual relevance of social interactions relates with group size. In our simulations we found that both these observables are an increasing function of group size, (Fig. 73.5(A)), despite the surprising fact that the proportion of fish spotting the predator decreases with group size (Fig. 73.5(B)).

73.5 Conclusions

We have presented a first attempt to relate a collective decision-making process to the explicit rules of motion for fish movement. We have shown that a self-propelled particle model can reproduce the increasing speed and accuracy with group size. In doing so we inferred the explicit values of the parameters providing the best match to experimental data. Finally, we investigated the possibility of extending the obtained results to a more general setting by testing the fitted model in a different environment.

When defining the model we initially considered just one social force: the attraction towards the center of mass of the interacting neighbours. In a previous work on the same fish species (*Gambusia holbrooki*) as in the Ward et al. experiment, Herbert-Read et al. find only a weak role of alignment and a strong role for attraction while analyzing the rules of motion of groups of swimming in a square tank [18]. Furthermore, Strömbom has shown that a rich and complex range of behaviour can be achieved from only local attraction and a blind angle [16]. However, we found that it was not possible to fit data by mean of attraction alone. A similar situation was found when we tried to fit parameters by introducing only alignment. Only the combined contribution of these two social forces allowed us to fit the data.

It is therefore clear that fitting a basic self-propelled particle model requires both the social forces of alignment and attraction.

Not only is alignment important, but it is actually more important than attraction in information transfer mediating. This result is consistent with the suggestion that alignment with neighbors can allow information to be transmitted rapidly through fish schools [19]. At first sight, it appears however to be in contrast with experimental observations on the same fish [18]. There are however fundamental differences in the two analyzed settings. Herbert-Read and co-workers inferred the rules of motion for groups of mosquitofish swimming freely in a square tank after a period of acquaintance, where no decision making nor predation risk are involved. In such a circumstance it is reasonable to assume that the fish aim primarily to maintain cohesion. Attraction to conspecifics is then the most relevant force to achieve this goal by, for example, preserving a common speed. However, in a situation where fish have to collectively decide between the two arms of the tank, one of which is occupied by the predator replica, the goals of the fish change. Furthermore, the experimental set up adopted by Ward et al. does not allow fish to spread too much, already ensuring that the group will be quite packed. In this context, one explanation of the importance of alignment is that a sharp direction change provides a social cue about which of two available branches to take. A clear turning by the spotting fish communicates to conspecifics that it has some extra knowledge about which path to take, and the easiest way for other fish to be sure to take the safe branch of the tank is to assume its same direction. That is to align with the turning fish.

It is possible that our results and interpretation are strictly linked to the modeling choices we made in fitting data. The SPP approach introduces a strict distinction between forces and makes it necessary to choose which ones to introduce for representing interactions between fish. Our decision of prioritizing alignment and attraction over other social forces is arbitrary, and further work could be done by exploring if it would be possible to fit Ward's data by using different forces within an SPP model or even by trying different models. For example, introducing repulsion along with attraction instead of alignment could have lead to results more compatible with observations emphasizing the role of attraction [18]. Models have shown that highly polarized groups can be obtained from attraction and repulsion without involving alignment [16, 20]. Another alternative approach would be to fit different models than the ones involving social forces acting on self-propelled particles. Good candidates could be models where individual rules of motion are based on retinal information processing [21] or on simple heuristics integrating information about the surrounding environment [22]. Models involving speed variation, which appears to be an important feature characterizing fish motion [18, 23], could also provide a better fit. An interesting question in this direction is whether the rules of motion found by Herbert-Read and co-workers alone can explain the main features of the decision-making process observed by Ward et al. This could be investigated by defining a data-driven model based on the rules of motion found in [18], assigning a spotting probability to individual fish and simulating it in a Y-maze like environment. Despite the preliminary nature of the work presented here, it is the first attempt we know of to relate the empirical outcome of a collective decision-making

process to the explicit rules of motion of animals. There is much additional research which can be done in this area.

The last step in our work has been to ask about the possible generalizations of our model. By simulating the model in open water with the parameters fitted from the Y-maze experiment, we were able to observe that both the proportion of "safe" fish and the proportion of fish escaping the predator due to interactions are an increasing function of group size. These results support the hypothesis that the decision-making accuracy of groups is typically greater than that of the single group members [2]. Our analysis suggests that the interactions involved in the decision-making process in the Y-shaped tank should be the same social forces leading to a successful predator avoidance also in open water, and therefore they might turn out to be environment-independent.

A final intriguing hypothesis emerging from our analysis of the model in open water is that increased accuracy with group size may be accompanied with a decreased probability of individuals detecting predators. We found that the proportion of fish spotting the predator decreases with group size, while the proportion of safe fish increases. This result is consistent with an apparent decreased vigilance with group size. It is however inconsistent with the idea that it is "many eyes" which makes the group safer. It is rather fewer eyes and more efficient transfer of information that allows groups to outperform individuals.

References

1. Dall SRX, Giraldeau LA, Olsson O, McNamara JM, Stephens DW (2005) Information and its use by animals in evolutionary ecology. Trends Ecol Evol 20(4):187–193
2. King AJ, Cowlishaw G (2007) When to use social information: the advantage of large group size in individual decision making. Biol Lett 3(2):137–139
3. Couzin ID (2009) Collective cognition in animal groups. Trends Cogn Sci 13(1):36–43
4. Treherne J, Foster W (1980) The effects of group size on predator avoidance in a marine insect. Anim Behav 28(4):1119–1122
5. Lima SL (1995) Back to the basics of anti-predatory vigilance: the group-size effect. Anim Behav 49(1):11–20
6. Ward AJW, Herbert-Read JE, Sumpter DJT, Krause J (2011) Fast and accurate decisions through collective vigilance in fish shoals. Proc Natl Acad Sci USA 108(6):2312–2315
7. Sumpter D, Buhl J, Biro D, Couzin I (2008) Information transfer in moving animal groups. Theory Biosci 127(2):177–186
8. Sumpter DJT, Krause J, James R, Couzin ID, Ward AJW (2008) Consensus decision making by fish. Curr Biol 18(22):1773–1777
9. Ward AJW, Sumpter DJT, Couzin ID, Hart PJB, Krause J (2008) Quorum decision-making facilitates information transfer in fish shoals. Proc Natl Acad Sci USA 105(19):6948–6953
10. Vicsek T, András Czirók EBJ, Cohen I (1995) Novel type of phase transition in a system of self-driven particles. Phys Rev Lett 75:1226
11. Czirók A, Vicsek T (2000) Collective behavior of interacting self-propelled particles. Physica A 281:17–29
12. Czirok A, Barabasi A, Vicsek T (1999) Collective motion of self-propelled particles: kinetic phase transition in one dimension. Phys Rev Lett 82(1):209–212
13. Couzin ID, Krause J, James R, Ruxton GD, Franks NR (2002) Collective memory and spatial sorting in animal groups. J Theor Biol 218(1):1–11

14. Vicsek T, Zafeiris A (2012) Collective motion. Phys Rep. doi:10.1016/j.physrep.2012.03.004
15. Mann RP (2011) Bayesian inference for identifying interaction rules in moving animal groups. PLoS ONE 6(8):e22827
16. Strombom D (2011) Collective motion from local attraction. J Theor Biol 283(1):145–151
17. Rountree RA, Sedberry GR (2009) A theoretical model of shoaling behavior based on a consideration of patterns of overlap among the visual fields of individual members. Acta Ethol 12(2):61–70
18. Herbert-Read JE, Perna A, Mann RP, Schaerf TM, Sumpter DJT, Ward AJW (2011) Inferring the rules of interaction of shoaling fish. Proc Natl Acad Sci USA 108(46):18726–18731
19. Radakov D (1973) Schooling in the ecology of fish. Wiley, New York
20. Romey WL (1996) Individual differences make a difference in the trajectories of simulated schools of fish. Ecol Model 92(1):65–77
21. Lemasson B, Anderson J, Goodwin R (2009) Collective motion in animal groups from a neurobiological perspective: the adaptive benefits of dynamic sensory loads and selective attention. J Theor Biol 261(4):501–510
22. Moussaïd M, Guillot EG, Moreau M, Fehrenbach J, Chabiron O, Lemercier S, Pettré J, Appert-Rolland C, Degond P, Theraulaz G (2012) Traffic instabilities in self-organized pedestrian crowds. PLoS Comput Biol 8(3):e1002442
23. Hemelrijk CK, Hildenbrandt H, Reinders J, Stamhuis EJ (2010) Emergence of oblong school shape: models and empirical data of fish. Ethology 116(11):1099–1112

Paper II

INTERFACE

rsif.royalsocietypublishing.org

Research

Cite this article: Bottinelli A, van Wilgenburg E, Sumpter DJT, Latty T. 2015 Local cost minimization in ant transport networks: from small-scale data to large-scale trade-offs. *J. R. Soc. Interface* **12**: 20150780.
http://dx.doi.org/10.1098/rsif.2015.0780

Received: 31 August 2015
Accepted: 29 September 2015

Subject Areas:
biomathematics

Keywords:
transport networks, network growth model, graph theory, ant collective behaviour, ant colony, network optimization

Author for correspondence:
A. Bottinelli
e-mail: arianna.bottinelli@math.uu.se

THE ROYAL SOCIETY
PUBLISHING

Local cost minimization in ant transport networks: from small-scale data to large-scale trade-offs

A. Bottinelli[1], E. van Wilgenburg[2], D. J. T. Sumpter[1] and T. Latty[3]

[1]Mathematics Department, Uppsala University, Uppsala, Sweden
[2]Department of Biological sciences, Fordham University, Bronx, NY, USA
[3]School of Biological Sciences, University of Sydney, Sydney, New South Wales, Australia

Transport networks distribute resources and information in many human and biological systems. Their construction requires optimization and balance of conflicting criteria such as robustness against disruptions, transport efficiency and building cost. The colonies of the polydomous Australian meat ant *Iridomyrmex purpureus* are a striking example of such a decentralized network, consisting of trails that connect spatially separated nests. Here we study the rules that underlie network construction in these ants. We find that a simple model of network growth, which we call the minimum linking model (MLM), is sufficient to explain the growth of real ant colonies. For larger networks, the MLM shows a qualitative similarity with a Euclidean minimum spanning tree, prioritizing cost and efficiency over robustness. We introduce a variant of our model to show that a balance between cost, efficiency and robustness can be also reproduced at larger scales than ant colonies. Remarkably, such a balance is influenced by a parameter reflecting the specific features of the modelled transport system. The extended MLM could thus be a suitable source of inspiration for the construction of cheap and efficient transport networks with non-zero robustness, suggesting possible applications in the design of human-made networks.

1. Introduction

Transport networks are important in a wide range of applications from communication systems, through logistics and urban planning [1–6]. Most networks involve a trade-off between efficiency, cost and robustness. For example, efficient transport systems are those that allow direct travel between any two points in the network. However, acquiring high efficiency might require a lot of paths, making networks costly to build and possibly to maintain. Even when a low cost and efficient transportation network can be found, for example, by conveniently reducing the number of links until there is just one link per node, the resulting network is not likely to be robust. Indeed in this case, the failure of a single connection is enough to break the network into two parts, compromising transportation on a global level. As the simultaneous optimization of cost, robustness and efficiency is not possible, human transportation systems are carefully planned to obtain the best balance between these competing design criteria [5,7–10]. In nature, we can find many transport networks that are built without centralized planning. Examples include the vascular networks of vertebrates [11,12], the mycelial networks of fungi [13,14] and the trail networks of social insects [15,16]. Most of these have evolved to satisfy environmental and evolutionary constraints, often providing near-optimal solutions with similar trade-offs to human systems [13,17–19].

Some ant species build trails that connect multiple nests and food sources within the same colony (polydomy), providing a striking example of decentralized transport networks that allows the exchange of resources among spatially separated sites [20–23]. The best known and most widely studied example is the Argentine ant [16,22–24]. When observed under laboratory conditions, these ants connect their nests using a trail network which resembles a minimum

spanning tree (MST). The MST minimizes the total length of the network and thus its cost. [16,25]. In the field, Argentine ants appear to form more robust networks. For example, Heller *et al*. [23] show a trail map that has multiple trails between nest sites. In Argentine ants, network formation is based on pheromone deposition and evaporation; this simple process has inspired a number of optimization algorithms [26–28].

Cost minimization is only one of the optimization criteria that constrain the ants. As in human networks, several polydomous ant species face the problem of balancing efficiency, robustness and cost. Such balance differs for different ant species and seems to be linked to their mechanism of network formation [15,20,29]. However, little is known about how ants actually obtain a certain equilibrium among competing network design criteria. What are the building mechanisms that lead to an effective balance of topological properties? And can these be used as a source of inspiration for the design of human-built networks?

In this paper, we aim to identify simple and biologically plausible building rules for networks featuring trade-offs between robustness, cost and efficiency.

We start studying transport network construction and optimization in the Australian meat ant, *Iridomyrmex purpureus*. Meat ants live in underground nests covered by a mound of gravel, sand and bits of vegetation. Their main food source is honeydew, a sugary secretion they collect from aphids living on nearby trees. Meat ants are polydomous, therefore, their colonies consist of several nests and trees connected by physical trails and can stretch up to hundreds of metres. Such trail systems are actual transport networks where ants travel and transfer food, eggs and larvae between nests [20,21,30]. A graphical representation of some of these colonies can be found in figure 1 and was reconstructed from empirical data [20]. We chose meat ants because of two main features. First, their networks are made of two different kinds of nodes (trees and nests), resembling a large number of human transport networks constituted by sources and sinks [1,31]. Second, trails are quite large and kept clear of all vegetation, and thus are probably costly to build and maintain [20]. Here we assume that both building and maintenance costs will be proportional to the length of the trail (also following [25,32]). Although the proportion factor might not be the same, we cannot discard that trails will have a maintenance cost once built as, for example, ants will have to cut growing grass [30]. Recent analysis by Cook *et al*. [29] and Cabanes *et al*. [32] argue that meat ants' transport networks balance efficiency and cost without giving up robustness, rather than prioritizing any single design goal. These two facts make meat ant transportation networks particularly interesting for understanding network construction. Ideally, we would extract building rules by observing colonies as they develop under natural conditions. However, meat ant colonies are very slow growing and can take 60–80 years to mature [21,30]. Therefore, here we propose an alternative way to determine the building rules underlying network formation from the observation of a large set of colonies.

We focus on the growth of the ants' transport network through a data-driven modelling approach. We propose a model for the sequential addition of new vertices and edges, as is seen in both natural and human transport networks [33]. Our approach is similar to that taken in [1,34] and in contrast to other models that optimize transport networks by rewiring an existing set of nodes [26,28,35,36]. Importantly, it is also consistent with how ants build their networks, starting with a single nest and building new ones as the ant population gets larger [30]. Note that we do not explicitly take into account the behaviour of individual ants. Instead, the global network building rules that we study here can be thought of as the result of underlying repeated local interactions between ants.

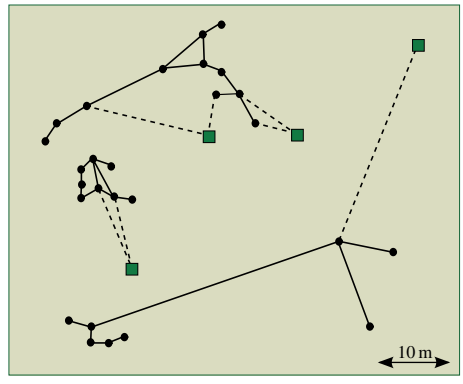

Figure 1. Graphical visualization of meat ants' colonies. The image shows three colonies of different size as detected through the GPS in [20]. Nests are represented by dots and trees by squares. Dashed lines are trails that connect the colony to trees and full lines represent trails between nests of the same colony. The scale is the same for all colonies as indicated at the bottom the figure. (Online version in colour.)

The paper is structured as follows. We first propose a data-driven model of network growth based on the sequential addition of new nodes (nests) and links (connecting trails). The spatial distribution of nodes is taken from data [20], while we implement several possible mechanisms of connection for the new nodes. All these mechanisms are biologically plausible and could in principle produce spatial networks resembling the observed meat ant colonies. Comparing with empirical data, we identify a combination of rules reproducing some key global patterns and we name it the 'minimum linking model' (MLM). When we test the MLM on the relevant topological properties of transport networks (efficiency, robustness, cost), we find that we can reproduce the same balance characterizing meat ant networks at the same network size of about 15 nodes. We are also interested in the performance of the model when representing large man-made transport networks that may be composed of thousands of nodes [1,4]. We scale the MLM up to 2000 nodes, finding that the scaling of robustness, cost and efficiency with network size is qualitatively similar as in an MST. That is, the MLM is a dynamical prescription of local optimization having similar properties to the MST, which is usually computed by connecting a given set of nodes so to optimize global cost [37]. Thus at large scale, the transport networks grown with the MLM prescription feature a balance between efficiency and cost only, discarding robustness. In the last part of this work, we re-introduce a large-scale balance between all the considered design criteria by defining a local extension of the MLM (named 'local minimum linking model', LMLM). We show how the specific balance depends on the source nodes' catchment area, reflecting the supply–demand

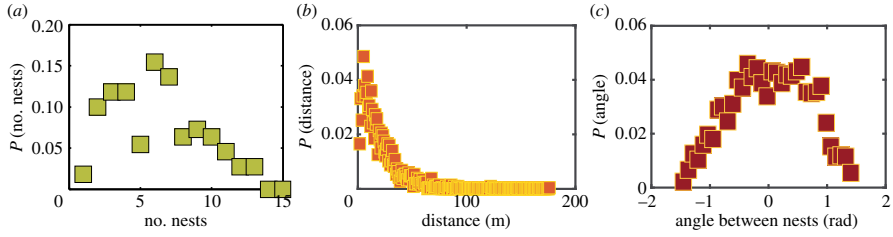

Figure 2. Experimental distributions providing initial conditions and positional statistics for the model. We extracted the following three distributions from experimental data in [20] and used them to initiate the model: (*a*) distribution of the number of nests per colony; (*b*) distribution of distances between nests within a colony, independent of the existence of trails connecting them; (*c*) distribution of the angular distance between nests within a colony with respect to their closest tree, independent of connecting trails. (Online version in colour.)

relationship between sources and sinks. This allows us to make a more realistic parallel with typical source–sink transport networks, opening possible applications in the design and management of human transport networks.

2. Model and methods

2.1. Mechanisms of network growth

Meat ant colonies consist of a network of connections between two different kinds of nodes, trees and nests, with undirected links in the form of ant trails [20] (figure 1). The algorithm we now propose is a general mechanism for building a spatial network, but in what follows we will interchangeably use biological terms such as colony, nest, tree and trail and abstract terms as network, node and edge.

The aim of our methodology is to test various plausible mechanisms for colony network construction. Ant colonies observed in the field grow by budding a new nest from older ones [30]. Then the new nest is linked to the rest of the colony and possibly to a tree by a trail that is kept clear of any kind of vegetation. In order to investigate the process of linking nests to trails, we start by making a number of basic assumptions about where the nests are placed with respect to trees and older nests.

2.1.1. Trees and initial territory

We assume a random distribution of trees in a square with the first nest (N1) placed in the centre of the square and connected to the closest tree. The density of trees in the surrounding square (0.002 trees m^{-2}) is compatible with that observed in [20]. This initial condition simulates how a new ant colony is founded, with the new queen landing and establishing a nest after the nuptial flight [30,38]. Also, it is in agreement with the observation that ants often build the shortest trail possible [20].

2.1.2. Number of nests

The distribution of the number of nests per colony is taken directly from data previously collected by Wilgenburg [20] (figure 2*a*). In each simulation, we choose the eventual colony size from this distribution. We then add the nests one at a time, connecting them to the network at each time step.

2.1.3. Placement of nests

On each time step, we choose a budding nest (BN) among the ones already belonging to the colony. A budding nest is the nest from which ants start searching the surrounding territory for a suitable spot to build a new nest. Such a search typically starts due to overcrowding that is related, in turn, to the age of the nest and its maturity [30]. Thus in our model, the probability that nest i is a budding nest is proportional to its age T_i:

$$P_B(i) = \frac{T_i}{\sum_i T_i}. \tag{2.1}$$

Once the budding nest is selected, we determine the placement of a new nest from the experimental statistics. That is (1) the distribution of distances between nests within a colony, independent of the existence of trails connecting them (figure 2*b*); and (2) the distribution of the angles between nests within a colony with respect to their closest tree (figure 2*c*). To compute (2), we consider one nest belonging to a colony and we label it FN (focal nest). Then we find the FN's closest tree (CT), and all the nests that are closer to this tree than the focal nest, FN. Let k be the number of such nests, then we label them CN(i) (closer nests), with $i = 1 \ldots k$. Finally, we compute the angle between the direction connecting FN with CT and FN with CN(i), for all i. The distribution (2) is computed over the angles obtained by iterating this procedure over all the nests belonging to each colony, treating them in turn as the focal nest (FN). This distribution implicitly represents physical and environmental constraints that ants have to account for while building their network. The computation algorithm follows from the empirical observation that meat ants tend to build new nests closer to food sources with respect to the rest of the colony [20,30]. The distributions described above do not contain any explicit constraint or information about the topology of ant transport networks. In numerical simulations, the position of the new nest (NN) with respect to the BN is then given by the polar coordinates (δ, α) (figure 3*b*). δ is taken from the distance distribution (figure 2*b*) and α from the angular distribution (figure 2*c*) and added to the direction connecting BN with its closest tree.

2.1.4. Linking schemes

We now test two different rules for connecting the new nest to the colony, and three rules to connect it to a tree. We assume that the new nest NN will make one and only one connection either to (i) BN: its budding nest or (ii) CN: its closest nest.

As in ant colonies only some nests are connected to trees, we propose three different criteria for building a connection

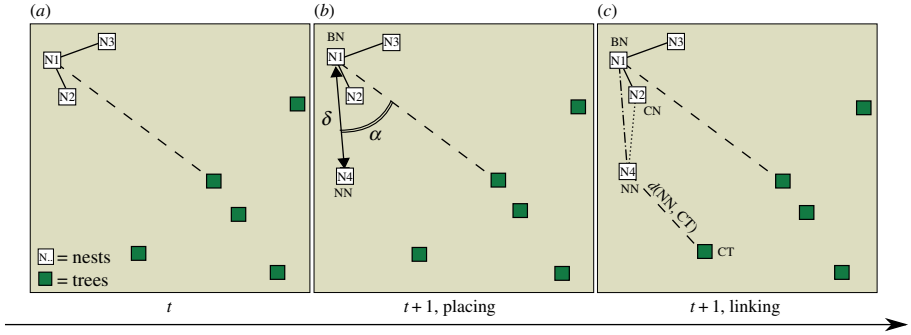

Figure 3. Illustration of the ants' network expansion model and the proposed wiring schemes. (*a*) Generic starting condition at time *t*. At time $t + 1$, the model adds a new nest (NN) and links it to the existing colony and possibly to a tree. (*b*) Positioning: extraction of a budding nest (BN) (equation (2.1)) and placement of the new nest at distance δ and angular deviation α extracted from the positional statistics in figure 2*b* and *c*. (*c*) Linking: connection of the new nest to the colony with two possible schemes: BN-linking (dotted-dashed line) or CN-linking (dotted line). We test three criteria for connecting NN to its closest tree CT (dashed line) depending on the distance *D* between NN and CT: (i) connect if *D* is the minimum over all the distances between CT and the other nests in the colony; (ii) connect if *D* is minimal over all the nest–tree distances; and (iii) connect if *D* is less than the distance between the NN and CN. (Online version in colour.)

Table 1. Summary of the main rules of the model and linking schemes.

rule	formula	description
choose the budding nest	$P_B(i) = T_i/\sum_i T_i$	the probability that a nest *i* is a budding nest is proportional to its age T_i
link to the colony	BN	links NN to the budding nets
	CN	links NN to the closest nest
link to the closest tree if	$D < \min_N(d(\mathrm{CT}, N))$	(1) *D* is minimum compared with all distances between CT and the other nests in the colony
	$D < \min_{N,T}(d(T, N))$	(2) *D* is a global minimum for all tree-colony distance
	$D < d(\mathrm{NN}, \mathrm{CN})$	(3) *D* is less than the distance between the new nest and its closest nest

between a new nest and its closest tree (CT). We do not possess information about the amount of resources provided by different trees, thus we assume that all trees are *a priori* equally likely to be linked. With such an assumption, in the model the cost and the advantage of annexing a tree depends only on its distance from the colony. Therefore, we compare the distance $D = d(\mathrm{NN},\mathrm{CT})$ between a new nest and its closest tree to other relevant distances in the colony, establishing a connection in three (alternative) cases:

(1) *D* is minimum compared with all distances between CT and the other nests in the colony, i.e.

$$D < \min_N(d(\mathrm{CT}, N)); \tag{2.2}$$

(2) *D* is a global minimum over all the distances between each nest and tree, independent of the existence of connections:

$$D < \min_{N,T}(d(T, N)); \tag{2.3}$$

(3) *D* is less than the distance between the new nest and its closest nest:

$$D < d(\mathrm{NN},\ \mathrm{CN}). \tag{2.4}$$

Connection scheme (1) is a local rule that tends to ensure a large number of trees per colony while minimizing the length of the trails needed to reach them. Scheme (2) establishes the least possible number of trails, connecting to a food source only if it is globally the cheapest option. Rule (3) is a local criteria assessing the advantage of transporting resources from CT rather than transporting them from CN. Altogether we have six combinations (BN1, BN2, BN3, CN1, CN2, CN3) of linking rules that are biologically reasonable and give different final topologies. See table 1 for a summary.

2.2. Model selection through topological quantities

We determine which of the six models above (BN1, BN2, BN3, CN1, CN2, CN3) best reproduces empirical data using two quantities: the number of hubs within a colony and the number of trees per colony. Following [20], we define 'hub' as any point at which two or more trails intersect. In the model, hubs naturally arise as a consequence of nest placement and of the connection rules. We simulate 300 realizations for each of the six combinations of connection rules. We compute the distributions of the number of hubs and of the number of trees per colony and we compare them with the corresponding distributions for the 142 colonies in [20]. We use the distribution of hubs to determine the best nest-linking rule, and the tree distribution to find the best rule to link the new nest to a tree.

2.3. Model validation on the main transport networks design criteria

After selecting the model that best reproduces the distribution of the number of hubs and trees, we verify whether

it also reproduces the relevant topological properties of meat ant transport networks and the balance that characterizes them. Following [32], we consider robustness, efficiency and cost as the relevant and competing design goals in transport network construction [2,13]. *Robustness* is defined as the probability that the network remains connected under the removal of one random link. This definition can be interpreted as a particular case of reliability polynomial for vertex cancellation [39]. In the case of ants, robustness measures the resilience of the network against, for example, trail disruptions due to natural causes or to predation [40]. The *efficiency* of a graph G built on N nodes is defined following [41] and extended for spatial networks as

$$E(G) = \frac{1}{N(N-1)} \sum_{i \neq j \in G} \frac{d^{\mathrm{e}}_{i,j}}{d_{i,j}}, \tag{2.5}$$

where i and j are nodes in G, $d^{\mathrm{e}}_{i,j}$ is their Euclidean distance and $d_{i,j}$ is the length of the shortest path connecting them on the network G. Efficiency represents how fast information and resources are exchanged over the network [29,41]. Finally, cost is defined as the total length of the trails connecting the network:

$$C(G) = \sum_{i \neq j \in G} d_{i,j}. \tag{2.6}$$

As discussed in the introduction, meat ants build physical trails by removing all vegetation from them [20]. Here we make the simple assumption that the longer the trail, the wider the area to be cleared while building the trail and to keep clean afterwards. Accordingly, both the costs of building and maintaining a trail are proportional to its length [25,32]. As we do not have experimental evidence about the proportion factors, it is reasonable to directly use the total length of the trails as the main characterizing quantity for the total cost. To test our selection procedure, we compare the distributions of these three quantities for the 142 colonies in [20] with 300 realizations of the best model.

2.4. Large-scale limit of the model

In this part of our work, we address the possible application of the selected model to the design of human transport networks requiring a balance between competing criteria. Man-made networks may be composed of thousands of nodes [1,4], thus we are interested in the large-scale behaviour of our model. Here we mainly focus on the evolution of topological quantities and their final balance with network size. We simulate the selected model up to 2000 nodes and, at different network sizes, we compute the average values of robustness, efficiency and cost over 300 instances of the model. As we do not have specific empirical data for large networks, we compare our model with the corresponding Euclidean MST. The MST, by definition, is the network of shortest length that connects a given set of nodes, optimizing cost at the expense of robustness [37]. At selected sizes, we use Prim's algorithm to build the MST connecting the existing nodes [42] and we compute the corresponding topological quantities. As regards the position of nodes, we follow the empirical distributions for distance and budding angle computed from [20] (figure 2*b* and *c*) together with the budding probability given by equation (2.1). As a consequence, the local density of nodes changes with the size of the network by construction. As older nodes are more likely to bud new ones, in particular, we expect the older, central part of the network to be denser than the peripheral one. This spatial distribution is compatible, for example, with empirical observations on urban densities [43]. Sources are randomly distributed in a large territory in order to reproduce the average tree density used in the small-scale simulations.

2.5. Local extension of the model

The final step in our work is to introduce a variation of the original source-linking rule in the large-scale simulations. The new connection scheme states that a link between a new nest (sink node) and its closest tree (source node) is established if their distance is minimal within a certain number of neighbouring nodes and their closest tree, independent of connections. We call the set of such nodes 'minimization neighbourhood', N_{neigh}, and we fix it to 20 nodes. With this choice, the introduced variation coincides with the original model on the typical size of an ant network. Thus, the new connection scheme can be seen as a 'local extension' of our original tree-linking rule. Such variation corresponds to the reasonable assumption that the resources provided by a source node can support only a finite amount of sink nodes. From the perspective of human-built networks, it is indeed the case for power plants, water stations or even schools and hospitals. We test the performances of the local version of the model simulating networks up to 2000 nodes and comparing the average values (computed from 300 realizations) of robustness, efficiency and cost with those obtained for the MST and with the original version of the model. Finally, we study the large-scale dependence of the balance between robustness, efficiency and cost as a function of the size of the minimization neighbourhood. We simulate the local version of the model for different neighbourhood sizes from $N_{\mathrm{neigh}} = 3$ to $N_{\mathrm{neigh}} = 100$, and we observe change in the asymptotic (at $N = 2000$) values of the relevant network properties.

3. Results and discussion

3.1. Model selection: the 'minimum linking model'

The results of the comparison between data and the simulations of the different connection schemes are shown in figure 4. As shown in figure 4*a*, linking to the closest nest (CN) best reproduces the distribution of the number of hubs within a colony for all the three tree-linking rules. The number of hubs does not allow us to clearly choose between the rules to connect new nests to trees. The number of trees per colony depends only on how links to trees are established, thus in figure 4*b* we compare data and simulations only for the three tree-linking rules. The comparison shows that the distribution for the number of trees is reproduced only by rule (2), i.e. by linking the new nest to its closest tree only if their distance is minimal among all the nest–tree distances within the colony.

The combination of the linking rules that best reproduces data, CN2, is also the one that minimizes the total length of the trails over all the proposed schemes, thus we name it the MLM.

3.2. Model validation on the design criteria of the main transport networks

Once we determined that the MLM is the model that best reproduces hubs and trees distributions out of the models proposed,

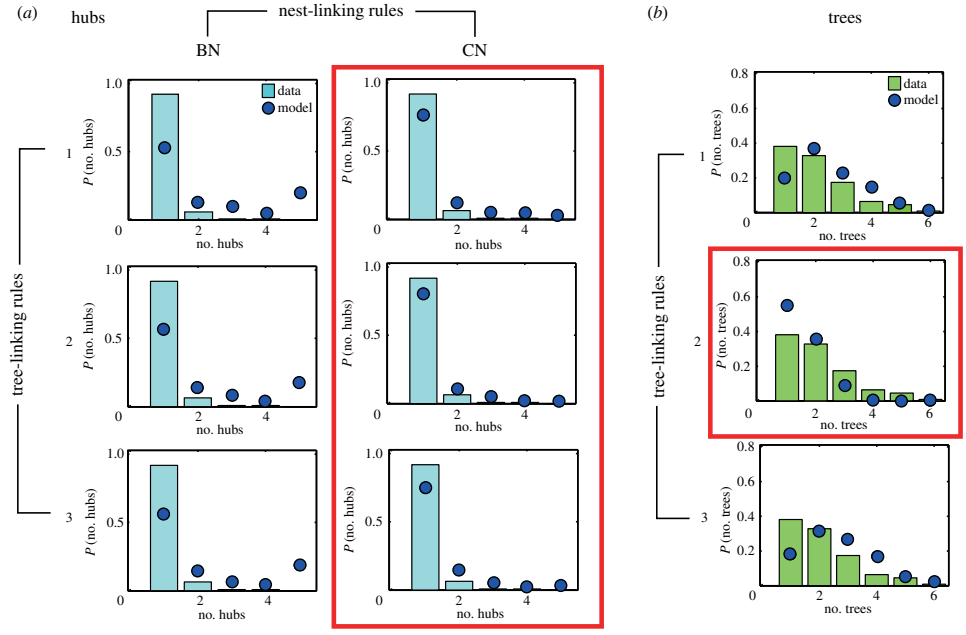

Figure 4. Selection of the MLM by comparison with empirical distributions. Histograms represent the empirical distributions, circles represent the model outcomes computed over 300 realizations. (*a*) The empirical distribution of the number of hubs per colony is compared with the distributions obtained simulating the six proposed linking schemes (CN and BN for the nests, columns; 1, 2, 3 for the trees, rows). The trend of the empirical distribution is reproduced only by linking the new nest to its closest nest (CN). (*b*) The empirical distribution of the number of trees per colony can be reproduced only by linking the new nest to its closest tree when their distance is minimal over all the nest–tree distances (rule 2). This distribution is independent of the nest-linking rules thus we show only the three cases for the tree-linking rules. The combination of the highlighted linking rules minimizes the total length of the trails over all the possible schemes defining the MLM. (Online version in colour.)

we check whether it also matches the relevant design criteria as observed in the meat ants' transport networks. In particular, we compare the model's distribution of robustness, efficiency and cost with the empirical ones (see Model and methods for the definitions). From this comparison, we see that the MLM produces the same key topological features of meat ants' transport networks (figure 5) and their characteristic balance. A graphical visualization of the simulated networks also shows that their structure is qualitatively similar to real ants' colonies as regards, for example, territorial extension and the presence of motifs such as triangular loops (cf. figures 1 and 6).

3.3. Large-scale limit of the model

We have shown that the MLM reproduces the meat ants' transport networks, balancing robustness, cost and efficiency through a simple prescription of local optimization. This is achieved on small networks of about 10–15 nodes, while human transport networks are typically larger, spanning from hundreds to thousands of nodes [1,4].

Large-scale simulations (up to 2000 nodes) show that the scaling of the MLM with network size is qualitatively similar to the one of an MST, albeit with some interesting differences. The first three plots in figure 7 compare the trends of the mean values of the MLM with the corresponding MST for robustness, efficiency and cost at increasing network size. The robustness of the MLM's networks tends to zero with network size, approaching the value that is typical of an MST (figure 7*a*). Efficiency in the MLM is a monotonically decreasing function of the number of nodes as in the MST. However, initially it is smaller than the efficiency of an MST, and becomes larger after a certain critical network size N^* that we estimated to be 230 nodes (figure 7*b*). Fitting the average cost gives a power scaling $C \sim N^{\alpha}$ for both models (figure 7*c*) with exponents $\alpha_{\mathrm{MLM}} = 0.71$ (s.e. = 0.03, $R^2 = 0.99$) and $\alpha_{\mathrm{MST}} = 0.69$ (s.e. = 0.03, $R^2 = 0.99$). The observed gap in the exponent $\Delta\alpha = 0.02$ is within both standard errors, thus the difference in cost scaling is not particularly significant. Consistently, the ratio of the network's mean cost of the MLM over the MST shows a sharp increase at small sizes that slows down significantly as N gets larger than the critical size N^* estimated from efficiency (inset in figure 7*c*).

The drop in robustness can be explained by the sub-linear growth of the average number of connected trees (source nodes) per colony that is shown in figure 7*d*. By construction, the only way to have a closed path (also called loop) in our model is when two different nests cast a connection to the same tree. Therefore, the lack of connected trees at larger sizes causes the lack of loops, which number becomes almost constant near N^* (figure 7*d*). The presence of loops is fundamental for robustness, as they provide more than one path to go from one node to another, making the network more robust against the random removal of links. It is

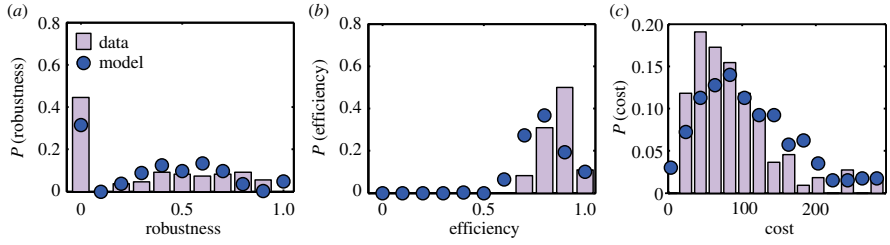

Figure 5. Comparison between simulations of the MLM and experimental data for the distributions of robustness, cost and efficiency. Empirical data are represented by the histograms and the model is represented by circles with distributions computed over 300 realizations. Comparing (*a*) robustness, (*b*) efficiency (equation (2.5)) and (*c*) cost (equation (2.6)) shows that the networks grown according to the MLM possess the same key topological features of meat ant transport networks. (Online version in colour.)

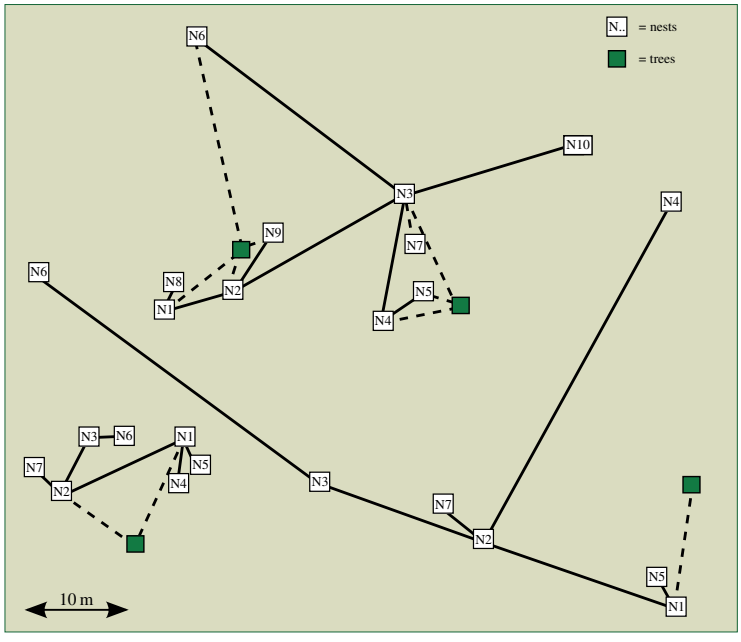

Figure 6. Visualization of selected realizations of the MLM. The scale is the same for all networks as shown at the bottom of the main panel. The comparison with figure 1 shows that the MLM produces outputs that are also visually similar to real ant colonies. In particular, network size can span from a few up to a tens of metres being compatible with the size of real colonies. Also, the model reproduces typical motifs found in ants' colonies such as triangular loops. (Online version in colour.)

likely that increasing the number of loops would also increase the network's efficiency. In our model, loops confer robustness to the network by adding a little cost at small size, however, they do not seem to constitute a particular advantage for the efficiency of the network. At sizes N larger than N^*, the number of loops becomes constant while the network keeps growing, meaning that it becomes less and less likely to obtain a connected network by removing a random link. Accordingly, robustness tends to zero.

At large sizes, the MLM features higher values of efficiency and cost with respect to the MST, the latter being still compatible with an MST as shown above. This can be explained by the fact that the MLM links new nodes to their nearest neighbour but, as the network gets larger, it becomes more and more likely that new nodes fall closer to old nodes than their previous nearest neighbour. This implies that the MLM features long-range links at large size, being more efficient than the corresponding MST, but not significantly more expensive.

Overall, the above results indicate that the MLM provides a dynamical framework for building networks that vary slightly from the MST, thereby balancing cost and efficiency at large scale.

3.4. Local extension of the model

In order to explore the model's potential in the framework of human-made transport networks, we introduced a local variation of the MLM where the tree-linking rule minimizes the distance D over a certain minimization neighbourhood N_{neigh} (see Model and methods for a detailed description). This

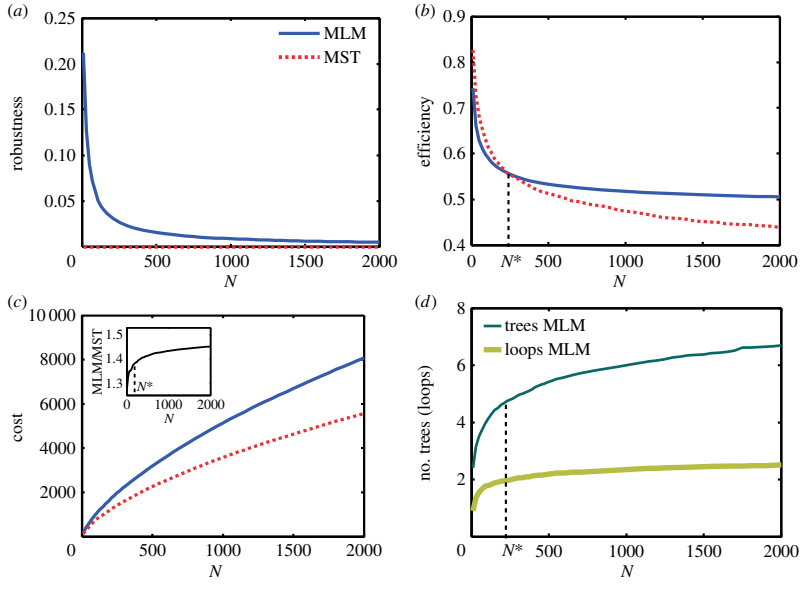

Figure 7. Large-scale behaviour of the MLM. Solid lines represent the average value of key topological features of the MLM as a function of network size. Dashed lines represent the scaling of the same quantities for the MST that was built at selected network size by rewiring the network's existing nodes. Mean values are averaged over 300 realizations. (*a*) Robustness: the MLM shows some robustness at small size that tends to zero with network size, reaching the typical value for the MST. (*b*) Efficiency: the MLM is less efficient than the corresponding MST at small size, while it is more efficient for sizes larger than a critical size $N^* = 230$. (*c*) Cost: in both MLM and MST, cost scales as a power law N^{α} with similar exponents $\alpha_{\mathrm{MLM}} = 0.71$ and $\alpha_{\mathrm{MST}} = 0.69$. (Inset) The ratio of the network's mean cost of the MLM over the MST shows a sharp increase at small sizes, which slows down significantly as $N > N^*$. (*d*) The average number of trees per colony and the number of loops (closed paths) grow sub-linearly with N, becoming almost constant after the critical size N^*. (Online version in colour.)

variation allows us to make a more realistic parallel with typical source–sinks transport networks. Indeed, it is reasonable to assume that a source node can support only a finite amount of sink nodes, such an amount constituting the minimization neighbourhood. As discussed below, it also makes it possible to build robust transport networks, reintroducing a balance between all the design criteria.

From now on we will refer to this variation as the LMLM.

When setting the neighbourhood size to $N_{\mathrm{neigh}} = 20$, the LMLM features an improvement in robustness and efficiency against a further increase in cost with respect to both the MST and our initial model. In figure 8, we compare the average values of robustness, efficiency and cost obtained by the three considered models (LMLM, MLM, MST). Robustness in the LMLM converges to a non-zero value estimated around 0.064, staying stably larger than for the MST and the MLM. This means that, in the modified model, the chance of obtaining a disconnected network under a random link removal is still high (93%), but consistently different from 100%. Efficiency in the LMLM shows the same initial decrease as observed in the MLM, intersecting both the MLM and the MST at the critical size N^* (estimated to 230 nodes, see the previous section). After the intersection at N^* it seems to tend to an asymptotic value, remaining significantly higher than in the MST and in the original MLM (figure 8*b*). The average cost for the local MLM scales as N^{α} with fitted exponent $\alpha_{\mathrm{LMLM}} = 0.76$ (s.e. = 0.05, $R^2 = 0.99$; figure 8*c*). The increase in the scaling exponent results in a linear growth of the cost difference of the two models (inset in figure 8*c*). Although the LMLM is growing faster than in the initial MLM, α_{LMLM} is within the standard deviation of the fit for α_{MLM}, while it is no longer compatible with the scaling exponent of the MST. Figure 8*d* shows that the average number of trees and loops per colony increases almost linearly with the size of the network. The linear growth in the number of loops explains the asymptotic convergence observed in the topological quantities, in particular the achievement of a constant non-zero value of robustness.

Our initial choice for the size of the minimization neighbourhood ($N_{\mathrm{neigh}} = 20$) was motivated by the conservation of the correspondence between LMLM and MLM for typical ant network sizes (where $N < 15$). However, this is not the only possible choice. In figure 9, we show how the neighbourhood size influences the trends of the relevant network design criteria and their asymptotic balance. As expected, the size of the local neighbourhood is directly related to the value of robustness through the number of loops, also influencing the value of cost and efficiency. In figure 9*a*, we report the trend of the mean value of the key design criteria with network size N for increasing size of the minimization neighbourhood from $N_{\mathrm{neigh}} = 3$ to $N_{\mathrm{neigh}} = 100$. Interestingly, for $N_{\mathrm{neigh}} = 3$ robustness is an increasing function of network size. This corresponds to a linear increase in cost with the number of nodes. To compare with the former trends in cost, now the scaling is a power law with $\alpha_{N_n=3} = 1$, leading to very expensive networks compared with the MLM ($\alpha_{\mathrm{MLM}} = 0.71$). Efficiency also is higher for smaller

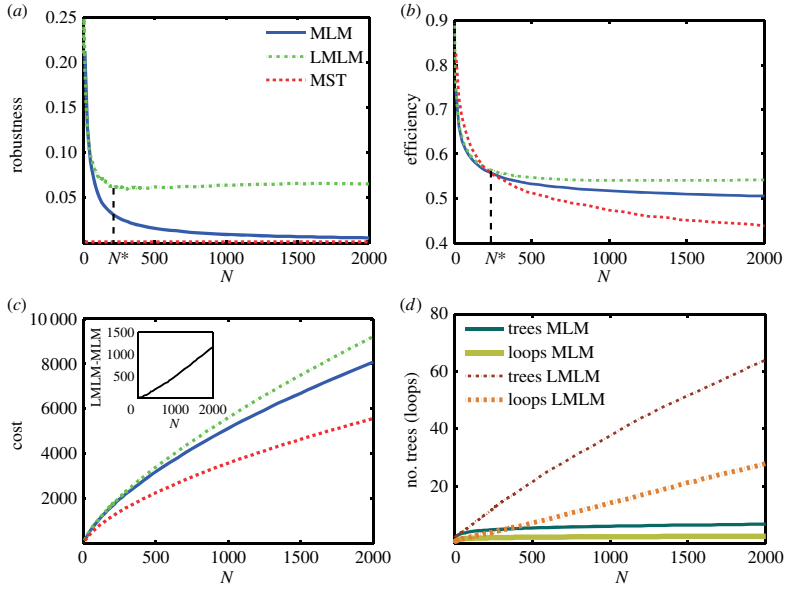

Figure 8. Large-scale behaviour of the LMLM and comparison with the original MLM and the MST. The first three panels in the figure show the comparison between the mean values given by the three analysed models (LMLM dotted-dashed lines, the original MLM full lines and the MST dashed lines) at increasing network size. The fourth panel shows the comparison between MLM and LMLM as regards the scaling of the number of loops and trees per colony. Mean values are averaged over 300 realizations and the MST is built by rewiring the nodes of each network grown with the MLM at selected network sizes. (*a*) Robustness in the LMLM converges to a non-zero value estimated around 0.064 and remains stably larger than in the MLM and MST. (*b*) Efficiency of the LMLM decreases like the MLM until N^* (230 nodes), then tends to an asymptotic value that is larger than in the original MLM. (*c*) Cost grows as a power law N^{α} with fitted exponent $\alpha_{\mathrm{LMLM}} = 0.76$, resulting in a linear growth of the cost difference of the two models (inset). (*d*) The average number of trees per colony appears to increase linearly with the size of the network, being compatible with the asymptotic behaviour of the key topological quantities. (Online version in colour.)

minimization neighbourhoods but its trend is not substantially affected by N_{neigh}. In particular, figure 9*b* shows that at large network size ($N = 2000$) high values of robustness (up to 0.7) can be obtained for small neighbourhood size, but require an almost a sixfold increase in the total cost with respect to the MLM (approximated with $N_{\mathrm{neigh}} = 100$). As already noted, the variation in the asymptotic value of efficiency is not as wide as for robustness.

Overall, our analysis indicates that the local version of the MLM provides a prescription for building transport networks that balance all the key topological properties at each network size. Remarkably, the point of equilibrium can be tuned by changing one parameter: the size of the minimization neighbourhood. This new parameter can be chosen according to the features of the modelled system. For example, in a certain transport network each source node might be able to serve a maximum number of sinks. Setting the size of the minimization neighbourhood accordingly, one could predict what balance could be reached using the LMLM prescription.

4. Conclusion and outlook

In this paper, we have used a selection procedure based on data to find the model that, out of the set we tested, best reproduces the main topological features of meat ant transport networks (figure 5) and the spatial structure of colonies (figures 1 and 6). In terms of network models, it would be difficult to imagine other simple, local and biologically plausible building rules that could be tested in this framework. Another approach, for example, through an individual-based model, would be to provide single-ant rules of motion. This would, however, require a totally different dataset in order to be tested. Such an approach would provide a specific tool tailored on meat ants that would be difficult to apply to other biological networks. Our procedure could be used both to extract the construction rules underlying network formation of other polydomous ants and to understand the emergence of topological patterns observed in other living systems. Given the increasing interest in studying the formation and topology of animal transportation networks [13–15,19,29], our methodology constitutes a way to infer the growth process of the network when observing it directly is difficult or costly. Using the same prescription on different biological networks would also allow for comparisons between different connection strategies across different species and systems. Do all polydomous ants, for example, use the same connection rules, and if not, which ecological and behavioural factors lead to the use of a particular rule?

In the case of meat ants, we found that the only plausible model matching the data was the MLM. This model turns out to be based on simple and biologically plausible rules, with local cost optimization as the key. Remarkably, the model constructs transport networks featuring a balance among global fundamental design criteria. Although our model gives insights into the formation process of ant networks, it is not based on direct observation as it would take

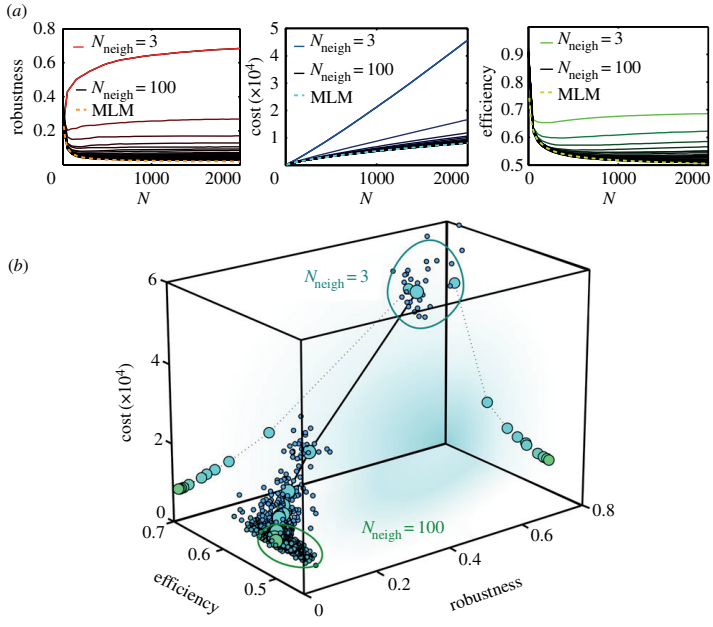

Figure 9. Dependence of the balance between design criteria on the size of the minimization neighbourhood (*a*) solid lines represent the mean values of the key design criteria with network size N at increasing size of the minimization neighbourhood from $N_{neigh} = 3$ (top), to $N_{neigh} = 100$ (bottom). Dashed lines represent the MLM. For $N_{neigh} = 3$ robustness is an increasing function of N. This corresponds to a linear increase of cost with the number of nodes ($\alpha_{N_n=3} = 1$), leading to very expensive networks compared with the MLM ($\alpha_{MLM} = 0.71$). (*b*) Evolution of the balance between cost, efficiency and robustness at $N = 2000$ from $N_{neigh} = 3$ (top) to $N_{neigh} = 100$ (bottom). Small circles represent individual simulations and large circles the average values. The full line in the three-dimensional plot represents the evolution of the average value of the equilibrium point between cost, efficiency and robustness. Dotted lines represent the cost–robustness and cost–efficiency balance (projected from the full one). $N_{neigh} = 3$ gives high asymptotic values of robustness (up to 0.7) but require almost a sixfold increase in the total cost with respect to the lower values for $N_{neigh} = 100$. In both panels efficiency is higher for smaller minimization neighbourhood but its trend is not substantially affected by N_{neigh}. (Online version in colour.)

decades to observe the establishment of a new nest and the connecting trails [38,44]. However, the model could suggest experiments that would shed light on meat ant behaviour. For example, our model can be used to predict how ant trail networks are reconstructed after a disruption such as the loss of a nest or the blocking of a trail. Manipulative field experiments could then confirm or refute the models predictions. Another interesting experiment would be to change the substrate meat ants move through while building their trail network. This would change the cost of constructing the network and could lead to different topologies and building strategies. It might also allow us to distinguish between building cost and maintenance cost of a trail, leading to a better understanding of how cost is relevant to network construction.

Scaling up to large networks, our focus is on understanding the global network features emerging from a rule of local minimization. At this stage, the model is abstracted from its initial biological meaning and we are mainly interested in the evolution of topological quantities and their balance point. Is there anything that we can learn from ants and apply it to a different system such as human transportation or distribution networks? When simulated for a large number of nodes, the MLM produces networks that, on average, feature a balance between efficiency and total cost at the expenses of robustness. Cost, in particular, is comparable with that obtained via an MST, meaning that the increase in efficiency is almost effortless. Robustness, however, tends to zero at increasing size, increasing the probability that the network will break into two after a small failure. When designing transport networks, robustness plays a fundamental role and is highly desirable [8,10]. However, the drop in robustness with network size is still interesting from a biological perspective and might explain why we do not observe colonies larger than 15 nests (see the size distribution in figure 2*a*). The model seems to suggest that the construction strategy adopted by meat ants cannot balance cost and robustness when a colony becomes too big. It might be that a colony requires a minimum value of robustness because of, for example, territorial competition with other colonies or resistance to predation. Thus, the optimal strategy might be to keep the colony smaller than a certain size by either splitting it or by establishing a new colony in another area through a nuptial flight. Future fieldwork could test our prediction by studying the relationship between colony size and splitting events in wild colonies.

In order for the MLM to be more suitable for informing human transport networks, it would need to include robustness as well as high efficiency and low cost. Moreover, it is not completely realistic to assume that a source node could provide for any arbitrary number of sink nodes. To address this, we have introduced a local variant of our model to relax the condition of cost minimization for the source-linking rule. In particular, we require that the cost of linking a new node to a

source is minimal over a neighbourhood of 20 nodes, called the minimization neighbourhood. This is equivalent to setting the catchment area of the sources to 20 sink nodes. The new model is significantly more expensive with respect to the cheapest possible option of an MST, but at large scale it performs better as regards robustness and efficiency. Therefore, the introduced variant re-establishes the sought after balance between all the considered topological properties. Remarkably, such equilibrium can be tuned by making the size of the minimization neighbourhood a parameter of the model. In particular, for a very small minimization neighbourhood it is possible to make robustness increase with network size. This parameter represents the sources' catchment area and thus is suited to reflect the features of the specific modelled transport network.

The LMLM seems very reasonable if thought of in a real-world situation such as the construction of a supply network or urban planning. For example, building a new suburb requires connections not only to the existing urban network but also to public services (schools, supermarkets, power plants). In this case, the size of the minimization neighbourhood could be tuned to reflect the typical local need for resources of the system under consideration. Then the model could advise whether it is convenient to build a connection to an existing source or if it is enough for the new area to access services though the existing network. Conversely, the model could predict the final robustness of the network obtained by minimizing connections cost, given the source–sink relationship characterizing the considered system. A further use of the extended MLM could be as a rebuilding prescription in case of disruption of links or nodes. Indeed, we argue that using our model to reconstruct part of a damaged transport network would be locally cheap, preserving efficiency and robustness on a global level. Our local variant could therefore be a suitable source of inspiration for the construction of robust and efficient transport networks characterized by a sources–sinks duality. Moreover, the dynamical nature of the MLM and of its local version fits the growing, evolutive aspect characterizing most human-made networks [37].

A similar model of local optimization was proposed and partially analysed by Fabrikant *et al*. [45] in the framework of the growth of the Internet. The analysis of Fabrikant *et al*. did not include sources, but introduced the mechanism of local cost minimization as a linking prescription, naming the resulting model 'dynamical MST'. Quantifying the actual difference between the dynamical MST or, equivalently, the sourceless MLM, with the actual MST would be an interesting theoretical challenge, giving an insight into the broader topic of the definition of topological distance between graphs. It might also be a useful analysis for the problem of the MST dynamical update, i.e. how to recompute the MST efficiently when adding new nodes [46]. It may well be that the ant construction model can give insights into these much larger networks, and that similar design principles are used in both cases.

5. Materials

In this paper, we refer to the maps of ant trail networks collected by Wilgenburg *et al*. [20] in the field in Australia in 2002. Such data are comprised of 142 trail networks maps where the coordinates of nests and trees were obtained with the aid of a GPS and the existence of connections between them recorded by hand and through aerial photography [20]. Simulations are performed using the software MATLAB.

Authors' contributions. A.B., T.L. and D.T.J.S. designed the study, developed the methodology and drafted the manuscript; A.B. implemented the model and performed numerical simulations and data analysis; E.v.W. collected and provided the data [20].

Competing interests. We declare we have no competing interests.

Funding. We thank the Branco Weiss Society in Science Fellowship and the Australian Research Council (DP110102998 and DP140103643) for financial support.

Acknowledgements. A.B. thanks M. Cosentino Lagomarsino, M. Gherardi, R. Louf and A. Perna for constructive discussion and feedback during the development of the study. The authors thank the referees for their constructive feedback.

References

1. Gastner MT, Newman MEJ. 2006 Shape and efficiency in spatial distribution networks. *J. Stat. Mech. Theor. Exp.* **2006**, P01015. (doi:10.1088/1742-5468/2006/01/P01015)
2. Tero A, Takagi S, Saigusa T, Ito K, Bebber DP, Fricker MD, Yumiki K, Kobayashi R, Nakagaki T. 2010 Rules for biologically inspired adaptive network design. *Science* **327**, 439–442. (doi:10.1126/science.1177894)
3. Crucitti P, Latora V, Porta S. 2006 Centrality measures in spatial networks of urban streets. *Phys. Rev. E* **73**, 036125. (doi:10.1103/PhysRevE.73.036125)
4. Buhl J, Gautrais J, Reeves N, Solé RV, Valverde S, Kuntz P, Theraulaz G. 2006 Topological patterns in street networks of self-organized urban settlements. *Eur. Phys. J. B* **49**, 513–522. (doi:10.1140/epjb/e2006-00085-1)
5. Boccaletti S, Latora V, Moreno Y, Chavez M, Hwang DU. 2006 Complex networks: structure and dynamics. *Phys. Rep.* **424**, 175–308. (doi:10.1016/j.physrep.2005.10.009)
6. Gorman SP, Kulkarni R. 2004 Spatial small worlds: new geographic patterns for an information economy. *Environ. Plan. B* **31**, 273–296. (doi:10.1068/b29118)
7. Louzada VHP, Daolio F, Herrmann HJ, Tomassini M. 2012 Generating robust and efficient networks under targeted attacks. (http://arxiv.org/abs/1207.1291)
8. Albert R, Jeong H, Barabasi A. 2000 Error and attack tolerance of complex networks. *Nature* **406**, 378–382. (doi:10.1038/35019019)
9. Schneider CM, Moreira AA, Andrade JS, Havlin S, Herrmann HJ. 2011 Mitigation of malicious attacks on networks. *Proc. Natl Acad. Sci. USA* **108**, 3838–3841. (doi:10.1073/pnas.1009440108)
10. Immers B, Yperman I, Stada J, Bleukx A. 2002 *Reliability and robustness of transportation networks. Problem survey and examples*. Leuvene, Belgium: Katholieke Universiteit Leuven.
11. Serini G, Ambrosi D, Giraudo E, Gamba A, Preziosi L, Bussolino F. 2003 Modeling the early stages of vascular network assembly. *EMBO J.* **22**, 1771–1779. (doi:10.1093/emboj/cdg176)
12. Folkman J, Haudenschild C. 1980 Angiogenesis *in vitro*. *Nature* **288**, 551–556. (doi:10.1038/288551a0)
13. Bebber DP, Hynes J, Darrah PR, Boddy L, Fricker MD. 2007 Biological solutions to transport network design. *Proc. R. Soc. B* **274**, 2307–2315. (doi:10.1098/rspb.2007.0459)
14. Heaton L, Obara B, Grau V, Jones N, Nakagaki T, Boddy L, Fricker MD. 2012 Analysis of fungal networks. *Fungal Biol. Rev.* **26**, 12–29. (doi:10.1016/j.fbr.2012.02.001)
15. Buhl J, Hicks K, Miller ER, Persey S, Alinvi O, Sumpter DJT. 2009 Shape and efficiency of wood ant foraging networks. *Behav. Ecol.*

Sociobiol. **63**, 451–460. (doi:10.1007/s00265-008-0680-7)

16. Perna A, Granovskiy B, Garnier S, Nicolis SC, Labédan M, Theraulaz G, Fourcassié V, Sumpter DJT. 2012 Individual rules for trail pattern formation in Argentine ants (*Linepithema humile*). *PLoS Comput. Biol.* **8**, e1002592. (doi:10.1371/journal.pcbi.1002592)
17. Buhl J, Gautrais J, Solé RV, Kuntz P, Valverde S, Deneubourg JL, Theraulaz G. 2004 Efficiency and robustness in ant networks of galleries. *Eur. Phys. J. B* **42**, 123–129. (doi:10.1140/epjb/e2004-00364-9)
18. Nakagaki T, Kobayashi R, Nishiura Y, Ueda T. 2004 Obtaining multiple separate food sources: behavioural intelligence in the *Physarum plasmodium*. *Proc. R. Soc. Lond. B* **271**, 2305–2310. (doi:10.1098/rspb.2004.2856)
19. Perna A, Latty T. 2014 Animal transportation networks. *J. R. Soc. Interface* **11**, 20140334. (doi:10.1098/rsif.2014.0334)
20. Van Wilgenburg E, Elgar MA. 2007 Colony structure and spatial distribution of food resources in the polydomous meat ant *Iridomyrmex purpureus*. *Insectes Sociaux* **54**, 5–10. (doi:10.1007/s00040-007-0903-3)
21. McIver JD. 1991 Dispersed central place foraging in Australian meat ants. *Insectes Sociaux* **38**, 129–137. (doi:10.1007/BF01240963)
22. Holway D, Case TJ. 2000 Mechanisms of dispersed central-place foraging in polydomous colonies of the argentine ant. *Anim. Behav.* **59**, 433–441. (doi:10.1006/anbe.1999.1329)
23. Heller N, Ingram K, Gordon D. 2008 Nest connectivity and colony structure in unicolonial argentine ants. *Insectes Sociaux* **55**, 397–403. (doi:10.1007/s00040-008-1019-0)
24. Aron S, Deneubourg J, Goss S, Pasteels J. 1990 Functional self-organisation illustrated by inter-nest traffic in ants: the case of the argentine ant. In *Biological motion*, vol. 89. Lecture Notes in Biomathematics (eds W Alt, G Hoffmann), pp. 533–547. Berlin, Germany: Springer.
25. Latty T, Ramsch K, Ito K, Nakagaki T, Sumpter DJT, Middendorf M, Beekman M. 2011 Structure and formation of ant transportation networks. *J. R. Soc. Interface* **8**, 1298–1306. (doi:10.1098/rsif.2010.0612)
26. Dorigo M, Caro G, Gambardella L. 1999 Ant algorithms for discrete optimization. *Artif. Life* **5**, 137–172. (doi:10.1162/106454699568728)
27. Mullen RJ, Monekosso D, Barman S, Remagnino P. 2009 A review of ant algorithms. *Expert Syst. Appl.* **36**, 9608–9617. (doi:10.1016/j.eswa.2009.01.020)
28. Dorigo M, Stützle T. 2003 The ant colony optimization metaheuristic: algorithms, applications, and advances. In *Handbook of metaheuristics*, pp. 250–285. Berlin, Germany: Springer.
29. Cook Z, Franks DW, Robinson EJH. 2014 Efficiency and robustness of ant colony transportation networks. *Behav. Ecol. Sociobiol.* **68**, 509–517. (doi:10.1007/s00265-013-1665-8)
30. Greaves T, Hughes RD. 1974 The population biology of the meat ant. *Aust. J. Entomol.* **13**, 329–351. (doi:10.1111/j.1440-6055.1974.tb02212.x)
31. Durand M. 2007 Structure of optimal transport networks subject to a global constraint. *Phys. Rev. Lett.* **98**, 088701. (doi:10.1103/PhysRevLett.98.088701)
32. Cabanes M, van Wilgenburg E, Beekman M, Latty T. 2014 Ants build transportation networks that optimize cost and efficiency at the expense of robustness. *Behav. Ecol.* **26**, 223–231. (doi:10.1093/beheco/aru175).
33. Barabsi A, Albert R. 1999 Emergence of scaling in random networks. *Science* **286**, 509–512. (doi:10.1126/science.286.5439.509)
34. Barthélemy M, Flammini A. 2008 Modeling urban street patterns. *Phys. Rev. Lett.* **100**, 138702. (doi:10.1103/PhysRevLett.100.138702)
35. Mathias N, Gopal V. 2001 Small worlds: how and why. *Phys. Rev. E* **63**, 021117. (doi:10.1103/PhysRevE.63.021117)
36. Gastner MT, Newman MEJ. 2006 The spatial structure of networks. *Eur. Phys. J. B* **49**, 247–252. (doi:10.1140/epjb/e2006-00046-8)
37. Barthélemy M. 2011 Spatial networks. *Phys. Rep.* **499**, 1–101. (doi:10.1016/j.physrep.2010.11.002)
38. Hölldobler B, Carlin NF. 1985 Colony founding, queen dominance and oligogyny in the Australian meat ant *Iridomyrmex purpureus*. *Behav. Ecol. Sociobiol.* **18**, 45–58.
39. Ellens W, Kooij RE. 2013 Graph measures and network robustness. (http://arxiv.org/abs/1311.5064)
40. Van Wilgenburg E, Elgar MA. 2007 Colony characteristics influence the risk of nest predation of a polydomous ant by a monotreme. *Biol. J. Linn. Soc.* **92**, 1–8. (doi:10.1111/j.1095-8312.2007.00868.x)
41. Vito L. 2001 Efficient behavior of small-world networks. *Phys. Rev. Lett.* **87**, 198701. (doi:10.1103/PhysRevLett.87.198701)
42. Tremblay J-P, Sorenson PG. 1984 *An introduction to data structures with applications*. New York, NY: McGraw-Hill, Inc.
43. Clark C. 1951 Urban population densities. *J. R. Stat. Soc. A* **114**, 490–496. (doi:10.2307/2981088)
44. Greenslade PJM. 1975 Dispersion and history of a population of the meat ant *Iridomyrmex purpureus* (Hymenoptera: Formicidae). *Aust. J. Zool.* **23**, 495–510. (doi:10.1071/Z09750495)
45. Fabrikant A, Koutsoupias E, Papadimitriou CH. 2002 Heuristically optimized tradeoffs: a new paradigm for power laws in the internet. In *Automata, languages and programming*, pp. 110–122. Berlin, Germany: Springer.
46. Chin F, Houck D. 1978 Algorithms for updating minimal spanning trees. *J. Comput. Syst. Sci.* **16**, 333–344. (doi:10.1016/0022-0000(78)90022-3)

Paper III

Balancing building and maintenance costs in growing transport networks

Arianna Bottinelli,[1] Rémi Louf,[2] and Marco Gherardi[3,4]

[1] *Mathematics Department, Uppsala University, Lägerhyddsvägen 1, Uppsala 75106, Sweden.*
[2] *Centre for Advanced Spatial Analysis, University College London, 90 Tottenham Court Road W1T4TJ London, United Kingdom.*
[3] *Sorbonne Universités, UPMC Univ Paris 06, UMR 7238, Computational and Quantitative Biology, 15 rue de l'École de Médecine Paris, France.*
[4] *Dipartimento di Fisica, Università degli Studi di Milano, via Celoria 16, 20133 Milano, Italy.*

The costs associated to the length of links impose unavoidable constraints to the growth of natural and artificial transport networks. When future network developments can not be predicted, building and maintenance costs require competing minimization mechanisms, and can not be optimized simultaneously. Hereby, we study the interplay of building and maintenance costs and its impact on the growth of transportation networks through a non-equilibrium model of network growth. We show cost balance is a sufficient ingredient for the emergence of tradeoffs between the network's total length and transport efficiency, of optimal strategies of construction, and of power-law temporal correlations in the growth history of the network. Analysis of empirical ant transport networks in the framework of this model suggests different ant species may adopt similar optimization strategies.

From roads, railways and power grids, to ant trails, leaf veins and blood vessels, transportation structures support the functions necessary to many natural and man-made systems [1–8]. Transport systems are typically represented as spatial networks, where the nodes are the distinct locations — such as cities or ant nests — and the links are the physical connections between these locations — such as roads or trails [9]. These networks are embedded in a metric space, and the length of links is used to quantify the cost of building and maintaining the connections [10]. These costs pose an unavoidable constraint to transport networks, which is intrinsically tied to their spatial nature. Together with the need for efficient transportation and for fault tolerance, it affects the growth and the topology of transport networks, having a profound impact on the systems that rely on them [10].

A great deal of theoretical and empirical research has been devoted to understand how diverse constraints influence the evolution of natural and man-made transport networks, and to identify minimal ingredients underlying the emergence of complex topologies [11–16]. The effects of competing design criteria have been explored, such as average shortest path versus link density [17] (or total length [18]), and total length versus synchronizability [19] or centrality [20]. Other models balance the length of single links with the gain in centrality [21], or efficiency [1], or they analyze the costs and benefits entailed by the creation of new links [22]. However, most of the existing models in quantitative geography and transport engineering assume that (i) the network is static and/or constituted by a pre-fixed and known set of nodes, (ii) it is either planned by a central authority, or the result of a completely self-organized process, and (iii) the length of a link is a proxy for both the costs of building *and* maintaining it [10]. Therefore, they neglect that (i) transport systems are typically built iteratively, often lacking information about future developments, as these may be beyond the time horizon of planners [9, 10]; (ii) due to such dynamic evolution, in long-lived infrastructures global planning has to compromise with local constraints and competing interests [9], and to alternate with local optimization processes; (iii) building costs and maintenance costs act on different time scales, constituting unavoidable competing constraints that cannot be optimized simultaneously.

These three aspects are strongly related. In a static scenario, the network of minimum length spanning a fixed set of nodes (the *minimum spanning tree*, MST) minimizes both maintenance and building costs [10]. In a dynamic setting, instead, when future node additions are not known in advance, or when the task of building links is partially delegated to local entities, these costs can not be minimized simultaneously. On one side, building cost is minimized by iterating the local rule of "linking each new node to the closest node in the network". However, the obtained structure (called *dynamical minimum spanning tree*, dMST [21]) does not minimize the total length of the network [16], thus attaining a sub-optimal maintenance cost. On the other side, globally rearranging the network to a MST every time a node is added does minimize the total length, but it requires to destroy old links and rebuild new ones, increasing the building cost. Moreover, maintenance costs must be sustained until links are abandoned or destroyed [23, 24], constraining the network on a longer time scale.

In this paper, we address these open issues by formulating an out-of-equilibrium model for the growth of transport networks in the context where the position of new nodes can not be predicted. By interpolating between the two pure optimization strategies (global, centrally planned MST, and local, decentralized dMST), the model explores the antagonism between the constraints associated with building and maintenance costs.

Model — Our model grows spatial networks starting from a single node and adding one node and one link at a time, so that resulting networks are trees (see Fig. 1). (In real transport networks, fault tolerance is achieved through the presence of cycles [25, 26]. Here we restrict to trees for simplicity.) Nodes appear with the flat mea-

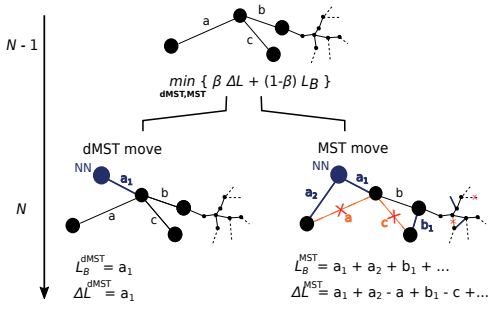

FIG. 1. (Color online) At each time step, the model grows a network by adding a new node (NN) at a random position. Depending on what move minimizes the linear combination of built length L_B and length variation ΔL, NN is either locally connected to the closest node in the network (dMST move) or the network is globally rewired to minimize the total length (MST move). In both cases only one link is added.

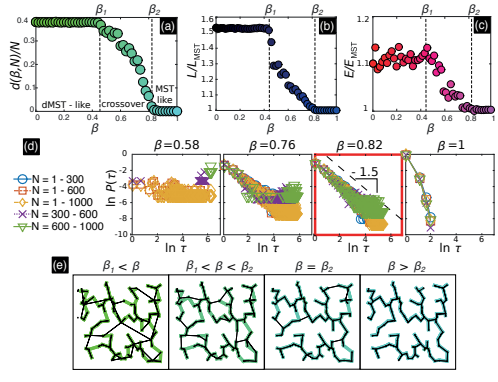

FIG. 2. (Color online) Structural properties and dynamical evolution of networks grown with different strategies β. The normalized (a) Hamming distance, (b) total length, and (c) efficiency reveal three classes of strategies: MST-like, crossover, and dMST-like, separated by two transition points β_1 and β_2. (d) The probability distribution of the waiting time between two consecutive MST moves $P(\tau)$ for different windows of network size. In β_2, $P(\tau)$ is a power-law of exponent ≈ 1.5 (highlighted box). (e) Realizations of the model (black thin line) for values of β in the three classes and for $\beta = \beta_2$ on the same 50 nodes sequence (black dots), superposed to the corresponding MST (light bold line).

sure on the unit square. When a new node at position x_N is added to the existing nodes having positions $\{x_0, \ldots, x_{N-1}\}$, either it is linked to the closest node ("dMST move"), or a number of links are destroyed and rebuilt in order to obtain the (unique) MST spanning all nodes at positions $\{x_0, \ldots, x_N\}$ ("MST move"), such that the functional

$$H(\beta, N) = \beta \Delta L(N) + (1-\beta) L_{\rm B}(N) \qquad (1)$$

is minimum. $L_{\rm B}$ is the length that needs to be built, and ΔL is the variation in the total length of the network (these are not equal, as ΔL includes negative contributions from the deleted links). To elaborate, both $H^{\rm MST}$ and $H^{\rm dMST}$ are computed every time a node is added, then the MST move is performed if $H^{\rm MST} < H^{\rm dMST}$, and the dMST move otherwise. The "strategy" β is the only parameter of the model, taking values in $[0, 1]$. Setting $\beta = 0$ prioritizes the minimization of $L_{\rm B}$ (as expected if building costs are dominant), and the network grows only by local dMST moves. Conversely, $\beta = 1$ minimizes ΔL (maintenance costs dominate), and the network is globally rewired to a MST at each step. When the two costs are comparable, intermediate values of β account for both global and local length minimization and the model can alternate between MST and dMST moves. It is useful to express the growth condition $H^{\rm MST} \gtrless H^{\rm dMST}$ in terms of the sum of the lengths of newly built and newly destroyed links, $L_{\rm B}$ and $L_{\rm D}$ respectively. For a MST move $\Delta L^{\rm MST} = L_{\rm B}^{\rm MST} - L_{\rm D}^{\rm MST}$, while $H^{\rm dMST} = L_{\rm B}^{\rm dMST}$, thus the condition becomes $L_{\rm B}^{\rm MST} - \beta L_{\rm D}^{\rm MST} \gtrless L_{\rm B}^{\rm dMST}$.

Results — For each value of β from 0 to 1 (by steps of 0.02), we numerically grow 70 networks up to $N_{\rm f} = 1000$ nodes by the rules of the model. Results are averaged over these 70 networks [Supplemental Material (SM)]. For each network, we measure the normalized Hamming distance $d(\beta, N)/N$, defined as the number of links that one has to create (and destroy) in order to turn the network into the MST spanning the same set of nodes, divided by the size of the network N [SM]. This quantity identifies three classes of strategies separated by two transition points, $\beta_1 \approx 0.45$ and $\beta_2 \approx 0.82$ [Fig. 2(a))]. "MST-like" strategies ($\beta > \beta_2$) grow networks with very small distances from the corresponding MST ($\beta = 1$). "dMST-like" strategies ($\beta < \beta_1$) grow networks similar to the one grown by iterating dMST moves only ($\beta = 0$). "Crossover" strategies ($\beta_1 < \beta < \beta_2$) smoothly interpolate from one extreme to the other. The phase boundaries and the value of $d(\beta, N)/N$ do not depend sensibly on network size after $N \approx 200$ [SM].

The existence of three classes is further confirmed by looking at the total length L and efficiency E of the same networks, normalized by the corresponding MST values and as a function of β [Fig. 2(b) and (c) and SM]. Efficiency quantifies how quickly information and resources are exchanged over a transport network [27, 28], and is often regarded as one of the main design goals in planning and building these networks [6, 11]. It is known that maximizing efficiency competes with minimizing total length [29]. Interestingly, our approach reveals that balancing building and maintenance costs entails a tradeoff between total length and efficiency [Fig. 2(b) and (c)], suggesting that the bias towards efficient transport observed in real networks may emerge under more general

conditions, via optimization of a function of length alone.

To better characterize the classes of strategies observed, we introduce the *waiting time* τ, defined as the number of steps from $N = 1$ to the first MST move, and then between two consecutive MST moves. Due to non-stationarity of the process, the probability distribution function $P(\tau)$ of the waiting time depends not only on β, but also on the size of the network [Fig. 2(d) and SM]. Before β_1, $P(\tau)$ is not defined, as the typical waiting times are larger than those attained by our simulations ($N_f = 1000$). Accordingly, the total length is never minimized through a MST move, and networks in this regime share only a few links with the corresponding MST, typically the shortest ones [Fig. 2(e)]. A mean field estimate of β_1 can be obtained by using the condition for choosing a MST move $L_{\rm B}^{\rm MST} - \beta L_{\rm D}^{\rm MST} < L_{\rm B}^{\rm dMST}$, and assuming that, when β is close to β_1 from above, a MST move destroys and rebuilds nearly all the network's links [Fig. 2(e)]. The typical length of a link in a MST of N nodes can be estimated as the average nearest-neighbor distance among N random points, i.e. $\sqrt{1/cN}$, where c is some constant. Thus, $L_B^{MST} \sim N\sqrt{1/cN} = \sqrt{N/c}$ and $L_{\rm B}^{\rm dMST} \sim \sqrt{1/cN}$, while $L_D^{MST} \sim \sum_{n=1}^{N} \sqrt{1/cn} \sim 2\sqrt{N/c}$. The left-hand side of the growth condition becomes $(1-2\beta)\sqrt{N/c}$. Since $L_{\rm B}^{\rm dMST}$ goes to zero for large N, the condition for at least one MST move to occur in this limit becomes $\beta > 1/2$, which is not far from the observed $\beta_1 \approx 0.45$.

The optimization condition also suggests that, at the onset of the crossover regime, the occurrence of a MST event is tied to the destruction of long links to build short ones. Accordingly, $P(\tau)$ shows MST events are rare and happen typically at large network size [Fig. 2(d)], where the difference between long links, built in the initial steps, and links that would be built in the MST is large. At increasing β, the probability of shorter waiting times increases for small network size, and MST events occur more likely. In the MST-like phase ($\beta \gtrsim \beta_2$), the growth condition is satisfied often, and $P(\tau)$ decays subpolinomially (exponentially for $\beta = 1$) at all network sizes. Remarkably, the dynamics displays long-range memory at the transition to the minimum-length phase β_2. Here $P(\tau)$ is a power law of exponent ≈ -1.5 at all sizes, and the waiting time τ has no typical scale (except the cut-off) contrary to the MST-like and dMST-like phases. As a consequence, the occurrence of a MST event is highly unpredictable at β_2, where waiting times are scale free. (For further discussion see the SM.)

We analyze the performances of different growth strategies in terms of their long-term total cost by means of three time-integrated quantities $\mathcal{L}_{\rm B}, \mathcal{L}_{\rm D}, \mathcal{L}_{\rm M}$, defined as

$$\mathcal{L}_*(N_f, \beta) = \sum_{N=1}^{N_f} L_*(N, \beta) / \sum_{N=1}^{N_f} L_*(N, \beta = 1). \qquad (2)$$

These quantities measure how much length was built ($* =$ B), destroyed ($* =$ D), or maintained ($* =$ M) up to $N_f = 1000$ by each strategy β. $L_{\rm B}(N, \beta)$ and $L_{\rm D}(N, \beta)$ are the instantaneous lengths built and destroyed between step $N-1$ and step N, and $L_{\rm M}(N, \beta)$ is the total length of the network at size N. All the measures are normalized by the values they take in a pure MST dynamics (i.e., at $\beta = 1$) with the same realization of the point process.

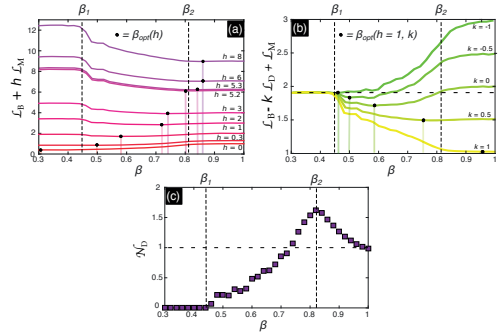

FIG. 3. (Color online) The integrated (up to $N_f = 1000$) cost landscapes (solid lines) for (a) building ($\mathcal{L}_{\rm B}$) and maintaining ($\mathcal{L}_{\rm M}$), at different values of the ratio h between their unit costs; (b) building, maintaining, and destroying ($\mathcal{L}_{\rm D}$) for $h = 1$. $k \in [-1, 1]$ is the unit cost of destroying material (if $k < 0$) or the advantage of recycling (if $k > 0$). The minimum of each cost landscape (dots) is the optimal strategy β_{opt} for the given value of h and k. (c) The integrated number of links that are destroyed and rebuilt ($\mathcal{N}_{\rm D}$) is maximum in β_2, revealing high non-extensive costs. Strategies above the horizontal dashed line destroy more links than the pure strategy $\beta = 1$.

In the simple scenario where the costs of maintenance and building per unit length have ratio h, the final cost of a network is given by $\mathcal{L}_{\rm B} + h\,\mathcal{L}_{\rm M}$. Plotting this total cost against β produces a cost landscape for each value of h [Fig. 3(a)]. Each cost landscape has an absolute minimum, which identifies the optimal strategy $\beta_{opt}(h)$ for the given ratio h. Interestingly, crossover strategies turn out to be optimal for a wide range of values of the ratio h ($0.3 \lesssim h \lesssim 5.2$). More complicated cost scenarios can be analyzed. For example, one may consider that building costs during a MST move may be reduced by recycling the material obtained from the destruction of existing links. On the contrary, when recycling is not possible, disposing of the destroyed material may bear additional costs. Such scenarios can be described by adding the time-integrated destroyed length to the total cost: $\mathcal{L}_{\rm B} + h\,\mathcal{L}_{\rm M} - k\,\mathcal{L}_{\rm D}$. The coefficient $k \in [-1, 1]$ is the fraction of destroyed material that can be recycled (if $k > 0$) or bearing additional disposal costs (if $k < 0$). Also in this scenario, crossover strategies play an important role in minimizing the total efforts for construction and maintenance of transport networks [Fig. 3(b), particular case of $h = 1$], realizing nontrivial tradeoffs between the competing costs. The optimal strategy is in the crossover regime even when destroying is as expensive as building

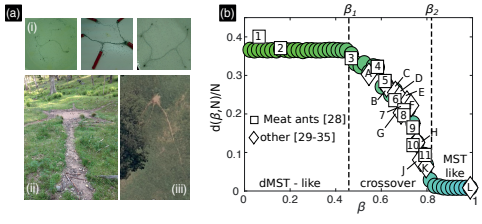

FIG. 4. (Color online) (a) Cost-optimized ant networks: (i) Argentine ants find the shortest path to connect their nests. Credit: Tanya Latty. (ii) Meat ant's nest with departing trails. Credit: Nathan Brown. (iii) Part of a meat ant's transport network from Google Earth. (b) Comparing the Hamming distance of ant transport networks (meat ants [30] are squares, other species [31–37] are diamonds) with our model suggests crossover strategies are relevant for different ant species.

and maintaining ($k = -1$), while MST-like strategies are optimal only when recycling strongly lowers the total cost.

All costs considered above are extensive in the length of the transport channels involved. However, length-independent costs may be present in empirical situations, for instance associated to setting up the sites for building and dismantling connections. These "fixed" costs depend on the number of links modified at each step, regardless of their length. We quantify these non-extensive costs via the total number of links that were destroyed (and rebuilt) $\mathcal{N}_{\rm D}(N,\beta) = \sum_{n=1}^{N} N_{\rm D}(n,\beta)/\sum_{n=1}^{N} N_{\rm D}(n,\beta=1)$. $N_{\rm D}$ is the number of links destroyed at each step, and the sum is normalized by the corresponding MST value, as in (2). Interestingly, β_2 is the strategy requiring the largest number of link deletions, and is therefore a point of strong non-optimality in terms of fixed costs [Fig. 3(c)]. Crossover strategies with $\beta \gtrsim 0.75$ and MST-like strategies require to destroy (and thus to re-build) more links than in the pure MST strategy [Fig. 3(c) horizontal dashed line].

Discussion — Albeit simple, our interpolating model presents a rich behavior, providing a general framework to understand the competing nature of construction and maintenance costs. In doing so, it addresses the interplay of central planning and local growth characterizing the growth of many man-made transport networks, offering insights in the long-term outcome of different short-term construction strategies. Unexpectedly, intermediate growth strategies are optimal in many cost scenarios, as they minimise the long-term total costs entailed by the infrastructure. Moreover, we showed balancing competing costs is a minimal sufficient ingredient for the emergence of the tradeoff between the network's total length and its transport efficiency, which is usually explained by more system-specific principles. Finally, the model displays a transition point with diverging characteristic time, similarly to the phenomenon of critical slowing down close to phase transitions in statistical mechanics, which maximizes the long-term number of links rewired.

A key premise in the formulation of the model is that the position of new nodes is not known beforehand. If the time scale of the arrival of new nodes is much larger than that of the transport processes on the network itself, then each new node needs to be connected before the position of successive nodes can be taken into account. A possible example in human systems is the evolution of bus routes [38, 39]. New areas can be quickly connected by adding further segments to bus lines stopping nearby (dMST move). However, if the whole network becomes suboptimal in terms of running costs, it may become necessary to re-design it globally (MST move). Our model suggests there may be an optimal re-organization frequency that minimizes total costs, including construction, maintenance, etc.

In nature, a striking example of cost-constrained transport networks are the trails built by polydomous ant colonies to connect spatially separated nests [8]. Under laboratory conditions, the Argentine ant *Linepithema humile* builds globally optimized transport networks that resemble MST or even Steiner trees (minimum spanning trees where the set of nodes is allowed to be enlarged) [40] [Fig. 4(a), top]. Conversely, the Australian meat ant *Iridomyrmex purpureus* tends to link each newly built nest to the closest one in the colony [16], as in the dMST move in our model [Fig. 4(a), bottom]. For these ants, it has been observed that, during colony growth, suboptimal connections can be progressively substituted with shorter ones and eventually abandoned [41], realising a dynamics similar to the one implemented by our model (although on a time scale comparable to that of node addition). Building on these observations, we used our model as a framework to quantify the trade-off between building and maintenance costs experienced by ants. For 30 published networks constructed by different ant species (*Linepithema humile* [31], *Iridomyrmex purpureus* [30, 32–34], *Formica lugubris* [35, 36] and *Camponotus gigas* [37], see SM for detailed description of the datasets and methods), we measured the normalized Hamming distance from the MST built on the same set of nodes, and assigned a strategy β to each network by comparison with the model prediction for $d(\beta,N)/N$ [Fig. 4(b)]. We ask wether this strategy may be informative of how building and maintenance costs affect ant's network growth. In all but one of the analyzed trail networks, the rescaled distance $d(\beta,N)/N$ from the corresponding MST departs from 0 at most as much as the typical dMSTs ($d(\beta,N)/N \approx 0.38$). Interestingly, for 27 colonies out of 30, the estimated strategy β is in the crossover regime (as a consequence of the distribution of their rescaled distances). This suggests both maintenance and building costs are relevant in the growth of ant networks, and that different species may share common underlying building principles and optimization strategies. Alternating between local and global interventions on the network may thus confer evolutionary advantages, and should be taken into account in the planning and in the analysis of human transport networks.

ACKNOWLEDGEMENTS

We would like to thank D.J.T. Sumpter, J.L. Silverberg, and M. Cosentino Lagomarsino for constructive feedback and stimulating discussions. A.B. acknowledges funding from the Centre for Interdisciplinary Mathematics (CIM).

[1] M. T. Gastner and M. E.J. Newman. Shape and efficiency in spatial distribution networks. *Journal of Statistical Mechanics: Theory and Experiment*, 2006(01):P01015, 2006.

[2] A. Tero, S. Takagi, T. Saigusa, K. Ito, D. P. Bebber, M. D. Fricker, K. Yumiki, R. Kobayashi, and T. Nakagaki. Rules for biologically inspired adaptive network design. *Science*, 327(5964):439–442, 2010.

[3] J. Buhl, J. Gautrais, N. Reeves, R.V. Solé, S. Valverde, P. Kuntz, and G. Theraulaz. Topological patterns in street networks of self-organized urban settlements. *The European Physical Journal B-Condensed Matter and Complex Systems*, 49(4):513–522, 2006.

[4] S. P. Gorman and R. Kulkarni. Spatial small worlds: new geographic patterns for an information economy. *Environment and Planning B: Planning and Design*, 31(2):273–296, 2004.

[5] G. Serini, D. Ambrosi, E. Giraudo, A. Gamba, L. Preziosi, and F. Bussolino. Modeling the early stages of vascular network assembly. *The EMBO Journal*, 22(8):1771–1779, 04 2003.

[6] D. P. Bebber, J. Hynes, P. R. Darrah, L. Boddy, and M. D. Fricker. Biological solutions to transport network design. *Proceedings of the Royal Society B: Biological Sciences*, 274(1623):2307–2315, 2007.

[7] J. Buhl, K. Hicks, E. R. Miller, S. Persey, O. Alinvi, and D. J.T. Sumpter. Shape and efficiency of wood ant foraging networks. *Behavioral Ecology and Sociobiology*, 63(3):451–460, 2009.

[8] A. Perna, B. Granovskiy, S. Garnier, S. C. Nicolis, M. Labédan, G. Theraulaz, V. Fourcassié, and D. J. T. Sumpter. Individual Rules for Trail Pattern Formation in Argentine Ants (Linepithema humile). *PLoS Computational Biology*, 8:2592, July 2012.

[9] F. Xie and D. Levinson. Modeling the growth of transportation networks: a comprehensive review. *Networks and Spatial Economics*, 9(3):291–307, 2009.

[10] M. Barthélemy. Spatial networks. *Physics Reports*, 499(1–3):1 – 101, 2011.

[11] M.T. Gastner and M.E.J. Newman. Optimal design of spatial distribution networks. *Phys. Rev. E*, 74:016117, 2006.

[12] J.R. Banavar, A. Maritan, and A. Rinaldo. Size and form in efficient transportation networks. *Nature*, 399:130, 1999.

[13] A. Maritan, F. Colaiori, A. Flammini, M. Cieplak, and J.R. Banavar. Universality classes of optimal networks. *Science*, 272:984–986, 1996.

[14] R. Guimerà, A. Diaz-Guilera, F. Vega-Redondo, A. Cabrales, and A. Arenas. Optimal network topologies for local search with congestion. *Phys. Rev. Lett.*, 89:248701, 2002.

[15] V. Colizza, J.R. Banavar, A. Maritan, and A. Rinaldo. Network structures from selection principles. *Phys. Rev. Lett.*, 92:198701, 2004.

[16] A. Bottinelli, E. van Wilgenburg, D. J. T. Sumpter, and T. Latty. Local cost minimization in ant transport networks: from small-scale data to large-scale trade-offs. *Journal of The Royal Society Interface*, 12(112), 2015.

[17] R. Ferrer i Cancho and R.V. Solé. Optimization in complex networks. In *Statistical Mechanics of Complex Networks*, volume 625 of *Lecture Notes in Physics*, pages 114–125. Springer, 2003.

[18] M. Brede. Coordinated and uncoordinated optimization of networks. *Phys. Rev. E*, 81:066104, 2010.

[19] M. Brede. Optimal synchronization in space. *Phys. Rev. E*, 81:025202(R), 2010.

[20] M. Barthélemy and A. Flammini. Optimal traffic networks. *J. Stat. Mech.*, (07):L07002, 2006.

[21] A. Fabrikant, E. Koutsoupias, and C. H. Papadimitriou. Heuristically optimized trade-offs: A new paradigm for power laws in the internet. In *Automata, languages and programming*, volume 2380 of *Lecture Notes in Computer Science*, pages 110–122. Springer, 2002.

[22] R. Louf, P. Jensen, and M. Barthelemy. Emergence of hierarchy in cost-driven growth of spatial networks. *Proceedings of the National Academy of Sciences*, 110(22):8824–8829, 2013.

[23] P. E. O'Sullivan. *Transport policy: geographic, economic, and planning aspects*. Rowman and Littlefield, 1980.

[24] J. H.E. Taplin, M. Qui, V. K. Salim, and R. Han. *Cost-benefit analysis and evolutionary computing: optimal scheduling of interactive road projects*. Edward Elgar Publishing, 2005.

[25] V. H.P. Louzada, F. Daolio, H. J. Herrmann, and M. Tomassini. Generating robust and efficient networks under targeted attacks. *arXiv preprint arXiv:1207.1291*, 2012.

[26] R. Albert, H. Jeong, and A. Barabasi. Error and attack tolerance of complex networks. *Nature*, 406(6794):378–382, 07 2000.

[27] V. Latora. Efficient behavior of small-world networks. *Physical Review Letters*, 87(19), 2001.

[28] Z. Cook, D. W. Franks, and E. J.H. Robinson. Efficiency and robustness of ant colony transportation networks. *Behavioral Ecology and Sociobiology*, 68(3):509–517, 2014.

[29] G. Cabanes, E. van Wilgenburg, M. Beekman, and T. Latty. Ants build transportation networks that optimize cost and efficiency at the expense of robustness. *Behavioral Ecology*, page aru175, 2014.

[30] E. Van Wilgenburg and M.A. Elgar. Colony structure and spatial distribution of food resources in the polydomous meat ant iridomyrmex purpureus. *Insectes sociaux*, 54(1):5–10, 2007.

[31] N.E. Heller, K.K. Ingram, and D.M. Gordon. Nest connectivity and colony structure in unicolonial argentine ants. *Insectes Sociaux*, 55(4):397–403, 2008.

[32] J.A. Holt. Observations on the relationships between meat ants and termites in tropical australia. *Journal of tropical ecology*, 6(03):379–382, 1990.

[33] A. N. Andersen and A. D. Patel. Meat ants as dominant members of australian ant communities: an experimental test of their influence on the foraging success and forager abundance of other species. *Oecologia*, 98(1).

[34] J.D. McIver. Dispersed central place foraging in australian meat ants. *Insectes Sociaux*, 38(2):129–137, 1991.

[35] G. Boudjema, G. Lempérière, M. Deschamps-Cottin, and D. G. Molland. Analysis and nonlinear modeling of the mound-building ant formica lugubris spatial multi-scale dynamic in a larch-tree stand of the southern french alps. *Ecological modelling*, 190(1), 2006.

[36] S. Ellis, D. W. Franks, and E. J.H. Robinson. Resource redistribution in polydomous ant nest networks: local or global? *Behavioral Ecology*, 25(5), 2014.

[37] M. Pfeiffer and K.E. Linsenmair. Contributions to the life history of the malaysian giant ant camponotus gigas (hymenoptera, formicidae). *Insectes Sociaux*, 47(2):123–132, 2000.

[38] J. Dodson, P. Mees, J. Stone, and M. Burke. The principles of public transport network planning: A review of the emerging literature with select examples. *Issues paper*, 15, 2011.

[39] S.V.C. Sekhar, W. L. Yue, and M.A.P. Taylor. An approach to transit path design using gis. *International Journal of Urban Sciences*, 8(1):28–39, 2004.

[40] T. Latty, K. Ramsch, K. Ito, T. Nakagaki, D. J.T. Sumpter, M. Middendorf, and M. Beekman. Structure and formation of ant transportation networks. *Journal of The Royal Society Interface*, 8(62):1298–1306, 2011.

[41] T. Greaves and R. D. Hughes. The population biology of the meat ant. *Australian Journal of Entomology*, 13(4):329–351, 1974.

Supplemental Material to "Optimal tradeoffs between building and maintenance costs in growing transport networks"

Arianna Bottinelli,[1] Rémi Louf,[2] and Marco Gherardi[3,4]

[1] *Mathematics Department, Uppsala University, Lägerhyddsvägen 1, Uppsala 75106, Sweden*
[2] *Centre for Advanced Spatial Analysis, University College London, 90 Tottenham Court Road W1T4TJ London, United Kingdom.*
[3] *Sorbonne Universités, UPMC Univ Paris 06, UMR 7238, Computational and Quantitative Biology, 15 rue de l'École de Médecine Paris, France*
[4] *Dipartimento di Fisica, Università degli Studi di Milano, via Celoria 16, 20133 Milano, Italy*

STRUCTURAL PROPERTIES

We define the Hamming distance as the number of links that one would need move in order to rewire the current graph G to the minimum spanning tree built on the same set of nodes MST_G at fixed β and at a certain network size N:

$$d(\beta, N) = \frac{|Adj(G(\beta, N)) - Adj(MST_G(N))|}{4}. \quad (1)$$

This is the matrix extension of the well known Hamming distance used in computer science to measure the distance between strings [1]. We grow numerically 70 networks up to $N = 1000$ nodes by the rules of the model for each value of β from 0 to 1 (by steps of 0.02). We choose to average on 70 networks due to the high computational costs, especially for $\beta \approx 1$. Indeed, 70 networks was a trade-off between reasonable computational time and sufficient statistics. For each network we construct the corresponding MST at each time step, compute the Hamming distance as defined above and average over the 70 instances. At all values of β, H turns out to be a linear increasing function of network size [Supplemental FIG. 1(a)]. After a short transient ($N \sim 100$), the rescaled hamming distance d/N is constant with respect to network size N, and can be used as a size-independent measure of the length optimization deriving from a certain strategy β.

Efficiency, robustness and total length are typically considered as the relevant design goals in transport network construction [2–4].

For a graph G built on N nodes the total length is defined as

$$L(G) = \sum_{e \in E(G)} l_e, \quad (2)$$

where e is a link belonging to $E(G)$, the set of links of G, and l_e is the euclidean length of the link. Efficiency is defined following [5] and extended for spatial networks as

$$E(G) = \frac{1}{N(N-1)} \sum_{i \neq j \in G} \frac{d^e_{i,j}}{d_{i,j}}, \quad (3)$$

where i and j are nodes in G, $d^e_{i,j}$ is their euclidean distance and $d_{i,j}$ is the length of the shortest path connecting them on the network G. Efficiency represents how fast information and resources are exchanged over the network

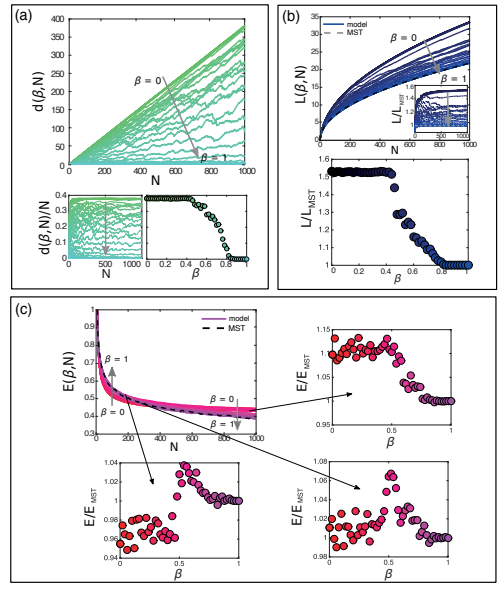

FIG. 1: Structural properties of the transport networks built by our model as a function of network size N and of the strategy β (colors online). Full lines represent networks grown according to our model at different values of β. Arrows indicate increasing values of β. In (b) and (c) the dashed line corresponds to independent simulations where nodes are connected to give a MST at each growth step. (a) Top: The Hamming distance as a function of N at different values of $\beta \in [0, 1]$. Bottom: the rescaled Hamming distance as a function of N (left) and β (right) for $N = 1000$. (b) Top: total network length as a function of N for different values of β, and rescaled by the length of the MST built on the same set of nodes (inset). Bottom: The rescaled total length as a function of β at $N = 1000$. (c) Top: Efficiency as a function of N at different values of β. Smaller plots: Efficiency normalized by the corresponding MST value during three growth stages of the network at $N = 200$, $N = 350$ and $N = 1000$ (counterclockwise).

[5, 6]. Robustness is defined as the probability that the network remains connected under the removal of a random link. Robustness measures network's resilience against targeted or random disruptions [7, 8]. In our specific case, the total length is the main design goal, leading the growth of the network. In our analysis we look at network efficiency as a consequence of length optimization, while robustness is trivially zero as we are dealing with trees. We compute the above measures for each network at each time step and average over the 70 instances.

The scaling of the total length as a function of N at different values of β is shown in Supplemental FIG. 1(b). At each value of β, the total length scales as $\sqrt{N}$ multiplied by a constant that depends on β, as estimated below. When divided by the total length of the corresponding MST (built on the same set of nodes), $L/L_{MST}(N)$ fluctuates around a constant value after $N \sim 250$ for all values of β. To summarize the asymptotical behaviour of the total length of the networks built by our model we take the rescaled total length L/L_{MST} at $N = 1000$ and plot it against β. Finally, the efficiency of our transport networks show a different behaviour depending on network size [Supplemental FIG. 1(c)]. When the network is small ($N \sim 200$) the dMST is less efficient than the corresponding MST. The ratio converges to 1 with increasing N. Around $N \sim 350$ the efficiency of the networks produced by our model is very close to the efficiency of a MST. Interestingly, the Hamming distance shows that the same efficiency is achieved by different network structures. At large network size, the rescaled efficiency shows the same three phases observed in the rescaled Hamming distance and in L/L_{MST}, with low values of β corresponding to highly efficient networks.

Asymptotically the growth strategy β tunes the tradeoff between total length and efficiency: for $\beta \lesssim \beta_1$ the strategy favors high efficiency by sacrificing the total length for $\beta \gtrsim \beta_2$ the networks have lower efficiency but are also shorter, and for $\beta_1 < \beta < \beta_2$ a smooth crossover is realized between these two regimes.

Mean field estimate for the scaling of the total length

For a network built on a random set of N nodes the total length can be written as $L = E < r >$, where E is the number of links and $< r >$ is the average length of links. For a Poisson distribution in 2D the distance between two first nearest neighbours is $< r_1 >= \frac{1}{2\sqrt{\rho}}$ $\rho = N/W$ is the density of points in the area W. For a tree $E = N - 1$, therefore:

$$L^{MST} = (N-1)\frac{1}{2\sqrt{\rho}} \sim \frac{\sqrt{W}}{2}\sqrt{N}. \qquad (4)$$

The building prescription of the dMST implies that every new node is linked to its first neighbour iteratively,

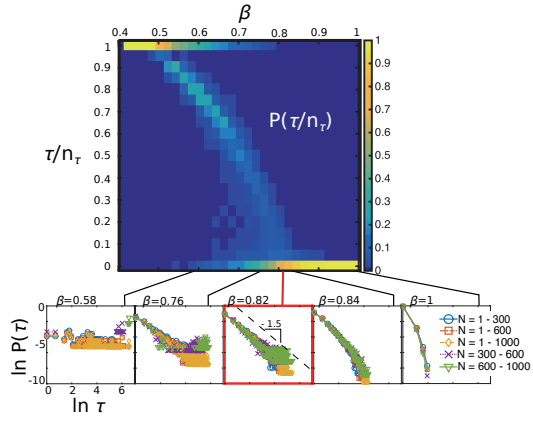

FIG. 2: The dynamics becomes bursty at the transition point β_2, with scale-free inter-event times (colors online). Top: the rescaled probability distribution $P(\tau/n_\tau)$ (color axis) of the inter-event time τ (y axis), as a function of β (x axis). Each distribution is normalized at fixed β, and conditioned on there being at least one MST event. Bottom: the probability distributions of τ (log-log scale) for different ranges of network size N, and different values of beta. The highlighted box corresponds to the transition β_2.

so it seems reasonable that:

$$L^{dMST} = \sum_{i=1}^{N} \frac{\sqrt{W}}{2\sqrt{i}} = \frac{\sqrt{W}}{2} H_N^{(\frac{1}{2})} \sim \sqrt{W}\sqrt{N}. \qquad (5)$$

$H_N^{(\frac{1}{2})}$ is the generalised harmonic number: $H_N^{(\frac{1}{2})} = 2\sqrt{N} + \zeta(1/2) + \ldots$, and $\zeta(1/2) = \sum_{k=1}^{\infty} 1/k^{1/2}$ is the Riemann Zeta function. At the first order $L_{TOT}^{dMST} \sim \sqrt{W}\sqrt{N}$. Therefore, the total length of the MST and dMST have the same scaling as a function of N, what changes is a constant.

DETAILED GROWTH DYNAMICS AND MEAN FIELD DISCUSSION

The *waiting time* τ is defined as the number of nodes added following a dMST prescription between two consecutive MST moves (and from the beginning to the first MST move). We use this quantity to characterize the growth dynamics of our networks depending on the strategy β. Due to non-stationarity of the process, the probability distribution function of τ turns out to depend on the time n_τ (corresponding to a certain size of the network) at which the MST move is performed. The typical τ shows an approximately linear scaling as a function of n_τ, so we focus on the rescaled waiting time τ/n_τ. The behaviour of the distribution $P(\tau/n_\tau)$ as a function of τ/n_τ and $\beta \in [0.4, 1]$ is reported in Supplemental FIG. 2.

Before β_1 the probability of a MST move is close to zero, and the typical waiting times are larger than those attained by our simulations ($N = 1000$).

The characteristic waiting time in the crossover regime is proportional to the size of the network. The ratio τ/n_τ is 1 around β_1 signaling that only one MST move is performed. As β increases towards the second transition value β_2, other MST events appear at small network size, accordingly $P(\tau/n_\tau)$ increases at $\tau/n_\tau \sim 0$ and for decreases steadily at $\tau/n_\tau > 0$.

For $\beta \gtrsim \beta_2$, the strategy largely prioritizes the minimization of total length and the network is rewired to a MST approximately at each time step. The typical waiting times do not depend on network size anymore and $P(\tau/n_\tau)$ is peaked in $\tau/n_\tau = 0$.

At the transition point $\beta = \beta_2$, $P(\tau/n_\tau)$ is positive for a wide range of values of τ/n_τ, and large waiting times are not suppressed. Correspondingly, $P(\tau)$ is power law distributed with exponent ~ -1.5.

Derivation of Eq. 2 in the main text

The probability of having a MST event $P(MST)$ can be expressed as follows. Starting from Eq.1 in the main text we can write $H^{MST}(N) = \beta(L^{MST}(N) - L(N-1,\beta)) + (1-\beta)L_B^{MST}(N,\beta)$ and $H^{dMST}(N) = L_B^{dMST}(N)$. $L^{MST}(N)$ is the total length of the Minimum spanning tree at size N. $L(N-1,\beta)$ is the total length of the network at size $N-1$ and depends on both N and β, as well as $L_B^{MST}(N,\beta)$, that is the total length that needs to be built to get a MST at size N from the network at size $N-1$. $L_B^{dMST}(N)$ is the length of the link that will connect the new node to its closest neighbour according to the dMST prescription. The total length of the MST at size N can be written as $L^{MST}(N) = L(N-1,\beta) + L_B^{MST}(N,\beta) - L_D^{MST}(N,\beta)$. $L_D^{MST}(N,\beta)$ is the sum of the lengths of the links that need to be destroyed during a global MST rewiring. Thus the equation governing the growth process can be written in a more compact fashion as:

$$P(MST) = P(L_B^{MST} - \beta L_D^{MST} < L_B^{dMST}). \quad (6)$$

Discussion of the growth dynamics

L_B^{dMST} can be estimated as the average distance between neighbouring nodes at size N, that for a Poisson point process is $\sqrt{1/cN}$ (c is a constant). L_D^{MST} and L_B^{MST} depend strongly on β and on the history of the network. For crossover values of β, it remains difficult to give a mean field approximation of the rewiring probability in terms of basic quantities. Equation 4 gives an insight on the mechanisms determining the final choice of a dMST or of a MST move.

The first term of the inequality shows that β is the proportion of destroyed length that is substantially subtracted from the built length when deciding which move will be performed on the network. The second term in the inequality tends to zero at large N, so that, asymptotically, the inequality can be satisfied only if the first term is negative. Accordingly, at fixed β we expect the probability of a MST event to decrease with network size, at least in the crossover phase.

These two contributions can be used to explain our model's dynamics using the lengths involved in the construction process. We start observing that, at size N, all the links built to give a MST will be on average $\sqrt{1/cN}$ long. Thus $L_B^{MST} \sim (N_D(N,\beta)+1)\sqrt{1/cN}$, where $N_D(N,\beta)$ is the number of links belonging to the network at size $N-1$ that are destroyed to build the MST at size N. The $+1$ refers to the link that needs to be added to connect the $N-th$ node. The destroyed length L_D^{MST} depends deeply on the history of the network. In the MST-like phase, it can be estimated as $L_D^{MST} \sim (L_D(N,\beta))\sqrt{1/c(N-1)}$, for we know that the network was almost surely an MST also at size N-1. Thus we see that for large beta the MST condition is easily satisfied, as L_D^{MST} is always slightly larger than L_B^{MST}.

In the crossover phase, when the most likely scenario is that just one rewiring occurs during the growth process, if any, we can suppose it will involve the whole network, so $L_D^{MST} \sim \sum_{n=1}^{N-1}\sqrt{1/cn}$ and $N_D \sim N-2$. So the comparison is now between $L_B^{MST} \sim (N-1)\sqrt{1/cN}$ and $L_D^{MST} \sim (\sqrt{(N-1)/c}-1)$. Some rearrangements let us write the MST condition as $\beta > (N-1)/[2\sqrt{N}(\sqrt{N-1}-1)] \to 1/2$, that is roughly where we see the first transition (N.B., this is conditioned to $N > 2$). This suggests that in the crossover regime, specially when β is closer to β_1, the only way to have a MST event is to destroy very long links to build short ones. This condition is likely to be achieved at large N, when the links built at the beginning of the process are likely to be very long ($\sim \sqrt{1/c}$) with respect to the ones that would be found in a MST at the same network size ($\sim \sqrt{1/cN}$). Once a MST rewiring has occurred, no long links are left, and the second term goes to zero with increasing N, explaining why when β is close to β_1 it is unlikely to observe more than one MST event. Increasing β makes long links less necessary, and the MST condition can be reached more and more often going towards β_2. Accordingly, the probability of short waiting times increases, specially at small network size where the second term in the inequality is still large. As a consequence, the typical waiting time becomes a fraction of the system size.

At β_2, the relationship between L_D^{MST} and L_B^{MST} seem to be balanced by the scaling in the built length L_B^{dMST} with network size. At all network sizes, this delicate equilibrium is often broken, but in few cases it can persist for several growth steps, resulting in the power-law scaling of $P(\tau)$ in all the considered N-windows [Supplemental FIG. 2, bottom]. The high number of links shared by MST and dMST in this regime requires to rewire very few links when a global length optimization is performed often. When waiting times get longer, the number of links that

need to be changed during a MST event increases. Despite being unfrequent in β_2, large waiting times belonging to the tail of the power law are responsible for 1/3 of the total number of destroyed and re-built links $\mathcal{L}_{\rm D}$.

DATA ANALYSIS

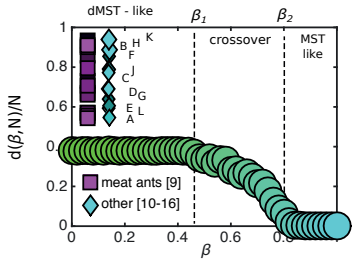

FIG. 3: Comparison between the Hamming distance of the randomized data networks with our model. Squares are transport networks from the meat ant dataset collected by Van Wilgenburg et al. [9], diamonds are further datasets from [10–16], the letters correspond to the labels in Table I.

For the data analysis we collected a total of 30 published ant networks constructed by the species *Linepithema humile* [10], *Iridomyrmex purpureus* [9, 11–13], *Formica lugubris* [14, 15] and *Camponotus gigas* [16]. The networks are at least 10 nodes big. For each transport network that is not already a tree (marked with * in Table I), we extract the minimum-length skeleton (the minimum spanning tree on the graph) and we measure the rescaled Hamming distance from the MST built on the same nodes. Finally, we assign a value of β to all of them by comparison with simulations of the model. In Supplemental Table I we report the explicit results of the analysis shown in FIG. 4(b) of the main text (d/N and β), as well as the size of the network N and the number of links L. Subsequently, we randomized each data network keeping a constant node degree and we applied the same procedure as described above to compute the Hamming distance and the corresponding β. Remarkably, randomized networks feature a typical Hamming distance that is larger than the maximum value obtained by our model, supporting our hypothesis that cost is a fundamental constraint in biological network formation [FIG. 3].

MATERIALS

Simulations are performed using the software Matlab.

[1] Richard W Hamming. Error detecting and error correcting codes. *Bell System technical journal*, 29(2):147–160, 1950.

[2] Guénaël Cabanes, Ellen van Wilgenburg, Madeleine Beekman, and Tanya Latty. Ants build transportation networks that optimize cost and efficiency at the expense of robustness. *Behavioral Ecology*, page aru175, 2014.

[3] Atsushi Tero, Seiji Takagi, Tetsu Saigusa, Kentaro Ito, Dan P Bebber, Mark D Fricker, Kenji Yumiki, Ryo Kobayashi, and Toshiyuki Nakagaki. Rules for biologically inspired adaptive network design. *Science*, 327(5964):439–442, 2010.

[4] Daniel P Bebber, Juliet Hynes, Peter R Darrah, Lynne Boddy, and Mark D Fricker. Biological solutions to transport network design. *Proceedings of the Royal Society B: Biological Sciences*, 274(1623):2307–2315, 2007.

[5] Vito Latora. Efficient behavior of small-world networks. *Physical Review Letters*, 87(19), 2001.

[6] Zoe Cook, Daniel W Franks, and Elva JH Robinson. Efficiency and robustness of ant colony transportation networks. *Behavioral Ecology and Sociobiology*, 68(3):509–517, 2014.

[7] Vitor HP Louzada, Fabio Daolio, Hans J Herrmann, and Marco Tomassini. Generating robust and efficient networks under targeted attacks. *arXiv preprint arXiv:1207.1291*, 2012.

[8] Ellen Van Wilgenburg and Mark A Elgar. Colony characteristics influence the risk of nest predation of a polydomous ant by a monotreme. *Biological Journal of the Linnean Society*, 92(1):1–8, 2007.

[9] E Van Wilgenburg and MA Elgar. Colony structure and spatial distribution of food resources in the polydomous meat ant iridomyrmex purpureus. *Insectes sociaux*, 54(1):5–10, 2007.

[10] NE Heller, KK Ingram, and DM Gordon. Nest connectivity and colony structure in unicolonial argentine ants. *Insectes Sociaux*, 55(4):397–403, 2008.

[11] JA Holt. Observations on the relationships between meat ants and termites in tropical australia. *Journal of tropical ecology*, 6(03):379–382, 1990.

[12] A. N. Andersen and A. D. Patel. Meat ants as dominant members of australian ant communities: an experimental test of their influence on the foraging success and forager abundance of other species. *Oecologia*, 98(1).

[13] JD McIver. Dispersed central place foraging in australian meat ants. *Insectes Sociaux*, 38(2):129–137, 1991.

[14] G. Boudjema, G. Lempérière, M. Deschamps-Cottin, and D. G. Molland. Analysis and nonlinear modeling of the mound-building ant formica lugubris spatial multi-scale dynamic in a larch-tree stand of the southern french alps. *Ecological modelling*, 190(1), 2006.

[15] S. Ellis, D. W. Franks, and E. J.H. Robinson. Resource redistribution in polydomous ant nest networks: local or global? *Behavioral Ecology*, 25(5), 2014.

[16] M Pfeiffer and KE Linsenmair. Contributions to the life history of the malaysian giant ant camponotus gigas (hymenoptera, formicidae). *Insectes Sociaux*, 47(2):123–132, 2000.

(a) □ Meat ant data from [9]

Data	N	L	d/N	β
1	12	11*	0.42	ND
2	13	12*	0.38	0
3	14	14*	0.36	0.46
4	15	16	0.34	0.58
	15	14*	0.34	0.58
	12	11	0.34	0.58
5	14	14	0.29	0.62
	14	15	0.29	0.62
6	16	16	0.25	0.68
	16	17	0.25	0.68
	12	11*	0.25	0.68
	12	13	0.25	0.68
7	14	15	0.21	0.7
8	15	15	0.22	0.7
9	12	13	0.17	0.74
	12	12	0.17	0.74
10	17	18*	0.12	0.76
11	12	11*	0.08	0.78
	12	12	0.08	0.78

(b) ◊ Further data from [10–16].

Data	N	L	d/N	β
A - *Linepithema humile* [10]	16	18	0.31	0.54
B - *Iridomyrmex purpureus* [11]	32	38	0.28	0.62
C - *Formica lugubris* [15]	19	24	0.26	0.66
D - *Formica lugubris* [15]	12	12	0.25	0.68
E - *Iridomyrmex purpureus* [12]	13	12*	0.23	0.72
F - *Formica lugubris* [15]	22	21*	0.23	0.72
G - *Formica lugubris* [15]	18	15	0.2	0.7
H - *Camponotus gigas* [16]	24	28	0.13	0.76
J - *Iridomyrmex purpureus* [13]	13	13	0.08	0.78
K - *Formica lugubris* [14]	34	34	0.06	0.8
L - *Formica lugubris* [15]	13	12*	0	1

TABLE I: Summary of the data analysis for FIG. 4(b) in the main text. (a): Transportation networks of the Meat ant *Iridomyrmex purpureus* [9] (squares in FIG. 4(b) in the main text and Supplemental FIG. 3). First column: reference in FIG. 4(b) and Supplemental FIG. 3. Ant networks corresponding to the same number have the same rescaled Hamming distance. Second column: number of nodes. Third column: number of links. Fourth column: rescaled hamming distance. Fifth column: estimated β. (b): Further data from [10–16] (diamonds in FIG. 4(b) and Supplemental FIG. 3). First column: reference in the figure - ant specie and reference in the bibliography. Second to fifth column as in table (a). In both tables, * indicates that the network is a tree, i.e. $L = N - 1$.

Paper IV

Emergent Structural Mechanisms for High-Density Collective Motion Inspired by Human Crowds

Arianna Bottinelli,[1,*] David T. J. Sumpter,[1,†] and Jesse L. Silverberg[2,‡]

[1] *Mathematics Department, Uppsala University, Lägerhyddsvägen 1, Uppsala 75106, Sweden*
[2] *Wyss Institute for Biologically Inspired Engineering, Harvard University, Boston MA, USA.*

Collective motion of large human crowds often depends on their density. In extreme cases like heavy metal concerts and Black Friday sales events, motion is dominated by physical interactions instead of conventional social norms. Here, we study an active matter model inspired by situations when large groups of people gather at a point of common interest. Our analysis takes an approach developed for jammed granular media and identifies Goldstone modes, soft spots, and stochastic resonance as structurally-driven mechanisms for potentially dangerous emergent collective motion.

PACS numbers: 89.75.Fb, 63.50.-x, 45.70.Vn

Studies of collective motion cover a broad range of systems including humans, fish, birds, locusts, cells, vibrated rice, colloids, actin-myosin networks, and even robots [1–3]. Often, theoretical models of these active matter systems take a Newtonian approach by calculating individual trajectories generated *in silico* from the sum of forces acting on each of N particles [3]. Of the work focusing on humans, social interactions such as collision avoidance, tendencies to stay near social in-group members, directional alignment, and preference for personal space have been examined to understand their role in emergent behavior [4–7]. Generally, these studies show order-disorder transitions are driven by the competition between social interactions and randomizing forces [8, 9]. Models based on these findings have been incorporated into predictive tools used to enhance crowd management strategies at major organized gatherings, however, the validity of this approach is diminished in extreme social situations such as riots, protests, and escape panic [10–12]. In these situations, conventional social interactions no longer apply [13], and the actual collective behavior can be quite different from model predictions [14, 15].

Situations involving large groups of people packed at high-densities provide a unique view of emergent collective behavior in extreme conditions [8, 10]. For example, attendees at heavy metal concerts often try to get as close as possible to the stage, but are unable to do so due to the sheer number of people trying to attain the same goal [Fig. 1(a)]. Consequently, the audience in this region of the concert venue becomes a densely packed shoulder-to-shoulder group with little room for individuals to freely move. Often, the stresses involved become dangerously high and security professionals standing behind physical barriers are required to pull audience members from the crowd for medical attention [16]. At Black Friday sales events, we find similar situations when individuals seeking low-cost consumer goods congregate at the entrance of a store before it opens [Fig. 1(b)]. As documented in many reports and online videos, these events can have tragic outcomes in the critical moments after the doors open and the crowd surges forward resulting in stampedes and trampling.

In extreme situations involving large high-density crowds, physical interactions between contacting bodies and the simultaneous collective desire of each individual to get to a stage, through a door, or to a particular location become the dominant considerations [5, 12, 17]. To generically capture these scenarios, we use a conventional force-based active matter model for human collective motion, but remove terms that account for social interaction. With this simplification, we have an *asocial* model for human collective behavior describing people aggregating around a common point of interest $\mathcal{P}$. Here, we place $\mathcal{P}$ at the side of a 2D $L \times L$ simulation box [Fig. 1(c)]. In this framework, each person i is modeled as a disk with radius $r_0 \ll L$ positioned at a point $\vec{r}_i(t)$ and subject to pairwise collision forces $\vec{F}_i^{\text{repulsion}}$, a self-propulsion force $\vec{F}_i^{\text{propulsion}}$, random force fluctuations from environmental stimuli $\vec{F}_i^{\text{noise}}$, and a rigid-wall collision force $\vec{F}_i^{\text{wall}}$.

For each of the N self-propelled particles (SPPs) in our model we have $\vec{F}_i^{\text{repulsion}} = \epsilon \sum_{j \neq i}^{N} (1 - r_{ij}/2r_0)^{3/2} \hat{r}_{ij}$, which takes non-zero values only when the distance between two particles $|\vec{r}_i - \vec{r}_j| = |r_{ij}\hat{r}_{ij}| = r_{ij} < 2r_0$ [8]; $\vec{F}_i^{\text{propulsion}} = \mu(v_0 - v_i)\hat{p}_i$, where v_0 is a constant preferred speed, v_i is the current speed of the i^{th} SPP, and $\hat{p}_i$ is a unit vector pointing from each particle's center to the common point of interest $\mathcal{P}$; $\vec{F}_i^{\text{noise}} = \vec{\eta}_i$ is a random force vector whose components $\eta_{i,\lambda}$ are drawn from a Gaussian distribution with zero mean and standard deviation σ defined by the correlation function $\langle \eta_{i,\lambda}(t)\eta_{i,\kappa}(t')\rangle = 2\mu^{-1}\sigma^2\delta_{\lambda\kappa}\delta(t-t')$, which ensures noise is spatially and temporally decorrelated. Collisions between the simulation box's boundaries and SPPs give rise to a force similar to the repulsion force, $\vec{F}_i^{\text{wall}} = \epsilon\,(1 - r_{iw}/r_0)^{3/2}\,\hat{r}_{iw}$, which is non-zero when the distance of the particle from the wall $r_{iw} < r_0$, and is directed along the wall's outward normal direction. The functional form of $\vec{F}_i^{\text{repulsion}}$ and $\vec{F}_i^{\text{wall}}$ comes from treating SPP collisions as a Hertzian

* arianna.bottinelli@math.uu.se
† david.sumpter@math.uu.se
‡ jesse.silverberg@wyss.harvard.edu

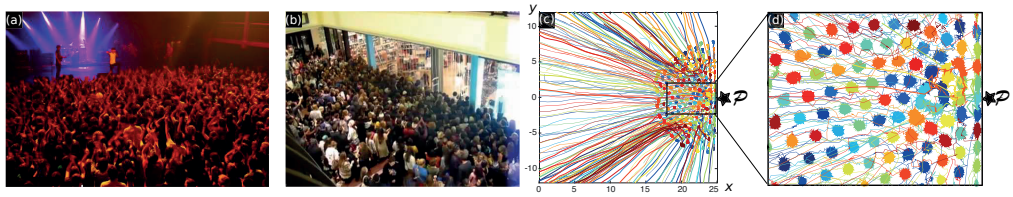

FIG. 1. (color online). Large dense groups of people give rise to emergent collective motion. (a) Attendees gather near the stage at a heavy metal concert. Credit: Ulrike Biets. (b) Customers gather for Black Friday sale to purchase low-cost consumer goods. Credit: Jerry Bailey. (c) Simulated trajectories of SPPs aggregating near a point of interest $\mathcal{P}$ located at the right-most edge of a simulation box. (d) Zoom in of trajectories show SPPs self-organize into a densely packed disordered aggregate.

contact problem (Supplemental Materials). In terms of the simulation unit length ℓ and unit time τ, we set the particle radius $r_0 = \ell/2$, the simulation box size $L = 50\ell$, the preferred speed $v_0 = \ell/\tau$ [12], the random force standard deviation $\sigma = \ell/\tau^2$ and the force scale coefficients $\epsilon = 25\ell/\tau^2$, $\mu = \tau^{-1}$ [8]. Results presented here are for $N = 200$ SPPs, though varying population size has little effect on our analysis (Supplemental Materials).

Simulations were initialized with random initial positions for each particle. Trajectories were evolved with Newton-Stomer-Verlet integration according to $\ddot{\vec{r}}_i = \vec{F}_i^{\text{repulsion}} + \vec{F}_i^{\text{propulsion}} + \vec{F}_i^{\text{noise}} + \vec{F}_i^{\text{wall}}$ for a total of $3,000\tau$ units of time [Fig. 1(c)], where each τ consists of 10 integration time steps. While data for the initial $\approx 50\tau$ was dominated by transient motion, we discarded the first 300τ from our analysis to avoid this far-from-equilibrium effect [Fig. 1(c), linear path segments]. By 300τ the SPPs aggregated near $\mathcal{P}$ and settled into a steady-state configuration with each particle making small random motions about their average position [Fig. 1(d)]. For the model parameters studied here, collisions and random force fluctuations contribute roughly equally to these motions, which can be seen by estimating the relevant time scales (Supplemental Materials). At average crowd density n, the collision time scale is $\tau_{\text{coll}} = 1/(2r_0v_0n) \approx (\pi/4)\tau$ and the noise time scale is $\tau_{\text{noise}} = v_0^2/2\mu\sigma^2 = \tau/2$, so that $\tau_{\text{coll}} \approx \tau_{\text{noise}}$ at steady-state. Thus, while $\vec{F}_i^{\text{propulsion}}$ acts as an external field confining SPPs, collision and noise forces drive position fluctuations and the aggregate's disordered structure [Fig. 1(d)].

Generally, we find a striking resemblance between these simulations of high-density crowds and previous studies of disordered packings [10, 18–20] (Supplemental Materials). In the context of jammed granular materials, a significant amount of effort has helped develop theoretical tools that connect local structure to dynamical response [21–27]. A key analysis method involves the displacement correlation matrix whose components are defined by $C_{ij} = \langle[\vec{r}_i(t) - \langle\vec{r}_i\rangle] \cdot [\vec{r}_j(t) - \langle\vec{r}_j\rangle]\rangle$. Here, $\vec{r}_i(t)$ is the instantaneous position at time t, $\langle\vec{r}_i\rangle$ is the mean position of the i^{th} SPP, and all averages $\langle\cdot\rangle$ are calculated by sampling position data every 10τ for a total of 270 measurements. This sampling was chosen to reduce effects of

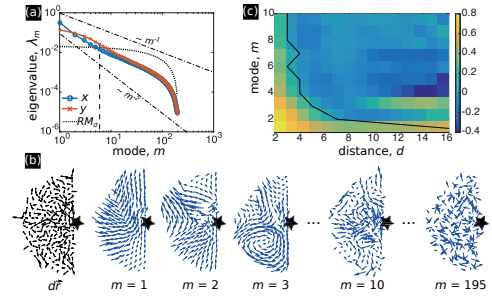

FIG. 2. (color online) Eigenmode analysis of asocial model for high-density human crowds. (a) Eigenvalue spectrum λ_m of the displacement correlation matrix exhibits scaling properties between $\lambda_m \sim m^{-1}$ and $\sim m^{-2}$ (black dashed lines). Low m eigenmodes in both x (blue) and y (orange) directions are larger than a random matrix model (RM_σ), and thus describe correlated motion. (b) Snapshot of instantaneous displacements $d\vec{r}$ and example vector fields for various eigenmodes. Lower m eigenmodes are more spatially correlated than higher m. (c) A heatmap of the polarization correlation function for the first 10 eigenmodes as a function of distance d between SPPs. Black line is where the correlation function decays to 0 demonstrating a long-range highly correlated mode for $m = 1$.

auto-correlated motion while still accumulating sufficient statistically independent measurements in a finite time [21]. In this computation, we exclude underconstrained SPPs that do not contribute to the overall collective motion. In the jamming literature these particles are called "rattlers," and they are distinguished by abnormally large position fluctuations [21]. In our analysis, we used a position fluctuation threshold of 4 standard deviations to identify rattlers. However, our results were self-consistent for values from 2 to 5 indicating the methodology is robust (Supplemental Materials).

To extract quantitative information from the SPP configuration, we computed eigenmodes $\vec{e}_m$ and eigenvalues λ_m of the displacement correlation matrix. In the harmonic theory of crystals, these normal modes fully charac-

terize the linear response of the system to perturbations [28]. For disordered materials, these modes convey information about structural stability as well as coherent and localized motion [22–24]. In non-equilibrium systems, only modes with eigenvalues that are sufficiently large play a role in determining the response to perturbations [21]. These modes must be carefully identified and interpreted due to differences between equilibrium and non-equilibrium dynamics (Supplemental Materials). Plotting the eigenvalue spectrum λ_m as a function of mode number m averaged over 10 runs with random initial conditions revealed an approximate power-law decay [Fig. 2(a), blue and orange data]. While the Debye model for 2D crystals obeys $\lambda_m \sim m^{-1}$ [Fig. 2(a), upper dashed line] [28], the simulation data has an exponent between -1 and -2. Using a random matrix model of uncorrelated Gaussian variables as a control for relevant modes [Fig. 2(a), black dotted line] (Supplemental Materials) [21], we see the lowest six eigenmodes contain information about correlated motion [Fig. 2(a), vertical black dashed line]. Plotting displacement vector fields for a few eigenmodes, we indeed find a higher degree of spatial correlation for lower m that rapidly diminishes with increasing mode number [Fig. 2(b)]. To quantify this observation, we measured the polarization of each mode's vector field and calculated the fluctuation correlation function for this order parameter (Supplemental Materials) [29]. Remarkably, we find the first eigenmode carries a system-spanning displacement modulation [Fig. 2(c), $m = 1$], whereas the correlation for higher modes rapidly decays over a few particle diameters [Fig. 2(c), $m > 1$].

To understand the origins of this long wavelength mode, we note self-propulsion toward $\mathcal{P}$ breaks XY translational symmetry, and therefore the Goldstone theorem implies the existence of low-frequency long-wavelength deformations [30–32]. This Goldstone mode is expected to arise at low m since eigenvalues are related to vibrational frequencies by $\lambda_m = \omega_m^{-2}$, and the largest eigenvalue in the spectrum occurs at the lowest mode number [Fig. 2(a)]. Thus, the system-spanning $m = 1$ eigenmode is the system's Goldstone Boson. In the context of active matter, this is known as the "Goldstone mode of the flock," and when excited, it drives the SPPs to move collectively as one [33–36]. We hypothesize a real-world example of this type of coherent long-range motion is "crowd crush" [13]. In these situations, a large number of people are suddenly displaced toward a wall, fence, or other architectural element resulting in dangerously high pressures and occasionally death [10, 37]. Determining if Goldstone modes are responsible for crowd crush would require careful image analysis of crowd structure and motion in the moments before such an event. Nevertheless, we expect any large dense gatherings to exhibit this type of long-range collective behavior since it originates from the general principle of symmetry breaking.

Another type of disaster found at high-density gatherings is when sudden unexpected movements of the crowd cause individuals to trip and fall. Because the majority of people are unaware this accident has happened, the rest of the crowd moves largely uninterrupted, resulting in injury or death due to trampling [10, 13, 38]. This is more general than the excitation of a pure Goldstone mode, and is better characterized by a superposition of modes. Thus, we focus on the particles that displace significantly more than average in a given mode m [Fig. 3(a), displacement threshold is 2.5 standard deviations more than average] (Supplemental Materials). Studies of jammed granular media show these particles, which tend to cluster in regions called "soft spots," correlate with structural rearrangements when the system is perturbed [24]. Superimposing data from the first 10 modes of a single simulation run reveals a soft spot near the core of the aggregate [Fig. 3(a)]. Regions along the perimeter also feature large displacements, but they are essentially underconstrained edge effects and therefore not relevant for our analysis [27]. Identifying SPPs undergoing the largest displacements in each mode up to $m = 10$ in all simulation runs show the region near the core of the crowd is the most likely area to find soft spots [Fig. 3(b), peak centered on $\rho \approx 2$]. Cross-correlating soft spot SPPs with their real-space dynamics confirmed these particles typically displace the greatest amount despite being confined within a disordered aggregate [Fig. 3(a)].

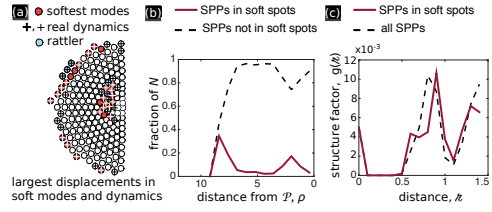

FIG. 3. (color online) Soft spots within the crowd undergo large displacements. (a) SPPs are shown as disks. Soft spots near the core of the aggregate colocalize with SPPs that displace the most in real dynamics. This region is subject to large structural rearrangements when the system is perturbed, and is likely a region where injury can occur. Apparent soft spots along the periphery are artifacts due to underconstrained edge effects. (b) Averaging over all simulation runs show soft spots generally occur near the core of the aggregate a radial distance $\rho \approx (2\pm1)$ away from $\mathcal{P}$. (c) Structure factor $g(\ell)$ measures the pair-wise SPP distribution of distances between particles and reveals structural features distinguishing SPPs in soft spots that suggest why they are subject to large displacements.

We further studied the relation between structural disorder and large displacements in soft spots by measuring the structure factor $g(\ell)$, which quantifies the distribution of distance ℓ between the center of adjacent particles (Supplemental Materials), and found that soft spot SPPs have an intrinsically different structure compared to the average population [Fig. 3(c)]. The secondary peak in $g(\ell)$ around $0.5 \lesssim \ell \lesssim 0.8$ [Fig. 3(c) solid line] indicates soft spot SPPs are more highly squeezed by some of their

neighbors, while the shifted peak centered on $\hat{\imath} \approx 0.9$ indicates they're also further away than average from other neighbors [Fig. 3(c), dashed line peak at $\hat{\imath} \approx 0.8$]. These data suggest soft spot SPPs are being compressed tightly in one direction, and as a consequence displace greater amounts in the orthogonal direction. As such, self-organized structural disorder is fundamental for large displacements and rearrangements [Fig. 3(a)] [24]. Because these large random rearrangements would likely be experienced as unexpected lurching movement for the average member of a human crowd, we hypothesize soft spots pose the greatest risk for tripping and subsequent trampling. If found true, real-time image analysis identifying soft spots in densely-packed human crowds may provide useful predictive power for preventing injuries.

Our results thus far have focused on structural origins of collective motion with all model parameters kept constant. In real life situations, not all people behave the same: some agitate more easily, others less so [9, 15]. Accordingly, we modify the asocial model to study how mechanisms for coherent collective motion are affected by active perturbations. Specifically, we introduce a second population of SPPs so that a fraction f exhibits a more agitated behavior, while the remaining fraction $1-f$ of the population is the same as before [8, 9]. We model these agitated SPPs with a larger distribution of force fluctuations in $\vec{F}_i^{\text{noise}}$ by increasing their standard deviation to $\sigma_a > \sigma$, and analyze the two parameter phase space of f and σ_a. We first consider the case $\sigma_a = 3\sigma$ and vary f from 0 to 1. Calculating the spectrum of eigenvalues λ_m shows the qualitative trends are independent of f, though numerical values of λ_m tend to increase with more agitators (Supplemental Materials). To understand how long-range collective motion is affected by agitated SPPs, we measured the polarization fluctuation correlation function for the first 10 modes while varying σ_a and f [Fig. 4]. Surprisingly, the correlation functions for $\sigma_a = 3\sigma$ show a qualitative transition with varying f unanticipated from the eigenvalue spectrum: the eigenvalues smoothly vary with mode number while the correlation functions exhibit new behaviors. For $f = 0.1$, a long-range correlated Goldstone mode is observed as before. However, multiple long-range correlated modes are observed for $f = 0.2$, and no long-range correlated modes are observed for $f > 0.3$. Examining other values of σ_a shows a similar transition with increasing f from a single well-defined long-range mode, to multiple long-range modes, to no long-range modes whatsoever [Fig. 4, rows left-to-right].

The low-agitation and high-agitation limits are intuitive. For low agitation [Fig. 4, white region], additional force fluctuations through increasing σ_a with low f or increasing f with low σ_a induce small perturbations to the overall structure. As such, the existence of a Goldstone mode at low m is anticipated based on the homogeneous population results [Fig. 2(c)]. For high agitation where the combined effect of σ_a and f is large [Fig. 4, dark gray shaded region], we expect local structure to break down and correlated motion to be marginalized. Consistent with this reasoning,

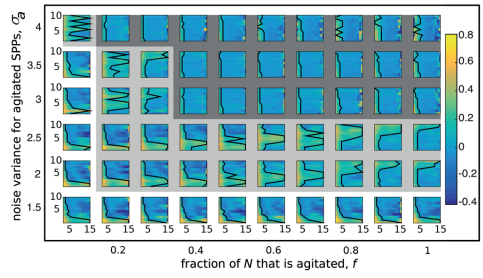

FIG. 4. (color online) Introducing a fraction f of agitated SPPs with variance σ_a in $\vec{F}_i^{\text{noise}}$ probes structural origins of collective motion. Each heat map is the polarization fluctuation correlation function for the first 10 eigenmodes as a function of distance d (same as Fig. 2(c)). Low fluctuations (white background) preserve the long-range highly-correlated Goldstone mode near $m = 1$. High fluctuations (dark gray background) destroy long-range correlated modes. Intermediate fluctuations (light gray background) add new modes with long-range correlations, indicating stochastic resonance.

we find no long-range modes in the high-agitation limit.

Between the high and low agitation limit, we find a boundary in the (f, σ_a) phase diagram characterized by multiple long-range modes [Fig. 4, light gray shaded region]. This result is striking because it shows moderate levels of noise produce new coherent motion. Noting that correlated motion allows mechanical information to be transferred across the aggregate, an appearance of multiple long-range modes implies greater information bandwidth. In certain settings, signal enhancement mediated by noise is called *stochastic resonance* [39, 40]. Generally, stochastic resonance is found in systems where nonlinear effects dampening signal propagation are suppressed by random noise. In our case, nonlinear effects suppressing conventional phonon modes come from structural packing disorder. Random noise from agitators increases the internal pressure within the aggregate, breaking-up the disordered configuration of particle-particle contacts. Consequently, phonon modes otherwise suppressed by packing disorder [Fig. 2(c), modes $m > 1$] reassert their presence [Fig. 4, additional long-range modes in light-gray region] (Supplemental Materials). In the context of our model, this indicates that modest random fluctuations can enhance overall collective motion, increasing the potential for injurious outcomes in high-density crowds.

Our analysis of collective motion in dense crowd simulations relies on trajectory data in order to identify and understand the emergence of Goldstone modes, soft spots, and stochastic resonance. With an eye to crowd safety, the dependence on measurable quantities combined with computer vision techniques [41, 42] provides significant potential for applications in real-time crowd management, which may help protect attendees at large gatherings by reducing emergent risks [10, 15, 38]. More theoretically,

the observation of Goldstone modes hints at a collective motion analogous to the Higgs Boson that may be found in collective speed modulations. To elaborate, active matter systems breaking continuous rotational symmetry can be represented by an orientation field quantifying the SPP vector headings. Long-range fluctuations in orientation correspond to the zero-energy Goldstone mode. Associated with this velocity vector *orientation* field is the velocity vector *speed* field. This speed field is subject to fluctuations with an energetic cost that does not go to zero at infinite wavelength, indicating the presence of a massive Boson otherwise known as the Higgs Boson. Developing an effective field theory around these ideas and incorporating quasi-particle-like excitations would likely present new opportunities to understand emergent collective motions, their interactions, and potential hazards in large social gatherings.

ACKNOWLEDGEMENTS

We thank U. Biets and J. Bailey for providing photographs used here. A.B. thanks A. Maffini for discussions during the early stages of the project. J.L.S. thanks M. Bierbaum, J. Sethna, and I. Cohen for useful discussions. Thanks to A. Gådin and J. Svensson for software development. A.B. acknowledges funding from the Centre for Interdisciplinary Mathematics (CIM). J.L.S. was independently funded.

[1] S. Camazine, *Self-organization in biological systems* (Princeton University Press, 2003).
[2] D. J. Sumpter, *Collective Animal Behavior* (Princeton University Press, 2010).
[3] T. Vicsek and A. Zafeiris, Phys. Rep. **517**, 71 (2012).
[4] D. Helbing and P. Molnar, Phys. Rev. E **51**, 4282 (1995).
[5] D. Helbing and A. Johansson, *Pedestrian, crowd and evacuation dynamics* (Springer, 2011).
[6] H. Xi, S. Lee, and Y.-J. Son, in *Human-in-the-Loop Simulations* (Springer, 2011) pp. 69–95.
[7] M. Moussaïd, D. Helbing, and G. Theraulaz, Proc. Natl. Acad. Sci. U.S.A. **108**, 6884 (2011).
[8] J. L. Silverberg, M. Bierbaum, J. P. Sethna, and I. Cohen, Phys. Rev. Lett. **110**, 228701 (2013).
[9] D. Helbing, I. J. Farkas, and T. Vicsek, Phys. Rev. Lett. **84**, 1240 (2000).
[10] D. Helbing, A. Johansson, and H. Z. Al-Abideen, Phys. Rev. E **75**, 046109 (2007).
[11] D. C. Duives, W. Daamen, and S. P. Hoogendoorn, Transport. Res. C - Emer. **37**, 193 (2013).
[12] D. Helbing, I. Farkas, and T. Vicsek, Nature **407**, 487 (2000).
[13] J. J. Fruin, Eng. for Crowd Safety **1**, 10 (1993).
[14] K. M. Zeitz, H. M. Tan, M. Grief, P. Couns, and C. J. Zeitz, Preshosp. Dis. Med. **24**, 32 (2009).
[15] E. A. Heide, in *The First 72 hours: A Community Approach to Disaster Preparedness*, edited by M. O'Leary (iUniverse, 2004) p. 337.
[16] T. Janchar, C. Samaddar, and D. Milzman, Am. J. Emerg. Med. **18**, 62 (2000).
[17] J. Bohannon, Science **310**, 219 (2005).
[18] D. Helbing, A. Johansson, J. Mathiesen, M. H. Jensen, and A. Hansen, Phys. Rev. Lett. **97**, 168001 (2006).
[19] E. Cristiani, B. Piccoli, and A. Tosin, Multiscale Model. Sim. **9**, 155 (2011).
[20] S. Faure and B. Maury, Math. Mod. Meth. Appl. S. **25**, 463 (2015).
[21] S. Henkes, C. Brito, and O. Dauchot, Soft Matter **8**, 6092 (2012).
[22] C. Brito, O. Dauchot, G. Biroli, and J.-P. Bouchaud, Soft Matter **6**, 3013 (2010).
[23] D. J. Ashton and J. P. Garrahan, Eur. Phys. J. E **30**, 303 (2009).
[24] M. L. Manning and A. J. Liu, Phys. Rev. Lett. **107**, 108302 (2011).
[25] S. Henkes, Y. Fily, and M. C. Marchetti, Phys. Rev. E **84**, 040301 (2011).
[26] N. Xu, V. Vitelli, A. Liu, and S. Nagel, Europhys. Lett. **90**, 56001 (2010).
[27] P. Charbonneau, E. I. Corwin, G. Parisi, and F. Zamponi, Phys. Rev. Lett. **114**, 125504 (2015).
[28] N. W. Ashcroft and N. D. Mermin, *Solid State Physics* (Thomson Learning, 1976) p. 120.
[29] W. Bialek, A. Cavagna, I. Giardina, T. Mora, O. Pohl, E. Silvestri, M. Viale, and A. M. Walczak, Proc. Natl. Acad. Sci. U.S.A. **111**, 7212 (2014).
[30] Y. Nambu, Phys. Rev. **117**, 648 (1960).
[31] J. Goldstone, Il Nuovo Cimento (1955-1965) **19**, 154 (1961).
[32] J. Sethna, *Statistical Mechanics: Entropy, Order Parameters, and Complexity* (Oxford University Press, 2006).
[33] J. Toner, Y. Tu, and S. Ramaswamy, Annals of Physics **318**, 170 (2005).
[34] S. Ramaswamy, Annu. Rev. Condens. Matter Phys. **1** (2010).
[35] A. Cavagna, A. Cimarelli, I. Giardina, G. Parisi, R. Santagati, F. Stefanini, and M. Viale, Proc. Natl. Acad. Sci. U.S.A. **107**, 11865 (2010), http://www.pnas.org/content/107/26/11865.full.pdf+html.
[36] W. Bialek, A. Cavagna, I. Giardina, T. Mora, O. Pohl, E. Silvestri, M. Viale, and A. M. Walczak, Proceedings of the National Academy of Sciences **111**, 7212 (2014).
[37] S. Takatori, W. Yan, and J. Brady, Phys. Rev. Lett. **113**, 028103 (2014).
[38] B. Krausz and C. Bauckhage, Comput. Vis. Image Und. **116**, 307 (2012).
[39] M. D. McDonnell and D. Abbott, PLoS Comput Biol **5**, e1000348 (2009).
[40] L. Gammaitoni, P. Hänggi, P. Jung, and F. Marchesoni, Rev. Mod. Phys. **70**, 223 (1998).
[41] J. S. J. Junior, S. Musse, and C. Jung, IEEE Signal Proc. Mag. **5**, 66 (2010).
[42] S. Ali, K. Nishino, D. Manocha, and M. Shah, *Modeling, Simulation and Visual Analysis of Crowds: A Multidisciplinary Perspective* (Springer, 2013).

Supplemental Material: Emergent Structural Mechanisms for High-Density Collective Motion Inspired by Human Crowds

Arianna Bottinelli,[1,*] David T. J. Sumpter,[1,†] and Jesse L. Silverberg[2,‡]

[1] *Mathematics Department, Uppsala University, Lägerhyddsvägen 1, Uppsala 75106, Sweden*
[2] *Wyss Institute for Biologically Inspired Engineering, Harvard University, Boston MA, USA.*

I. DETAILED INFORMATION ON SIMULATION AND DATA ANALYSIS

a. Simulations. Each simulation takes place in a square room of side $L = 50$ length units ℓ with the center of the room placed at the origin $[0, 0]$. N individual humans are modeled as self-propelled particles (SPPs) with radius $r_0 = \ell/2$, and placed at random initial positions with zero initial speed. The equation of motion described in the main text is numerically integrated using the Newton-Stomer-Verlet algorithm. At each time step the algorithm computes the total force $\vec{F}_{\rm tot}(t)$ acting on each individual in its current position $\vec{r}(t)$. The position is updated using the current speed $\vec{v}(t)$ according to

$$\vec{r}(t+1) = \vec{r}(t) + \vec{v}(t)\Delta T + \frac{1}{2}\vec{F}_{\rm tot}(t)(\Delta T)^2. \qquad (1)$$

The algorithm then computes the force $\vec{F}_{\rm tot}(t+1)$ acting on each individual in its new position, and updates the speed:

$$\vec{v}(t+1) = \vec{v}(t) + \frac{1}{2}(\vec{F}_{\rm tot}(t) + \vec{F}_{\rm tot}(t+1))\Delta T. \qquad (2)$$

We choose $\Delta T = 0.1$ because this value is small enough to make the trajectories smooth, but large enough to achieve a reasonable computational time. For the time series data we analyzed in the main text, random forces and collisions operate at similar time scales. Consequently, the motion of SPPs, which is confined to regions roughly the same size as the particle's diameter, rapidly scrambles the particle trajectories over a short distance. This prevents numerical integration errors from adding up, and moreover, tends to average integration errors out because the dense aggregate of SPPs is stable over long periods of time. Every 10 time steps of the simulation we record each particle's position and the pressure due to radial contact forces $P_i = (2\pi r_0)^{-1}(\sum_j F_{i,j}^{\rm repulsion} + \sum_w F_{i,w}^{\rm wall})$. We run our simulations for $T = 30,000$ time steps, corresponding to $3,000\tau$.

b. Model parameters and time scales. As described in the main text, our model parameters are set by the fundamental simulation unit length ℓ and unit time τ. This allows us to maintain careful control over the relative force and time scales, while not explicitly committing to dimensionful units. For example, the SPP preferred speed v_0 is set to ℓ/τ, which means v_0 is the "unit speed" in arbitrary simulation units. Choices for other units are based around this notion of dimensionless parameters. For example, the SPPs radius r_0 is simply chosen as $\ell/2$, which means that in the absence of any other interactions, a SPP would be inclined to move a distance equal to its diameter in the time τ. This choice approximates relaxed pedestrian motion if we were to set τ equal to one second. Indeed, empirical observations have reported that $v_0/r_0 \approx 2$ in calm pedestrian motion [1], which is in agreement with our parameter choice. Along similar lines, we choose $L \gtrsim \ell\sqrt{N}$ to avoid finite size effects. In this case, the simulation box size L must be larger than the characteristic aggregated SPP group size $\sim \ell\sqrt{N}$. For the case discussed in the main text where the number of SPPs is $N = 200$, we set $L = 50\ell$ to satisfy the inequality. Larger values of L are also sufficient.

The self-propulsion force coefficient μ was chosen to be τ^{-1} since it represents the exponential relaxation time for this force. This can be seen by setting mass equal to 1, and writing a simplified differential equation for $\vec{F}_i^{\rm propulsion}$: $dv/dt = \mu(v_0 - v)$, which has a solution $v(t) = v_0[1 - \exp(-\mu t)]$ when $v(t = 0) = 0$. If we again take $\mu^{-1} = \tau$ to be one second, then in the absence of any other interactions, it would only take a SPP a few seconds to reach its preferred speed when starting from zero initial velocity.

In order for SPP collisions to be counterbalanced by random noise force fluctuations, the collision time scale $\tau_{\rm coll}$ and the random force time scale $\tau_{\rm noise}$ must be comparable. Here, the random collision time scale $\tau_{\rm coll} = 1/(2r_0 v_0 n) \approx (\pi/4)\tau$ is the mean-free path $(2r_0 n)^{-1} \approx (\pi/2)r_0$ divided by the preferred speed v_0, where an estimate of the average crowd density $n \approx N/\pi(\sqrt{N}r_0)^2$ is obtained by noting the steady-state configuration of SPPs is roughly a half-circle with radius $\sqrt{N}r_0$ surrounding $\mathcal{P}$. Similarly, the noise time scale $\tau_{\rm noise} = v_0^2/2\mu\sigma^2$ can be found by calculating the amount of time required for random noise to change the correlation function $\langle[v_i(\tau_{\rm noise}) - v_i(0)]^2\rangle = 2\mu^{-1}\sigma^2\tau_{\rm noise}$ by an amount equal to v_0^2. Hence, $\tau_{\rm noise} = \mu v_0^2/2\sigma^2$. Because the unit speed v_0 is fixed by the fundamental simulation units, and μ is set by the self-propulsion relaxation time, we simply let $\sigma = \ell/\tau^2$ to satisfy $\tau_{\rm noise} = \tau/2 \approx \tau_{\rm coll}$ at steady-state.

Both particle-particle and particle-wall collisions are subject to a Hertzian contact repulsion force with coefficient ϵ. In the context of contact mechanics, the

* arianna.bottinelli@math.uu.se
† david.sumpter@math.uu.se
‡ jesse.silverberg@wyss.harvard.edu

Hertzian force provides the simplest description of the repulsion force arising from the contact of two elastic spherical bodies. The classical solution in the case of non-adhesive and frictionless elastic contact is given by $F_H = (4/3)ER^{1/2}d^{3/2}$, where E is a combination of elastic moduli and Poisson ratio, R is the body's effective radius, and d is the indentation depth. The assumption that there are no friction and adhesion forces means that F_H is directed normally to the surface of contact. In our case, $R = r_0/2$, $d = 2r_0 - r_{ij}$, and the normal direction is the direction joining the center of mass of the two particles. Therefore ϵ is a function of elastic material properties and constant for all SPPs. Such a repulsion term is often used to simulate jammed soft granular materials [2], but has been used to simulate human crowds, successfully reproducing instances of collective behavior at heavy metal concerts [3]. Though the functional form of contact forces were varied in previous work, it was not found to have significant impact on the model's overall phenomenology [3]. For consistency and continuity, we retained the force $\sim (\text{strain})^{3/2}$ relation. Other choices for the collision force have also been considered in the literature. For example, Moussaid et al. [4] and Helbing et al. [1] choose an even simpler linear repulsion force where $F_{ij} = k(r_i + r_j - r_{ij})$, while in another paper Helbing et al. [5] use an exponential repulsion of the form $F_{ij} = A\exp[(r_i + r_j - r_{ij})/B]$, where A denotes the interaction strength and B the range of repulsive interaction. Both these choices reproduce most of the phenomena observed in real crowds at high density such as turbulence at bottlenecks and stop-and-go waves [6].

Because the Hertzian contact force used in the main text is non-singular, we require the coefficient to be sufficiently large that particles do not completely overlap. To this end, we set $\epsilon = 25\ell/\tau^2$ so that the collision force scale is larger than the self-propulsion force scale $\mu v_0 = \ell/\tau^2$ and the noise force scale $\eta \sim \sigma = \ell/\tau^2$. While choosing simple Hertzian contact forces implies strong assumptions on the physics of the system, it reproduces the fact that bodies can be partially compressed and it captures the nonlinearity of the stresses involved. At the same time, this expression is easily implemented numerically and involves only one free parameter, making the effects easy to interpret.

c. The correlation matrix. As the starting point of our analysis, we use the simulated trajectories to compute the displacement covariance matrix C_p [7]. We treat separately the x and y components of the position vector $\vec{r}_i(t) = \langle x_i(t), y_i(t)\rangle$ to avoid convolving fluctuations in orthogonal directions. The simulation reaches steady state after $\approx 50\tau$, but we discard the first 300τ to eliminate far-from-equilibrium transients. Of the remaining $2,700\tau$, we sample data every 10τ, so that we have 270 time points. The obtained time points are separated by 100 simulation time steps to ensure statistical independence [7].

The equilibrium position $\langle x_i\rangle$ is obtained by averaging each SPPs position over 270 time points. The displacements $\delta x_i(t) = x_i(t) - \langle x_i\rangle$ around the mean position are used to compute the correlation matrix at the sampled time steps. The covariance matrix for the simulation is obtained by averaging over the independent time points:

$$C_{p_x} = \langle [x_i(t) - \langle x_i\rangle] \cdot [x_j(t) - \langle x_j\rangle]\rangle, \tag{3}$$

with a similar computation for the y component. The 270 independent time points are sufficient for the covariance matrix to converge to the true correlation matrix of the underlying statistical process [7]. In other words, the averaging is sufficient to obtain equivalence between time and ensemble average so that C_p can be identified as the correlation matrix.

d. Interpretation of C_p. For thermally equilibrated systems and in the approximation of harmonic oscillations, the dynamical matrix D (the Hessian of the pair interaction potential divided by the mass) contains all the information about the time-evolution of the system. The eigenmodes of D represent the vibrational modes of the system, $D|\lambda_m\rangle = \omega_m^2|\lambda_m\rangle$, where ω_m are the vibrational frequencies of the system, and ω_m^2 can be interpreted as the energy that has to be transferred to the system to activate the corresponding vibration. Here, $m = 1 \dots 2N$, where N is the number of particles in the system, and because x and y are orthogonal directions, the total number of eigenvalues is $2N$. For these systems, the correlation matrix is proportional to the inverse of the dynamical matrix D, thus the eigenvectors of C_p are simultaneous eigenvectors of D, while their eigenvalues are inversely proportional such that $\omega_m^2 \sim 1/\lambda_m$. For thermal systems at equilibrium, the spectrum of C_p can then be interpreted as the vibrational modes of an equivalent system of harmonic springs (shadow system). The vibrational properties of the two systems might not be exactly the same, but studying the shadow system is enough to extract the properties of the real system.

In our case, we are dealing with active matter and the observed dynamics is the result of the interplay between self-propulsion, repulsion, noise forces, and the environmental constraint of walls. Our system is not at thermal equilibrium, and the spectrum of C_p cannot be strictly interpreted as vibrational modes. We thus perform a Principal Component Analysis (PCA) on C_p to extract the components of the fluctuations that carry the information of correlated motion by comparison with the random matrix case RM_σ.

e. The Random Matrix Model RM_σ. We use a Random Model of uncorrelated Gaussian variables to test what are the relevant eigenmodes in our system. We compute the correlation matrix of a set of random displacements normally distributed with zero mean and variance σ_{RM}. The variance is the same as the simulated displacements around each SPPs equilibrium position. The eigenmodes computed from C_p with eigenvalues larger than the largest eigenvalue of the RM_σ model contain the relevant information about correlations. In our case we see that the first ten modes are above noise before removing the rattlers, while six modes are above noise after [Fig. 1].

f. Measures. For each component of the correlation matrix we compute the eigenvalues λ_m and the eigenvectors $\vec{e}^{\,i}_m$, $i, m = 1 \dots N$ in the x and y directions for a total of $2N$ eigenvalues. The eigenvalues taken in decreasing order and plotted as a function of their index m give the spectrum of the correlation matrix (for separated components x and y). Using the analogy with vibrational theory, we call $\omega_m^2 = \lambda_m^{-1}$ the energy of the m-th mode, from which one can compute the density of states, DOS(ω^2). The DOS carries information about the rigidity of a solid to collective motion, but since the equipartition of energy is violated for active matter, one should be careful when analyzing this quantity. The participation ratio $P_r(m) = (\sum_{i=1}^{N} |e^i_m|)^2/[N(\sum_{i=1}^{N} |e^i_m|^4)]$, with $|e^i_m| = ((e^i_{m_x})^2 + (e^i_{m_y})^2)^{1/2}$ is constructed by combining the x and y components [8]. In crystal theory the participation ratio of a mode describes how many particles in the system move in a given mode, and runs between 0 (fully localized) to 1 (fully extended). If we think about modes as collective dynamics, another useful characterization of their collective nature and spatial coherence is given by the mean polarization $\vec{\Phi}(m) = N^{-1} \sum_{i=1}^{N} \vec{e}^{\,i}_m / |\vec{e}^{\,i}_m|$ and the correlation function of the fluctuations around it

$$C_m(d) = \langle (\vec{e}^{\,i}_m - \vec{\Phi}(m))(\vec{e}^{\,j}_m - \vec{\Phi}(m)) \rangle_{d_{i,j}=d}, \qquad (4)$$

From this computation, we define the correlation length $l_c(m)$ such that $C_m(l_c) = 0$ [9]. In order to characterize the structure around SPPs in soft spots, we use the two particle radial structure factor $g(r) = \sum_{i=1}^{N} \sum_{j \neq i}^{N} \delta(r - r_{ij})/[N(N-1)]$, which measures the radial distribution of distances between neighboring SPPs. In our analysis, the eigenvalue spectrum, density of states, participation ratio, correlation function, and structure factor are averaged over 10 independent simulations of the dynamics with random initial conditions.

g. Choice of the rattler's threshold. In the literature, rattlers are underconstrained particles that feature an abnormally large displacement in the lowest energy modes [7]. They are a consequence of local structure: neighbors pack inhomogeneously and form cages where these particles get trapped and vibrate without participating in collective movement. In this sense, one can expect to find rattlers in trivially underconstrained areas, but it is not possible to predict *a priori* where they will localize since structural constraints arise from local self-organized disorder. Following the analysis developed for granular materials [7], we identify rattlers from the eigenmode analysis, eliminate these particles from our consideration, and recompute the eigenmodes and eigenvalues for a new C_p that only considers the population of non-rattlers. This procedure is necessary so that the lowest energy modes are not zero energy vibrations localized on a single particle (i.e. the rattler). Instead, this two-step computation of C_p ensures we accurately measure collective motion of the system.

The identification criteria for rattlers we utilize comes from previous work [7]: a particle i is a rattler if $dr^i_m \geq \langle dr_m \rangle + \xi_r \sigma_m$, where $dr^i_m = |e^i_m| = ((e^i_{m_x})^2 + (e^i_{m_y})^2)^{1/2}$ is the displacement of the particle i on the m-th mode, $\langle dr_m \rangle$ is the average displacement of the particles on that mode, σ_m their standard deviation, and ξ_r is a fixed threshold. In order to fix a value for ξ_r we compute C_p, its eigenvalues, and eigenvectors. We identify rattlers in the eigenmodes corresponding to the first 10 modes with ξ from 2 to 5. We consider the first ten modes as they are the most prominent compared to random fluctuations as identified by the random matrix model RM_σ. After identifying the rattlers, we eliminate them and re-compute C_p, its eigenvalues, and eigenvectors. We compute the spectrum, the DOS, the participation ratio, and we average over 10 independent instances.

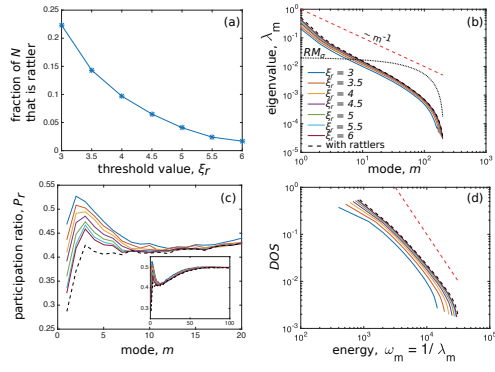

FIG. 1. Outcome of the choice of different thresholds when looking for rattlers and comparison with the random matrix model (RM_σ, dotted line). (a) The fraction of rattlers is a monotonically decreasing function of the threshold value ξ_r. (b) Comparison of the spectrum of the eigenvalues with the random matrix case before removing the rattlers (dashed black line) and after at different values of the threshold (solid colored lines). Depending on the value of ξ_r, the first five to ten modes are larger then the random matrix case (dotted black line). Debye model for harmonic crystals (red dashed line) is shown for reference. (c) The Participation ratio increases for the lowest energy modes when rattlers are removed at all values of the threshold ξ_r. Inset shows same data for modes up to $m = 100$. (d) Comparison of the density of states before removing rattlers (black dashed line) and after (solid colored lines) at different values of the threshold ξ_r. Debye model for harmonic crystals (red dashed line) is shown for reference.

We compare the above measures with and without the rattlers for different values of the threshold [Fig. 1]. The trend of the spectrum of the eigenvalues and of the density of states is not affected by removing the rattlers. In particular, we find the first modes remain above random noise [Fig. 1(b)]. The participation ratio [Fig. 1(c)] is increased at all values of ξ_r, suggesting that the rattlers we removed were particles that fluctuated the most in the considered modes. Thus, we fix the rattlers threshold at

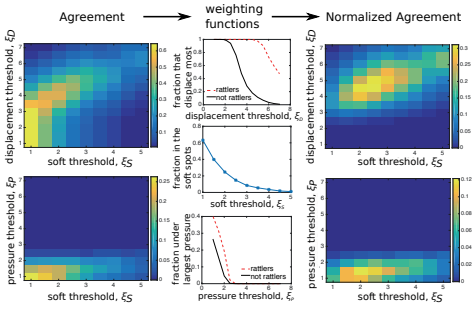

FIG. 2. The agreement functions before (left column) and after (right column) normalization by the weighting functions (central column) that measure the size of the sets S, P, D representing soft spots (S), large pressure (P), and large displacement (D).

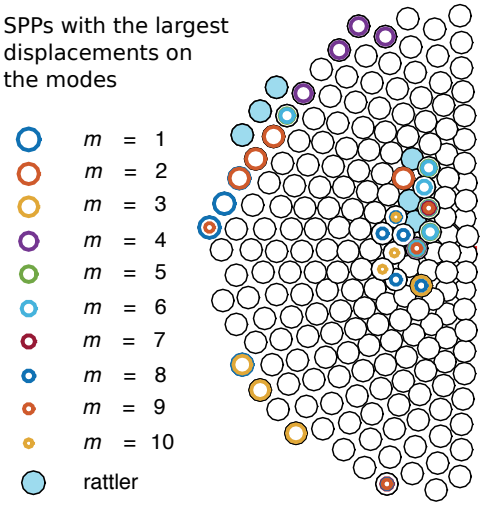

FIG. 3. Each SPP is shown as a disk. Superimposing data for the first 10 modes shows that soft spots appear in multiple modes in the same general area. Apparent soft spots along the periphery are artifacts due to underconstrained edge effects.

$\xi_r = 4$. With this value the rattlers are about 10% of the total population [Fig. 1(a)].

h. Choice of threshold for soft spots. As was done for rattlers, we need to set a threshold for identifying particles featuring large displacement on the softest modes. These particles are the ones that displace most when a mode is activated and we might expect them to behave qualitatively differently than other particles. In particular we test if the particles participating the most in soft modes (S) are the same particles featuring a large displacement in the real dynamics (D) and, separately, if they are subject to large pressure (P). We use the same criteria used for identifying rattlers and test a set of thresholds ξ_* from 1 to 5 standard deviations with respect to the mean displacement or pressure value, where $* = S, D, P$. After identifying the sets corresponding to each threshold, we compute their "normalized agreement," as $\nu_S \nu_D |S \cap D| / |S \cup D|$. Here, $\nu_* = 1 - N_*/N$ is a weighting function that dampens the measure of the overlap if the two sets are oversampling the total population.

For a large set of thresholds of D and S, the particles that participate most in the soft modes are also the ones that feature the largest displacements in the real trajectory. The normalized agreement function for S and D is maximum for $\xi_S = 2.5$ and $\xi_D = 4.5$ [Fig. 2, top]. Thus, we identify soft spot SPPs as the ones that have displacements larger than 2.5 standard deviations on at least one soft mode. Experiencing large pressure (P) does not seem to correlate with being a soft spot SPP [Fig. 2, bottom]. Indeed, the percentage of particles that are not rattlers and experience a pressure larger than one standard deviation is low [Fig. 2, bottom, central plot]. Simulation measurements show the highest pressures, and therefore the highest pressure fluctuations, are located in close proximity to the point of interest $\mathcal{P}$ [Fig. 5(a)]. Conversely, soft spots are located some distance from $\mathcal{P}$ either at the SPP aggregate's boarder or in a more centralized region [Fig. 3]. As a consequence, the highest agreement is obtained for the lowest pressure and soft spot thresholds [Fig. 2, bottom left]. However, $\xi_S = 1$ means that the particles in soft spots would be more than 50% of the population, making this measure ineffective for identifying individuals under large pressure. In other words, low pressure thresholds include too many SPPs. Even when correcting for this oversampling, we find the normalized agreement between S and P has only slightly increased optimal threshold values, but the overall agreement becomes extremely low (0.12). This shows that soft spots are not a good candidate for identifying individuals experiencing the largest pressure. We can intuitively understand this result by noting individuals in soft spots are partially underconstrained as shown by $g(\boldsymbol{z})$, and therefore subject to reduced forces overall [Fig. 3(c), main text].

SIZE EFFECT

To check for finite size effects in our analysis we simulated the same dynamics as described in the main text for $N = 500$ and $N = 80$. We apply the same procedure as in the case $N = 200$ and we consider the measures that are relevant for the analysis described in the main text [Fig. 4]. We find the crowd pressure increases with crowd size from $23.8P_0$ for $N = 80$ to $56.5P_0$ for $N = 500$, where $P_0 = \mu v_0 (2\pi r_0)^{-1}$ is the inertial swim pressure of a SPP of radius r_0 and moving with speed v_0 [10]. This

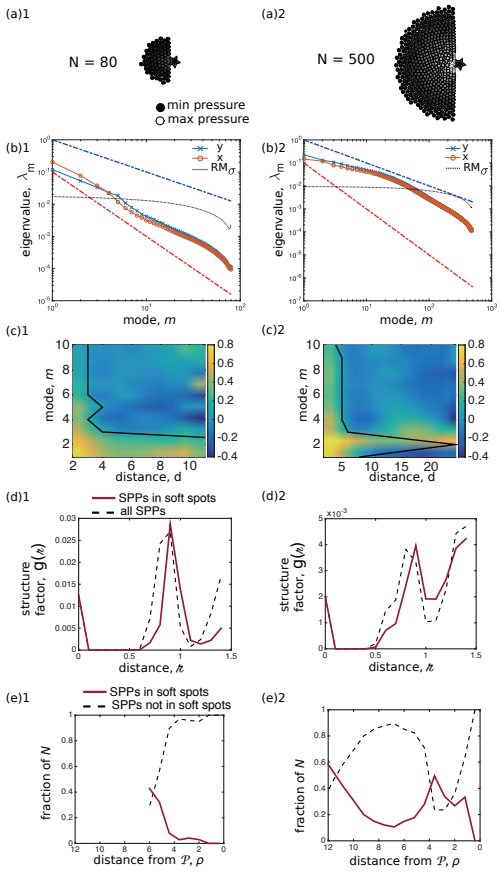

FIG. 4. Main measures at small ($N = 80$, column 1) and large ($N = 500$, column 2) system size. (a) Each circle represents a SPP. In both (a)1 and (a)2 the color scale is normalized so that the maximum pressure (lightest circles) is $56.5P_0$ and the minimum pressure is 0. (b) Spectrum in the x (circles) and y (crosses) direction compared with the random matrix model (dotted line). (c) Correlation function (heatmap) and correlation length (line). The gradient scale is identical in (c)1 and (c)2. (d) Structure factor for the particles in the central soft spot (solid line) compared with the average structure (dashed line). (e) Proportion of particles in the soft spots (solid line) and outside the soft spots (dashed line) as a function of the distance ρ from $\mathcal{P}$.

result is in agreement with the empirical observation that crowd pressure builds up with the number of people involved. The eigenvalue spectrum preserves its shape and thus seems to be a genuine feature of the dynamics. For increasing N, additional modes rise above the random matrix model for uncorrelated noise, RM_σ. The lowest energy modes are still correlated over long ranges. In particular for $N = 500$ the first mode shows high correlation at short distance and high anti-correlation at long distance, while the second mode's correlation length spans the size of the system. However the energy gap between these two modes is smaller than for smaller system sizes. For both $N = 500$ and $N = 80$ the structure factor $g(\hbar)$ shows that the particles belonging to the core soft spot are slightly less constrained than the average structure. At the edge of the simulated crowd, the number of SPPs with large displacement on the softest modes is large in both cases, while the size of the core soft spot increases with N.

THE ROLE OF LOCAL STRUCTURE AND RESEMBLANCE TO ORDERED PACKINGS

The densest 2D arrangement of hard discs packed in uniform conditions is a well-studied problem whose solution is a hexagonal lattice. In the model studied here, we do not have uniform conditions, however, a region of the steady-state SPP configuration shows similarities with hexagonal packings. This particle configuration arises in a self-organized fashion from the competition between attraction toward the point of interest $\mathcal{P}$, and body-body contact repulsion. Such competition between forces generates a pressure gradient that is highest at $\mathcal{P}$ and decreases with distance away from this point [Fig. 5(a)]. If the pressure was uniform, a true hexagonal lattice may be expected. However, the pressure gradient simply drives particles to pack in a fashion commensurate with the local force balance. As such, we only see hexagonal-like arrangements in a limited region where pressure is sufficiently low and the number of neighbors is sufficiently high to surround each particle. Near $\mathcal{P}$ where the pressure is highest, we see the packing becomes significantly more disordered since the particles can partially overlap through the body-body force interactions, leading to more than six interacting neighbors [Fig. 5(b)].

The fact that there is no long-range lattice structure can be seen also through the full structure factor $g(\hbar)$, which gives information about the local structure around particles in a way that cannot be inferred from globally averaged structural properties [11]. Indeed, the $g(\hbar)$ measurement reveals that the overall structure has clear short range order [Fig. 5(c), peaks where $\hbar < 3$] but no long range order [Fig. 5(c), generally smooth distribution where $\hbar > 3$], indicating that there is no regular lattice.

CORRELATION WITH INCREASED ACTIVITY

We model behavioral diversity by increasing noise fluctuations $\sigma_a \in [1.5, 4]$ for different fractions of SPPs $f \in [0.1, 1]$ placed in random positions within the crowd. When looking at the spectrum of C_p, the eigenvalues

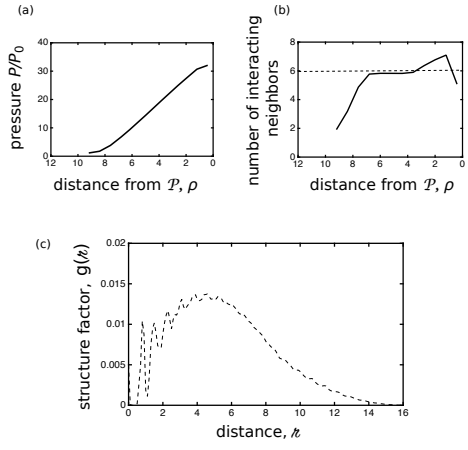

FIG. 5. Additional structural measurements. (a) Normalized pressure P/P_0 on each SPP averaged over all particles at distance ρ from the point of interest $\mathcal{P}$. The data shows a linear pressure gradient that is maximum at $\mathcal{P}$ and decreases away from this point. (b) Average number of interacting neighbors at a distance ρ from the point of interest $\mathcal{P}$. Hexagonal close packings of hard discs have six interacting neighbors, which is added as a dashed line for reference. (c) The structure factor $g(\aleph)$ shows short range order (peaks for $\aleph < 3$), but no long-range order ($\aleph > 3$). All data in (a) and (b) is generated and averaged from 10 random initial conditions.

steadily increase at increasing activity level σ_a and at increasing active population fraction f [Fig. 6(a)], with more and more modes becoming relevant in describing the dynamics. Correspondingly, the energy needed to excite these modes drops significantly. For example, the five lowest energy modes at $f = 0.1$ and $\sigma_a = 2.5$ need half of the excitation energy that is needed when everyone is calm ($f = 0$) [Fig. 6(b)]. This means that a fixed amount of energy provided to the system would excite an increasing number of modes as more active people are present. This could be explained by the increase in the size of soft spots, i.e. the number of individuals composing them, with both f and σ_a [Fig. 6(c)]. Intuitively, one might expect that individuals with larger σ_a would be detected as rattlers or as belonging to a soft spot, having a larger displacement on the softest modes. This does not seem to be the case as unstable areas can double their size even when a small fraction of the population becomes very active, as for example for $f = 0.1$ and $\sigma_a = 3.5$.

The heatmap for the correlation function of the fluctuations around the mean polarization for eigenmodes up to $m = 60$ [Fig. 6(d)] expands on the corresponding figure in the main text and confirms our interpretation for modes with $m > 10$. At increasing f and σ_a we observe that coherence decreases for low energy modes and increases for higher energy modes. Interestingly, for intermediate values of σ_a and f several modes feature long range correlation. When both σ_a and f are very large ($\sigma_a = 3, 3.5$, $f > 0.6$ and $\sigma_a = 4$, $f > 0.1$) our analysis does not find long-range correlated modes.

MECHANICAL SIGNAL TRANSMISSION ENHANCEMENT VIA STOCHASTIC RESONANCE

Insofar as information can be sent by mechanical oscillations similar to the way information can be sent by electromagnetic oscillations, our interpretation of new long-range modes in agitated SPPs as stochastic resonance can be understood by the following passage [12]:

> Over the last two decades, stochastic resonance has continuously attracted considerable attention. The term is given to a phenomenon that is manifest in nonlinear systems whereby generally feeble input information (such as a weak signal) can be amplified and optimized by the assistance of noise. The effect requires three basic ingredients: (i) an energetic activation barrier or, more generally, a form of threshold; (ii) a weak coherent input (such as a periodic signal); (iii) a source of noise that is inherent in the system, or that adds to the coherent input.

In our model, the weak signals to be amplified are oscillations with frequencies corresponding to modes $m > 1$ (ingredient ii). These modes can carry "mechanical information," but are prevented from propagating by the disordered geometry of the SPP packing (ingredient i). Unlike ordered packings where phonons can span the system, the $m > 1$ modes are spatially localized [Fig. 2(c) and 4, main text]. By adding a population of agitated SPPs to the system (ingredient iii), this source of noise breaks up the signal-localizing packing disorder, so that the "feeble input information" is no longer spatially localized, but instead, propagates through the system.

An alternative description of stochastic resonance describes the phenomenon as [13]:

> Stochastic resonance is said to be observed when increases in levels of unpredictable fluctuations e.g., random noise cause an increase in a metric of the quality of signal transmission or detection performance, rather than a decrease.

In our case, agitation adds more system-spanning modes, and hence increases the potential signal transmission bandwidth. Indeed, direct counting of the number of system-spanning modes shows the intermediate-agitation regime typically has 2 to 5 long-range modes for the parameters studied [Fig. 7].

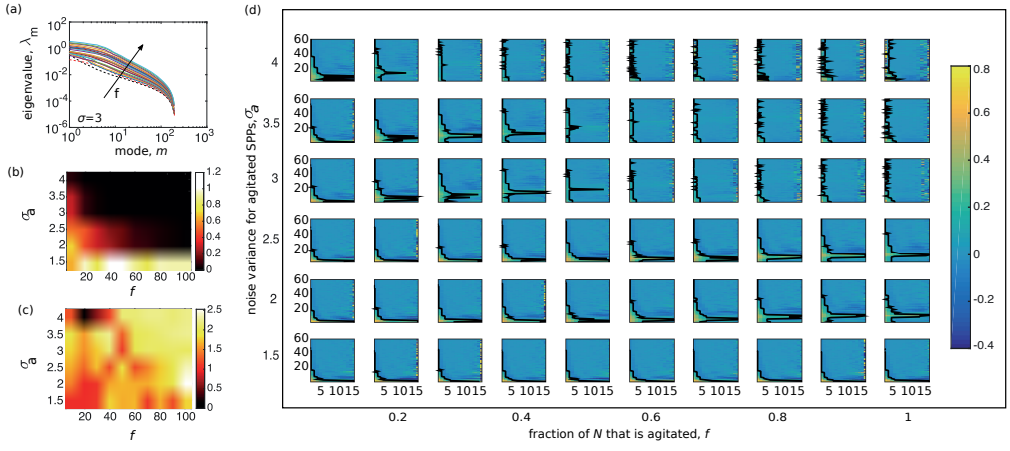

FIG. 6. Effects of increasing the fraction of active people f featuring a larger noise strength σ_a. (a) At fixed $\sigma_a = 3$, increasing f increases all eigenvalues of the spectrum with respect to the homogeneous population where $f = 0$. (b) The sum of the excitation energies of the first five eigenmodes as a function of f and σ_a divided by the corresponding quantity at $f = 0$. Excitation energies significantly drop at increasing active population and activity level. (c) The size of soft spots at different f and σ_a divided by the average soft spot size in the homogeneous population is an increasing function of f and σ_a. (d) Correlation function of the fluctuations around the mean polarization order parameter with increasing f and σ_a up to the 60^{th} mode (heatmap). The correlation length (black line) is plotted as a function of mode number m in each subplot.

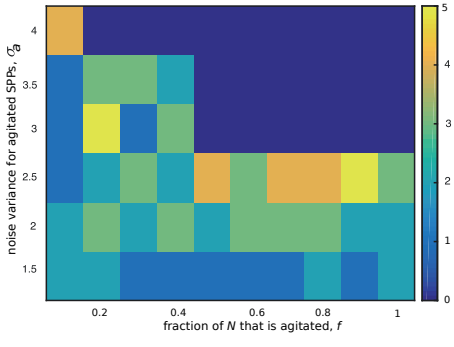

FIG. 7. Enhancement of mechanical signal transmission through agitation of dense crowds is evident by counting the number of long-range modes present in the system. Each cell in the heat map corresponds to a given (σ_a, f) parameter choice and represents the number of long-range modes.

METHODS

Crowd simulations are performed in C. The program was adapted from the original version by Andreas Gådin and John Svensson, which itself was inspired by previous work [3]. Data analysis was performed with MATLAB. As described in the main text, our initial analysis of the model's dynamics was averaged over 10 runs with random initial conditions, where each run provided 270 statistically independent measurements of the correlation matrix. We then modified the model to include two populations of SPPs, where each population is characterized by a distinct value for the noise force variance. In this analysis, we performed a sweep of the two-dimensional parameter space for $6 \times 10 = 60$ different parameter values. Our data for each parameter pair was similarly analyzed for 10 different random initial conditions, adding 600 simulation runs to our analysis. Again, each simulation run provided 270 statistically independent measurements of the correlation matrix. We also analyzed different population sizes, demonstrating the phenomenology is independent of the number of particles [Fig. 4]. This data adds 20 simulation runs, for a grand total of 620 simulations and 167,400 statistically independent measurements of the correlation matrix exploring three distinct model parameters.

The specific functional form of the forces studied here was chosen to be consistent with previous studies in the literature [3, 6]. Indeed, this minimal model for active matter has previously demonstrated a rich set of phenomenology such as stop-and-go waves, turbulence, and phase transitions [6]. While our choice to vary model parameters instead of model forces has its advantages, the opposite approach is certainly worth considering because it would provide evidence for the generality of our observations. For example, Goldstone modes can be reasonably expected in any active matter model that breaks

continuous symmetry, and thus should be found independent of the specific interaction forces. Soft modes, on the other hand, arise from disordered packings and may not be present if the interactions cause particles to form regular lattices. Future studies focusing on identifying such model-dependent phenomenology are likely to play a critical role in our understanding of both active matter and human collective motion. In addition, experimental advances providing new observations and testing existing theories must come hand-in-hand with these theoretical developments so that the field may continue to progress.

[1] D. Helbing, I. Farkas, and T. Vicsek, Nature **407**, 487 (2000).

[2] M. Van Hecke, Journal of Physics: Condensed Matter **22**, 033101 (2009).

[3] J. L. Silverberg, M. Bierbaum, J. P. Sethna, and I. Cohen, Phys. Rev. Lett. **110**, 228701 (2013).

[4] M. Moussaïd, D. Helbing, and G. Theraulaz, Proc. Natl. Acad. Sci. U.S.A. **108**, 6884 (2011).

[5] D. Helbing and A. Johansson, arXiv preprint arXiv:1309.1609 (2013).

[6] D. C. Duives, W. Daamen, and S. P. Hoogendoorn, Transport. Res. C - Emer. **37**, 193 (2013).

[7] S. Henkes, C. Brito, and O. Dauchot, Soft Matter **8**, 6092 (2012).

[8] N. Xu, V. Vitelli, A. Liu, and S. Nagel, Europhys. Lett. **90**, 56001 (2010).

[9] W. Bialek, A. Cavagna, I. Giardina, T. Mora, O. Pohl, E. Silvestri, M. Viale, and A. M. Walczak, Proc. Natl. Acad. Sci. U.S.A. **111**, 7212 (2014).

[10] S. Takatori, W. Yan, and J. Brady, Phys. Rev. Lett. **113**, 028103 (2014).

[11] B. B. Laird and H. Schober, Phys. Rev. Lett. **66**, 636 (1991).

[12] L. Gammaitoni, P. Hänggi, P. Jung, and F. Marchesoni, Rev. Mod. Phys. **70**, 223 (1998).

[13] M. D. McDonnell and D. Abbott, PLoS Comput Biol **5**, e1000348 (2009).